AN EXPERIMENTAL INVESTIGATION OF THE PROPULSIVE THRUST OF OSCILLATING FOILS OF DIFFERENT PLANFORMS

LUKSA LUZNIK

An Experimental Investigation of the Propulsive Thrust of Oscillating Foils of Different Planforms

By

©Luksa Luznik, B.Eng.

A thesis submitted to the School of Graduate Studies in partial fulfilment of the requirements for the degree of Master of Engineering

Faculty of Engineering and Applied Science

Memorial University of Newfoundland

July, 1997

St. John's Newfoundland Canada

Abstract

A second design loop in the development of the computer controlled oscillating motion apparatus was completed as a part of this research. Specifically, work was concentrated in two areas: first, modifications to the existing motion control software with the aim to produce a continuous sinusoidal motion, and second, design of a dynamometer to measure more accurately the thrust developed by the oscillating foil.

Bench tests conducted with the changes in the motion control indicated that the limitations to produce true sinusoidal oscillatory motion were due to the oscillating apparatus drive system. A single degree of freedom dynamometer consisted of two flexible vertical sheets to which a rigid plate was connected forming a U frame. This design allowed for sensitivity in the fore and aft direction, but was very rigid in the transverse direction. The oscillating apparatus was supported by the frame, and thrust or drag forces developed by the oscillating foil were transmitted through this frame to the load cell.

An experimental study to measure developed thrust from a series of rigid foils subjected to unsteady, oscillatory motion has been conducted in the towing tank at Memorial University of Newfoundland. The foils tested consisted of a rectangular planform, a straight tapered and swept back planform, as well as the planform with curved leading edge, similar to the flukes of a fin whale. The foils had the same

aspect ratio of 6. Two foils were fabricated out of brass, and another was made out of wood. The brass foils had a span of 200 mm, while the wooden foil had a span of 400 mm. In the experiment the heave amplitude to chord ratio was large (of order 1) and the pitch amplitudes tested were :6, 13, 17.5 and 21 deg. The pitching axis position was fixed at chord/2, and pitch led heave by 90 deg.

Results of developed thrust from different planforms are presented and examined with respect to four areas of interest: large amplitude motion, effects of different planforms on developed thrust, foil performance at large angles of attack, and a comparison of an existing 3D unsteady flow panel code to predict developed thrust with the experimental results.

Comparison of experimental results with the panel method showed that for small reduced frequencies and angles of attack, agreement in the magnitude of the thrust coefficient was good. At large reduced frequencies and angles of attack results from the panel method underpredicted the developed thrust. This discrepancy in results was due to separation and dynamic stall which occurred in the range of 33 to 40 deg. angle of attack. The combination of a leading edge sweep and taper of the foil's planform has a marked difference in developed thrust compared to the foil with a straight leading edge. This was due to different stall behaviour over foils with leading edge sweep compared to the stall of foils with a straight leading edge.

Acknowledgements

I would like to thank the following organizations for providing financial support for this work: Natural Sciences and Engineering Research Council through the Research Grant held by Dr. Neil Bose, Centre for Cold Ocean Resources Engineering for their support through C-CORE Graduate Fellowship in the period from September 1995 to September 1996, and the School of Graduate Studies and Faculty of Engineering and Applied Science for support through teaching assistantship.

My deepest and sincere gratitude goes to my supervisor Dr. Neil Bose for offering me this research topic, his continuing support, constructive guidance and invaluable advice throughout this project. Dr. Bose, the enthusiastic discussions that we had over the last two years of my graduate studies left me with the impression that my thoughts are not just mine. This was, and is a delightful feeling.

In addition, I would like to thank my co-supervisor Professor W. G. Smith for his supervision and advice. In particular, I would like to acknowledge his valuable comments on the design of the dynamometer, and for reading my thesis.

I also wish to express my thanks to Dr. Pengfei Liu, formerly the graduate student in the Faculty of Engineering and Applied Science, Memorial University of Newfoundland, for allowing me to use his panel method code for the purpose of

the comparison of experimental and theoretical results. His time and effort in assisting me with the code is greatly appreciated. My thanks also goes to Mr. David L. Greening for the help with familiarization with the oscillating foil apparatus during the initial stage of the project.

I extend my thanks to the professors in my graduate courses. Most notably to Dr. J. Sharp, Dr. M. Hinchey, and Dr. G. Sabin for presenting courses which I found to be particularly helpful in my research. Thanks are also due to the National Research Council of Canada, Institute for Marine Dynamics, for allowing me the use of their cavitation tunnel.

On a personal note, I would like to express thanks to my office mate Robert C. Brown for the helpful discussions throughout the master's program, and help with the fabrication of the wooden foil model.

Finally, I am indebted forever to my parents Nikola and Maria for their continuous encouragement, understanding and support.

Contents

List of Figures

List of Tables

Chapter 1

Introduction

1.1 General

Over the centuries the inquisitive human mind has found inexhaustible sources of inspiration in the natural world. In marine environments one just needs to see with what grace and ease dolphins, our most acquainted friends from the sea, propel themselves through the water.

The story of modern experimental and theoretical interest in fish propulsion started with the work of Gray (1936) when he compared the estimated available muscle power that a dolphin can deliver, and the power needed to achieve its swimming speed. The conclusion, known as "Gray's paradox" was that a dolphin is too weak to attain its swimming speed. So either a dolphin has the required muscular power to achieve high speeds, or it is a very efficient swimmer. Gray's paradox has not been resolved today, 60 years after its formulation. However, the work of Gray inspired an avalanche of theoretical, and with the emergence of computers, numerical studies concentrating on hydrodynamic performance and swimming efficiency of fishes and cetacean mammals.

The classical unsteady aerodynamic theory of oscillating foils originally developed as a result of interest in aircraft flutter problems (von Karman and Burgers, 1935),

has found extensive use in bio fluid dynamics. This is due to the fact that the propulsion of the fastest aquatic animals that include tunnyfishes, sharks and many cetacean mammals have adopted the mode of propulsion Lighthill (1969) termed *carangiform* with high aspect ratio tails of crescent-moon shape. Forward thrust is generated exclusively by the oscillation of the caudal fin mounted on the slender tail section of the heavy body, Van Dam (1982). If these fishes and cetacean mammals are relatively efficient swimmers, as is generally thought, then their propulsors, tail or flukes, must be very efficient. Indeed, the peak efficiency for the flukes of an immature fin whale (*Balaenoptera physalus)* has been estimated to be around 87% by Bose and Lien (1989). However, the open water efficiency of a screw propeller which has a dominant role in marine propulsion today may be around 50% to 60% and it is difficult to increase this beyond 75%. This clearly indicates the importance of altemative types of propulsors and the fact that there is still a lot to learn from the natural world as far as propulsion devices are concerned. This is even more so as the 20th century comes to a close, and our consumption of limited fossil fuel reserves shows no decline, but rather increases from year to year.

The focus of this thesis is to study the propulsive performance of flapping foils, which are the main propulsors for all fast fish and cetacean mammals. The study falls under the field of unsteady hydrodynamics, and the potentially beneficial effects of unsteadiness such as the propulsive vortical signature, controlled

periodic vortex generation, and stall delay will be discussed.

In wing theory, for simplicity, unsteady effects have often been ignored. In practical engineering applications no matter how carefully a fluid dynamic device is designed, separation and unsteadiness behind moving bodies are often unavoidable because of maneuvering motions, or interaction with ambient turbulence. From this point of view, the concepts of unsteady motion and potential benefits of unsteadiness, which are discussed in this thesis, are by no means restricted to marine propulsion. Its applicability is pertinent to the wide range of unsteady hydro/aerodynamic fields; aeronautical and turbomachinery fields being two of the obvious ones.

1.2 Objectives of the Research

The primary aim of this research was to investigate the performance of an innovative propulsion system which conceptually mimics the superior propulsive characteristics of advanced swimming animals. This was done by concentrating work in two main areas:

- Measurement and analysis of forward thrust developed by an oscillating foil. Specifically, three sets of foils of the same aspect ratio but different planform were tested in the towing tank.

- Comparison of experimental results with theoretical calculations. Emphasis was placed on large amplitude motions.

1.3 Description of Swimming Simulation

In this work the *carangiform* mode (Lighthill, 1970) of propulsion is considered i.e. heaving and pitching in the vertical plane which is the characteristic tail fluke motion of cetacean mammals such as whales and dolphins. The same motion turned 90 deg. represents the oscillations in the horizontal plane (sway and yaw) of lunate tail fishes.

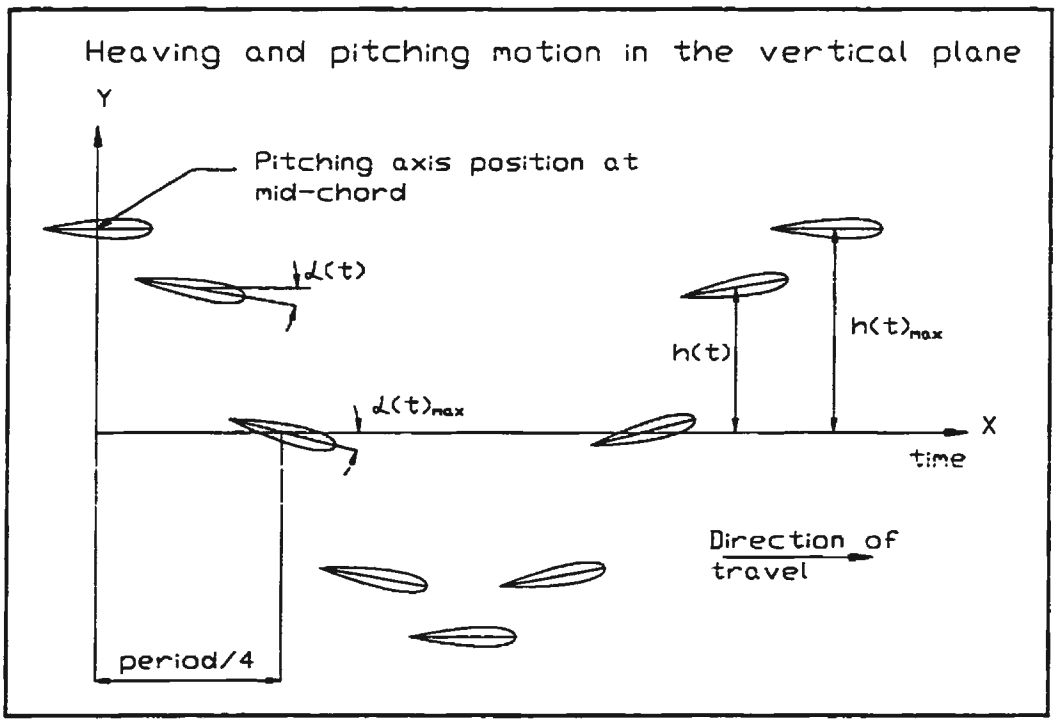

Figure 1.1 Oscillating Motion of the Foil

It is assumed that the foil section is **rigid** and its undisturbed position lies on the *x* axis with the origin at its mid-chord, and positive *y* axis direction upward. As the

foil is oscillated with a given heave amplitude it also pitches around the axis which is perpendicular to the chord line of the foil. Swimming is approximated with a sinusoidal motion with a constant 90 deg. phase angle (figure 1.1) between pitch and heave following Lighthill (1970) equation:

$$y = h\cos(\omega t) + \alpha (x - b)\sin(\omega t) \tag{1.1}$$

where y is the displacement of any point x on the foil, h and α are heaving and pitching amplitudes respectively, b is the pitching axis position relative to the mid-chord of the foil, and ω is the circular frequency.

1.4 Dimensional Analysis

As a starting point in this research work, a dimensional analysis of the problem of oscillating foils was performed. The aim of this analysis was to obtain the functional equation in which the non-dimensional parameters relevant to the phenomena are identified (Sharp et al., 1983). The first step in dimensional analysis was to select pertinent quantities which play a role in the problem of rigid oscillating foils. They are:

- Foil geometry or characteristic length: This includes chord c, span s and aspect ratio AR.
- Mean forward speed of an oscillating foil U.
- Motion variables: Heave amplitude h, pitch amplitude α, pitching axis position b, phase lag between pitch and heave ϕ, and frequency of

oscillation ω.

- Pressure p: To obtain a functional relationship for lift generation only, pressure need not be included in the analysis. This is because lift is caused by the difference in dynamic pressure between the upper and lower side of a foil and static pressure cancels out. As the dynamic pressure of a fluid particle is proportional to the velocity squared, the pressure term would be redundant if included in analysis. However for cavitating foils pressure has to be taken into consideration because cavitation inception is pressure dependent.
- Viscosity μ: Viscosity is important as it is responsible for determining the circulation around a foil.

It is expected that the following variables are sufficient to describe the unsteady flow around a heaving and pitching foil:

$$T = f[U, \alpha, \omega, \phi, p, c, s, \mu, \rho, b, h, AR] \tag{1.2}$$

where T denotes mean thrust or drag force developed by an oscillating foil, and ρ denotes fluid density. Here it was assumed that the foil cross section is geometrically similar to the prototype, so only three characteristic dimensions are used to specify foil shape, namely chord length c, foil span s, and aspect ratio AR. Using the method of linear proportionalities for dimensional analysis described by Sharp (1981), a convenient solution for thrust T after compounding is:

$$\left(\frac{T}{\rho U^2 s^2}\right) = f_1\left[\left(\frac{U}{\omega c}\right), \left(\frac{p}{\rho U^2}\right), \left(\frac{\nu}{Uc}\right), \left(\frac{h}{c}\right), \left(\frac{s}{c}\right), \left(\frac{b}{c}\right), \alpha, \phi, AR\right] \qquad (1.3)$$

Functional equation (1.3) indicates that oscillating foils can be studied in terms of ten non-dimensional parameters. The first term is the ratio of thrust force to inertial force and is represented by a thrust coefficient C_t equal to:

$$C_t = \frac{T}{\frac{1}{2}\rho U^2 S} \qquad (1.4)$$

where *S* is the foil's surface area, and where the other parameters are as defined above. The second term is a time constant and it signifies the importance of time-dependent phenomena. This term in the form:

$$k = \frac{\omega c}{2U} \qquad (1.5)$$

is traditionally known as the "*reduced frequency*" *k* and the relevant characteristic length is a streamwise dimension represented by the foil's chord length *c*. Another form of this non-dimensional parameter, indicating a wake shedding frequency behind an oscillating foil is the Strouhal number defined as:

$$St = \frac{fA}{U} \qquad (1.6)$$

where *A* denotes the width of the wake (or vertical distance travelled by the foil's trailing edge during half a cycle of oscillating motion), and *f* is the frequency in Hz. Here the characteristic length is perpendicular to the flow represented by the width of the wake *A*.

The third term in equation (1.3) is a pressure coefficient usually in the form:

$p/(\frac{1}{2}\rho U^2)$, the fourth term is the well known Reynolds number, and the fifth term is the ratio of heave amplitude to chord length. Term *s/c* is the aspect ratio for a rectangular planform, and *b/c* is the ratio of pitching axis position to the chord length. The last three non-dimensional parameters are the amplitude of pitch oscillation α, the phase angle between pitch and heave ϕ, and the aspect ratio *AR*.

The grouping together of a number of individual variables that are relevant to the problem of oscillating foils into a smaller number of non-dimensional parameters provided a basis for the organization of the experimental program. Also, as it will be shown in Chapter 5, dimensional analysis provided a guide to the comprehensive way in which experimental data together with theoretical results should be presented.

Chapter 2

Literature Survey

2.1 General

The aim of this section is to give an overview of the research development in the field of unsteady hydrodynamics with application to oscillating foils and their potential as a new type of propulsor. Most of the discussion will be focused on published experimental results on oscillating foils, as well as available unsteady flow visualization results. Theoretical and numerical work is only touched upon and only a few studies relevant to the present work are described. Theoretical treatments of any phenomena are justifiable as long as the assumptions inherent in the theory are realistic. The limitations of theoretical and numerical assumptions used today in oscillating foil studies will be highlighted. Also an attempt will be made to explain some of the fundamental differences between steady and unsteady hydrodynamics. The aim is to provide a background and a valuable framework against which this research can be viewed.

2.2 Experimental Results

Triantafyllou et al. (1996) show the results of systematic tests of a heaving and pitching foil. The set up consisted of a NACA 0012 foil with 10 cm chord and 60 cm span pitching about the $b=c/3$ position measured from the foil's leading edge. Aluminium end plates were fitted to avoid three-dimensional end effects. Tests

were done at three different heave amplitude to chord ratios h/c=0.25, 0.5, 0.75, and several nominal angles of attack[1] ranging from 5 to 30 deg. An important result from these experiments is that they illustrate a difference between steady and unsteady propulsion. To avoid stall, the basic principle of fixed-wing flight is to keep the angle of attack well below about 15 deg. However, the authors do not report on the occurrence of noticeable stall until the angle of attack exceeded 30 deg. This suggests that criteria indicating a stall for fixed wings, does not apply to oscillating foils because the unsteady effects can fundamentally alter the stall process for oscillating foils (McCroskey, 1977). Further, leading edge separation was observed at large angles of attack resulting in a dynamic stall vortex. The authors suggest that this vortex did not deteriorate foil performance, but on the contrary maximum propulsive efficiency[2] of 87% at Strouhal number=0.3 and a phase angle of 70 deg. occurred when this dynamic stall vortex merged with the shed trailing edge vortex to form a single vortex per half cycle of motion (Triantafyllou et al., 1995). Also, their results show that heave amplitude to chord ratio is a significant parameter with respect to the magnitude of the developed thrust: larger heave amplitude ratios resulted in increased thrust values.

---

[1]Nominal angle of attack is the angle between the foil's nose-tail plane and the resultant kinematic velocity vector which for the oscillating foil is a function of time. Angles reported here refer to the maximum angles. For a detailed definition of the angle of attack see Chapters 4 and 5.

[2]Propulsive efficiency is defined as the ratio of the work done by the mean forward thrust to the mean rate at which work is done by the foil movements on the surrounding fluid (Lighthill, 1970; Chopra and Kambe, 1977)

Koochesfahani (1989) used measured average velocity profiles behind an airfoil pitching about its quarter-chord point (measured from the foil's leading edge) to estimate the mean streamwise force on the airfoil. The thrust was measured for two cases of oscillatory pitch motion: amplitude 2 deg., and 4 deg. The ratio of the foil's trailing edge excursion to chord length *(a/c)* was small: 0.026 for 2 deg. pitch amplitude, and 0.052 for 4 deg. pitch amplitude. Here the foil's trailing edge excursion *a* is taken as half of the width of the wake denoted by *A* in equation (1.6). Koochesfahani provided a plot of the force coefficient versus reduced frequency *k* (see the definition in equation 1.5) for two cases of pitch amplitude. His results indicate that the reduced frequency for the onset of positive thrust generation depends on the oscillation amplitude. This was manifested in that at 4 deg. pitch amplitude thrust changed sign from drag to forward thrust at smaller reduced frequency than at 2 deg. pitch amplitude.

Yamaguchi and Bose (1994), show results for a heaving and pitching rectangular foil (*AR*=3), about the quarter-chord point. The ratio *h/c* in this experiment was 0.6 and the pitch motion led the heave motion by 90 deg. Thrust coefficient was plotted as a function of advance coefficient *J*, which according to their nomenclature is:

$$J = 2\left(\frac{h}{c}\right)\frac{1}{St} \qquad (2.1)$$

where *St* is defined as in equation (1.6). At $J \approx 15$ which corresponds to $St \approx 0.08$ thrust coefficient is approximately zero, which is in accordance with Triantafyllou

et al. (1996) results.

For periodic oscillation of the foil, the fluid dynamic phenomena can be characterised by the non-dimensional frequency parameters: reduced frequency k, advance coefficient J, and Strouhal number St. These non-dimensional parameters are defined using different characteristic lengths: foil chord c, heave amplitude h, and width of the wake A (foil's trailing edge double excursion), respectively. Different researchers select the parameter to represent the phenomena based on the characteristic length that they deem important. Thus, three different characteristic lengths have a predominant role in oscillating foil dynamics.

2.3 Flow Visualisation

The main ingredients of the classical unsteady aerodynamic theory of oscillating foils, which have found extensive use in bio-fluid dynamics, are foils of small thickness, potential flow formulations along with linearized body boundary conditions, small perturbation velocities, thin vortex sheets, and the assumption of a planar vortex wake (Wu 1961, 1971; Lighthill, 1970; Chopra, 1974; Chopra and Kambe, 1977). On the other hand flow visualisations of oscillating foils have indicated that the wake has a strong tendency to organize itself into a series of vortices. Since in the unsteady flow case the wake shape is a direct result of the foil's circulation history, visualisation of the wake behind the foil is useful as a

comparison between visual observations and theoretical calculations (Katz and Plotkin, 1991). If the calculated wake shape is similar to the observed one then it would be safe to assume that the calculated foil's lift history is similar to the experimental one. Other useful information can be obtained from flow visualisation. From observations of the orientation of vortices periodically shed from the trailing edge, the propulsive vortical signature i.e. whether the foil develops drag or forward thrust can be deduced.

Most of the flow visualisation results reviewed for this research were limited to a two dimensional heaving and/or pitching foil, thus vorticity shed from the foil tips is neglected. The most comprehensive observations of the wake structure behind an airfoil in unsteady flow has been given by Kadlec and Davis (1979). An airfoil executing pitching motion about $c/4$ (measured from the foil's leading edge) was oscillated at various reduced frequencies and two non-dimensional pitch amplitudes a/c=0.02 and 0.04, where a is the excursion of the foil's trailing edge. Based on visualisation photographs, the authors concluded that the distortion of the wake just downstream of the foil was strongly dependent on the reduced frequency k and (a/c) ratio. In their figure 7 reproduced here in figure 2.1 they show three different observed regions behind a flapping foil; **region I** corresponding to small reduced frequencies includes wakes of small distortion , **region II** describes those wakes that begin to break up into vortex like disturbances resembling the well known Karman street (Triantafyllou et al., 1993), and **region**

III corresponding to large reduced frequency where wake distortion is so great that it rolls up into itself forming a series of discrete vortices.

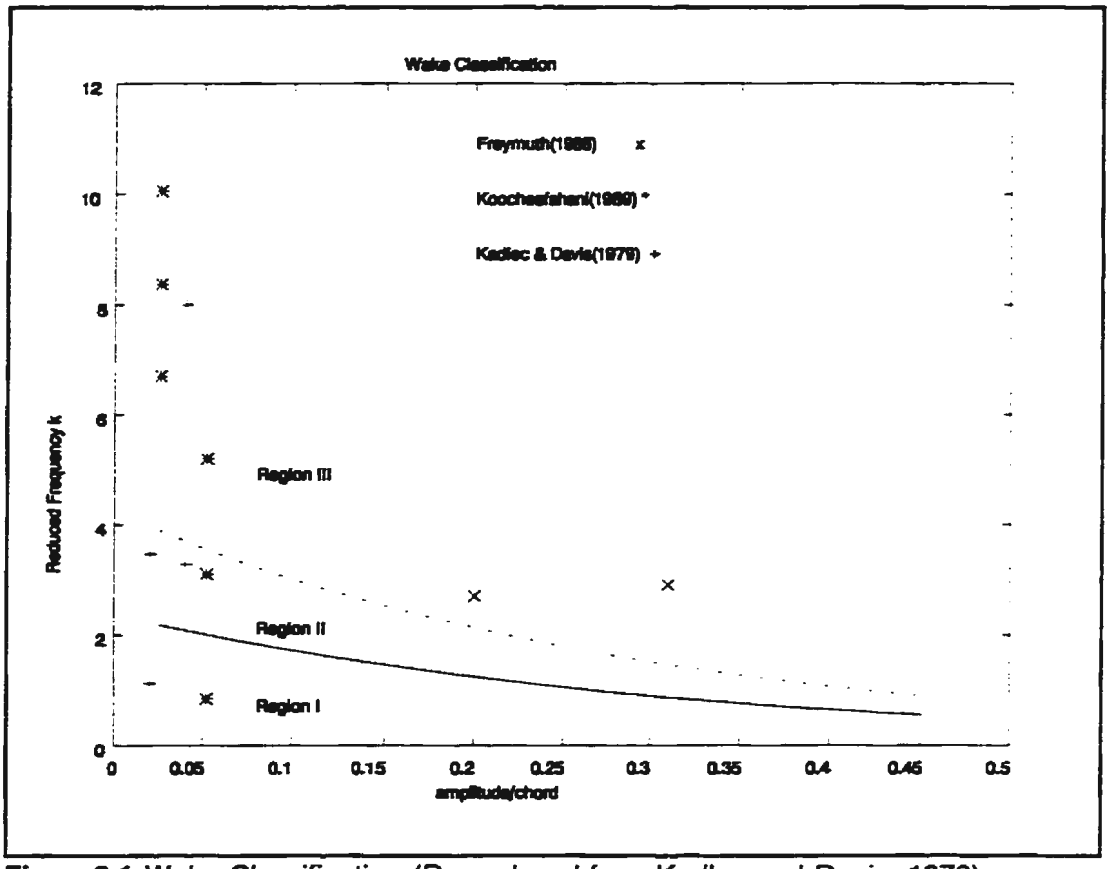

Figure 2.1 Wake Classification (Reproduced from Kadlec and Davis, 1979)

A similar wake configuration is shown in Koochesfahani (1989) for an airfoil pitching about its quarter-chord point. The reduced frequency *k* and amplitude to chord ratio *a/c* of the conditions examined are shown as data points in figure 2.1. The trailing edge amplitude to chord ratio was small: 0.026 for 2 deg. pitch amplitude and 0.052 for 4 deg. pitch amplitude. In addition to qualitative observations, Koochesfahani used the frequency-shifted laser Doppler velocimeter technique (LDV) to measure the streamwise component of the velocity vector in

the wake of the pitching foil. His measurements of the mean velocity profiles at the trailing edge (x/c=1) confirm visual observations of Kadlec and Davis (1979) that in **region II** a typical wake profile of Karman vortex shedding with velocity deficit is formed (an airfoil with drag). In **region III** where the wake has a strong tendency to organize itself into a series of vortices the mean velocity profile was transformed into a wake with velocity excess (no longer a wake but actually a jet, i.e. a forward thrust producing airfoil). Thus, in this case the pitching foil behaved as a propulsive system for which generation of a jet-like flow in the downstream direction is required by the momentum theory. Vortex streets with a placement of vortices so that they induce on each other a downstream motion would provide the requisite jet-like wake profile.

In figure 2.1 all data plotted which fall into **region III** indicate a propulsive vortical signature or jet-like wake profile. A schematic of this vortex street configuration is illustrated in figure 2.2a, and the actual deposition of vortices for one cycle is as follows: Flow is from right to left. During the upward stroke an anticlockwise vortex appears and is convected away from the trailing edge, then, during the downward stroke a clockwise vortex appears and is deposited above and to the right of the previous vortex. Thus two vortices of opposite sign are shed per cycle, where top and bottom vortices induce a velocity component in the downstream direction. Kadlec and Davis (1979) and Kochesfahani(1989) obtained vortical characteristics for a pitching foil. Freymuth (1988) complemented their results by providing vortical

characteristics for a foil in pure heave motion. Although derived from different modes of oscillation, visual observations suggest that deposition and the mechanics of vortex roll-up in the wake of an oscillating foil are the same for both pitch and heave motion.

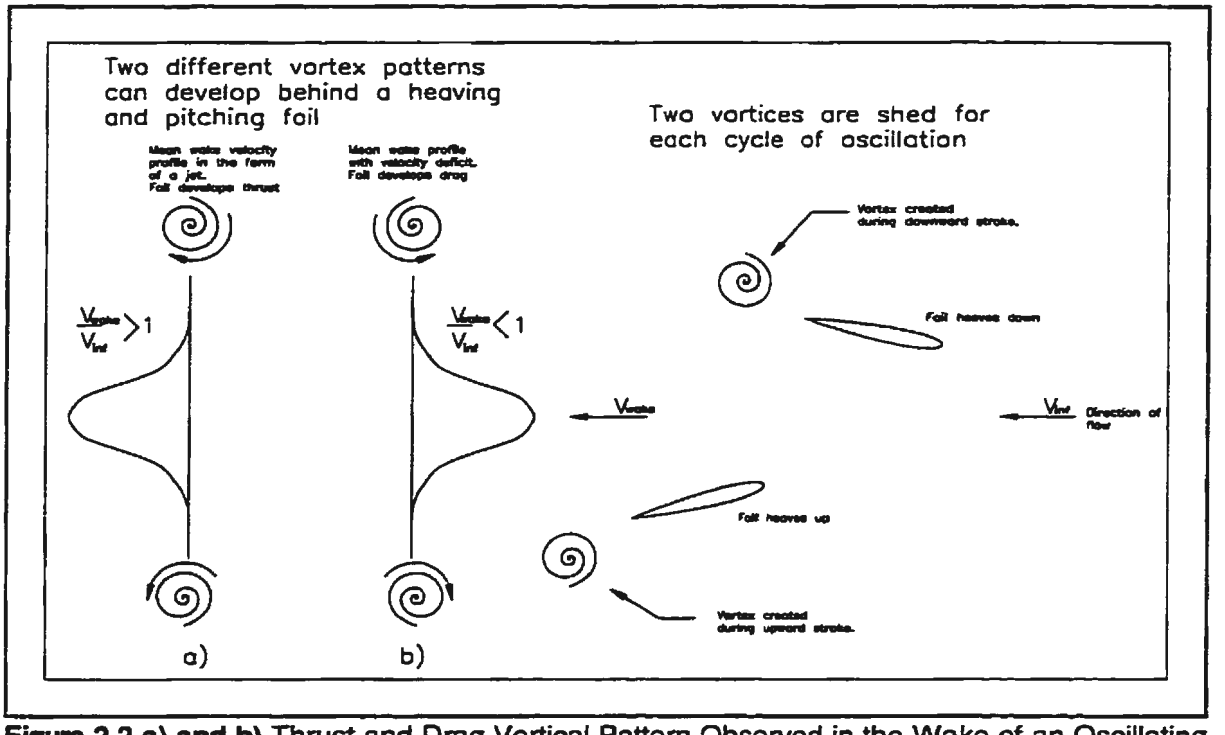

Figure 2.2 a) and b) Thrust and Drag Vortical Pattern Observed in the Wake of an Oscillating Foil

The concept of a propulsive vortical signature as depicted in figure 2.2a is not new. It was theoretically deduced by von Karman and Burgers (1935) for the case of a two dimensional flat plate. If the flow fluctuates as it does if the foil executes time dependent motion, then the circulation Γ and the pressure distribution around the foil fluctuates too. Each change in circulation around sections of the foil is accompanied by the shedding of free vorticity from the trailing edge region into the

wake. The total bound circulation[3] as a function of time for a flat plate pitching about the foil's leading edge, using small amplitude theory is (Katz and Plotkin, 1991):

$$\Gamma = \pi c \left(U\alpha_o \sin(\omega t) + h_o \omega \sin(\omega t) + \frac{3}{4} c\alpha_o \omega \cos(\omega t) \right) \qquad (2.2)$$

Here harmonic oscillations of the following form are assumed: $h=h_o\cos(\omega t)$, $\alpha=\alpha_o\sin(\omega t)$, and the direction of flow is from right to left (Katz and Plotkin, 1991). As an example, in figure 2.3 the total bound circulation Γ (full line) is plotted against time together with the foil displacement h (broken line) for the following motion particulars: chord length c=0.056 m, free stream velocity U=0.3 m/s, heave amplitude h=0.070 m, pitch amplitude α=6 deg, and frequency of oscillation ω=4.4 rad./sec (the reason for selecting these motion parameters will become apparent later in the thesis). It can be seen that when the foil is at its highest point, the circulation is positive and is increasing. A vortex will detach itself from the trailing edge with rotation opposite to the direction of the circulation such that the Kelvin theorem ($D\Gamma/Dt=0$ for the closed curve enclosing the foil and its wake) is satisfied. Since the circulation around the foil is positive (anticlockwise), the vortex in the wake is clockwise. On the other hand, when the foil is at its lowest position, the circulation is decreasing and a vortex will detach with an anticlockwise circulation (von Karman and Burgers, 1935). The orientation of the shed vortices is similar to that depicted in figure 2.2a, which indicates a jet velocity profile in the foil's wake.

[3]Bound circulation is circulation on the foil that gives rise to the creation of the hydrodynamic lift.

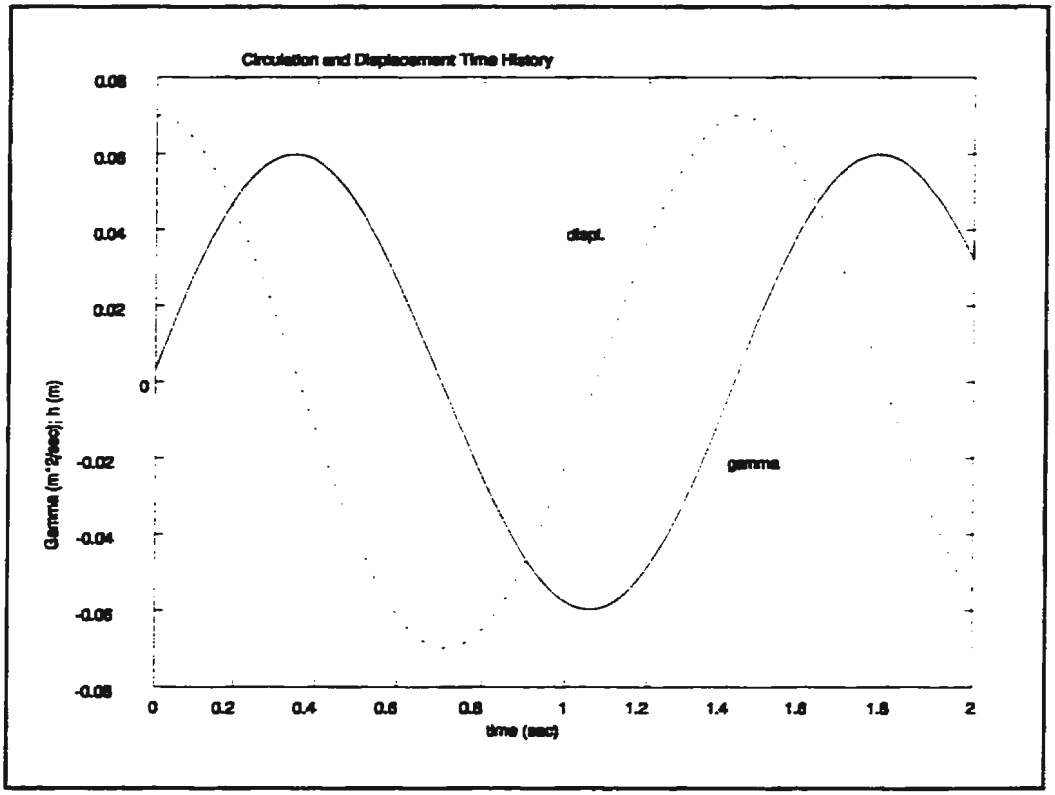

Figure 2.3 Circulation Distribution

In the field of theoretical hydrodynamics, thin vortex sheets have been studied by several investigators. In the classical hydrodynamics text, Lamb (1945) used small amplitude wave theory (Airy Theory) to show that lines of separation are inherently unstable. Even small perturbations which always occur in the flow will result in vortex sheet disintegration. Airy Theory, though, is a linear theory and therefore it does not provide a full picture of vortex sheet development. Rosenhead, whose work is cited in von Karman and Burgers (1935), computed the further development of the vortex sheet by taking into account the non-linear terms in the perturbations. This non-linear process of sheet roll-up into discrete vortices was described qualitatively by Prandtl and Tietjens (1935).

Katz and Weihs (1978) studied numerically the behaviour of the non-linear processes of wake roll-up patterns behind a zero-thickness lifting airfoil performing small amplitude oscillations. They used discrete vortex singular elements to represent both the airfoil and shed vorticity. Their basic conclusion was that the influence of the wake relaxation (vortex roll-up) had no significant effect on the momentary lift coefficient in oscillatory motion. However, this may not be the case for more realistic geometries such as finite thickness airfoils (fulfilment of the boundary conditions on the actual surface), large amplitudes of oscillation, and high reduced frequencies.

That there is a correlation between vortex roll-up in the near wake and forward thrust experienced by the oscillating foil (region III in figure 2.1) is the subject of a paper by Triantafyllou et al. (1993). In this work it is proposed that optimal thrust development is related to a maximum spatial growth of vortices developed by a flapping foil. They used velocity profiles measured by Koochesfahani (1989) and performed a linear stability analysis by solving the inviscid Orr-Sommerfeld equation (Triantafyllou et al., 1986; Oertel, 1990) to obtain a dispersion relation for the flow in question. The response in classical linear stability theory is assumed to be of the form: $Y=Ye^{j(kx-\omega t)}$, where the frequency ω is assumed to be complex. If the frequencies calculated from the dispersion relation have a positive imaginary part then instabilities in the flow will grow in space and time and will result in the formation of waves which ultimately roll-up into an array of vortices.

This apparent contradiction between Katz and Weihs (1978) result and the proposal by Triantafyllou et al. (1993) could be probably that these researchers are approaching the problem from two different points of view. In the Katz and Weihs calculations the reduced frequencies as well as amplitude of oscillations were small. This means that curvature of the shed vortex sheet was small and roll-up occurred well downstream of the foil. In Triantafyllou et al. (1993) a foil performed large amplitude motions, and the reduced frequency was large. This resulted in vortex roll-up occurring immediately behind or within one chord length of the foil.

Freymuth (1988) provides excellent flow visualizations of the near wake of an oscillating airfoil for large amplitude motion. The amplitude to chord ratio was 0.2 and 0.3 for pure heave and pure pitch motion respectively. In the case of a pure pitch motion, pitching axis was fixed at $c/4$ measured from the foil's leading edge. Reduced frequencies were large enough, so that the foil was operated in region III (see figure 2.1). Flow visualization photographs suggest a propulsive vortical signature as shown in figure 2.2a. In addition, Freymuth reports the occurrence of a "weak separation over the leading edge" which essentially is a dynamic stall. Dynamic stall usually refers to unsteady separation and the stall phenomena on foils that are forced to execute time-dependent motion. Experiments have shown that the flow field around an oscillating foil can be characterised by the degree of flow separation and that for a given foil, the primary parameter that determines the degree of separation is the maximum nominal angle of attack (McCroskey, 1982).

Freymuth does not give the value of this angle, but from information provided on the motion, the maximum nominal angle of attack for the downward heave motion was calculated to be 52.2 deg. For the pitch motion the maximum angle of pitch was 25 deg. ($\alpha_{max}=\alpha_{mean}+\alpha_{ampl}$). These angles are well in excess of the static-stall angle for the NACA 0015 foil section used in the experiment (Moran, 1984). Hence it is likely that dynamic stall occurred during the downward motion in both heave and pitch oscillations.

From the flow visualization photographs (Freymuth, 1988, figures 2 and 3) it can be seen that the vertical extent of the leading edge vortex (extent of the viscous zone) is about the order of magnitude of the foil thickness and is present during most of the half cycle in both heave and pitch cases. Further development of this leading edge vortex is as follows: a vortex-like (clockwise) disturbance that was created during the downward stroke in the leading edge region, moved downstream over the upper surface of the airfoil. It merged with a clockwise trailing edge vortex, thus reinforcing this vortex. Since the vortex pattern was one indicating a jet velocity profile in the wake, this experimental observation is an excellent example of a possible beneficial effect associated with unsteady motion. Energy associated with the vortex is used to enhance the propulsive vortex signature, and hence possibly improves foil performance. Freymuth also reports that an increase in the maximum nominal angle of attack resulted in severe leading edge separation and an associated erosion in propulsive signature. The

leading edge vortex was no longer incorporated into the appropriate trailing edge vortex. Freymuth's (1988) photographs and conclusions support Triantafyllou et al. (1996), who have alluded to this behaviour with a foil oscillating with large amplitude (h/c=0.75), and large angles of attack.

Flow visualisation experiments were done by Gopalkrishnan et al. (1994) to investigate the feasibility of free shear flow control and energy extraction from the large eddies in the flow. They conducted an experiment which aimed at altering the vortex street produced by a bluff object through the use of an oscillating foil. The conclusion of the Gopalkrishnan flow visualisation experiments was that the oscillating foil can reposition the vortices, and reduce, or enhance their strength. Repositioning occurs primarily through the action of the foil suction, and can turn, for example, a regular Karman vortex street (with a wake-like average velocity profile) into a reverse Karman street (with a jet-like velocity profile).

Chapter 3

Oscillating Foil Apparatus

3.1 General

The focus of this thesis was to study the propulsive performance of oscillating foils which are the main propulsors of fast fishes and cetacean mammals. The aim of the oscillating foil apparatus was to mimic the unsteady oscillatory motion of the tail of advanced swimming animals by producing a coupled heave and pitch motion in the vertical plane. The oscillating foil apparatus was designed and manufactured prior to the present work, and design details and descriptions of the functions of each individual component of the apparatus can be found in Greening (1996).

The present work with this oscillating foil apparatus represents a second design loop in the development of the computer controlled oscillating motion apparatus. Based on Greening's (1996) recommendations, modifications to the motion control program were done as a part of this work. These modifications and their limitations are discussed in this chapter.

3.2 Drive System

The drive system of the oscillating apparatus consisted of two numerically controlled AeroTech DC servo motors with a resolution range of 20,000 steps/rev. Both motors were equipped with a 10/1 ratio gear box, and the maximum

continuous power output of the motors was 146 W. The motors were controlled by a *Unidex 14* multi-axis motion controller which received motion commands from an indexer installed on the PC bus slot of a 80386 computer. This allowed any language which has the ability to do I/O to be used for programming the *Unidex 14*, and for manipulating the motion control by the personal computer.

Rotation from the motors was transferred to two solid stainless steel shafts through a pulley/belt system as shown in figure 3.1. Alignment of the shafts was accomplished by running each drive shaft through two linear bearings and one teflon bushing. Both the forward and aft shaft were identical except that the forward drive shaft had a pivot joint inserted in it to allow the shafts to operate out of phase. Vertical shaft displacement in terms of a number of motor steps, produced the required heave motion, and phase lag between the shaft's oscillation allowed for the required angular displacement. The mounting pod to which a model foil was attached, was connected to the shafts by pin connections (points P and Q in figure 3.1). The shape of the mounting pod, and lower parts of the driving shafts were such that they minimized the flow disturbances around the foils (Greening, 1996).

The oscillating apparatus sensor system included two Linear Variable Differential Transformers (LVDT) connected to each shaft with the aim to measure with precision the shaft's displacement.

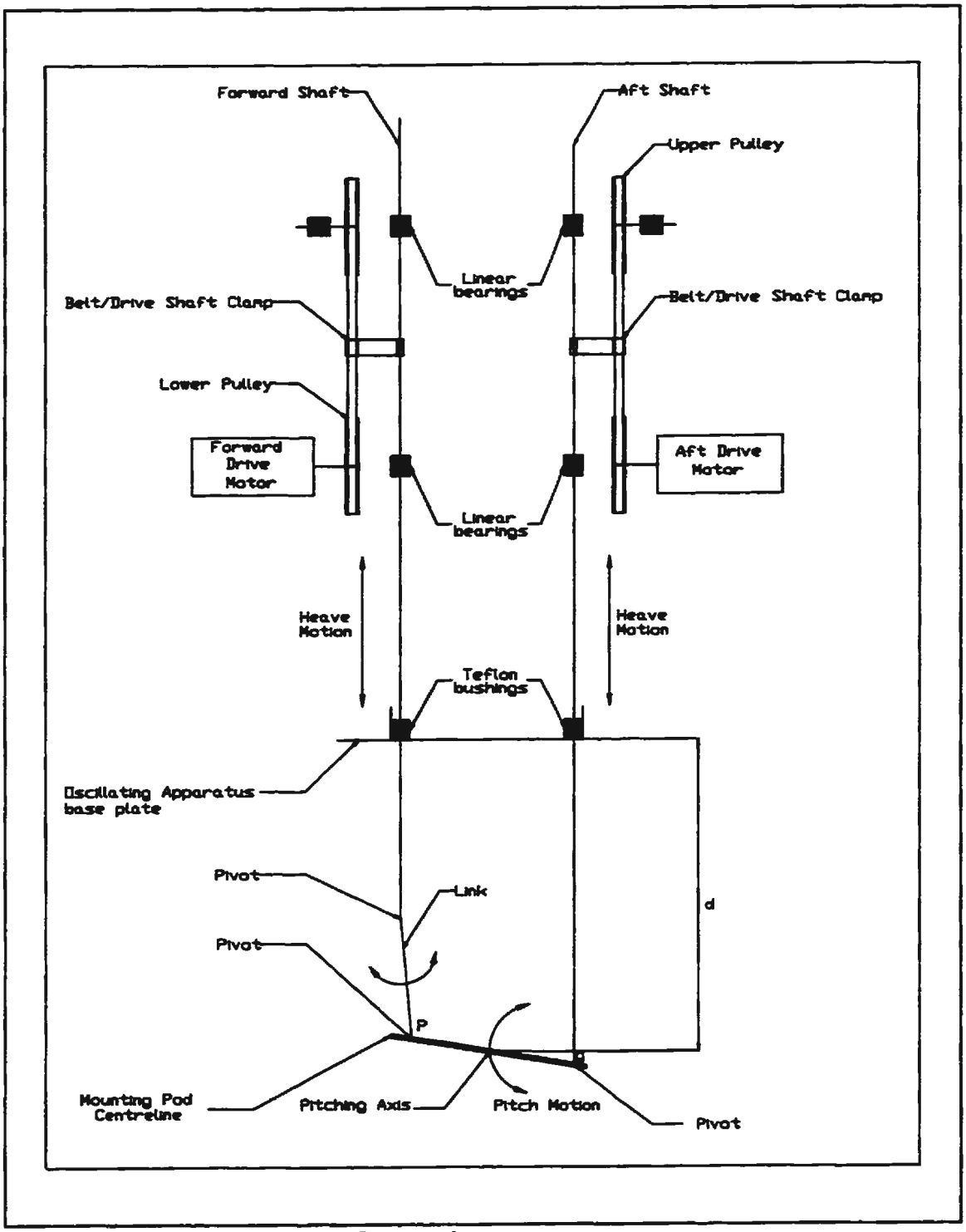

Figure 3.1 Oscillating Apparatus Schematic

3.3 Motion Development

A Microsoft QuickBasic© program was written with the purpose of controlling the shaft's oscillating motion and to home the foil models at the end of the test period. Also the program allowed for automatic creation of desired motion files, based on input parameters consisting of frequency of oscillation, heave and pitch amplitude, and the position of the pitching axis.

The horizontal distances of the forward and aft shafts from the origin are defined as *a* and *c*, while *b* is the pitching axis position with respect to the origin, (see figure 3.2). The pivot points where the drive shafts are connected to the mounting pod are denoted by *P* and *Q* for the forward and aft shaft respectively.

Following equation (1.1) which describes the displacement of any point along the chord line of the foil, the equation of motion for pivot points *P* and *Q* are respectively:

$$\begin{aligned} y_P &= h\cos(\omega t) + \alpha(a-b)\sin(\omega t); \\ y_Q &= h\cos(\omega t) + \alpha(c-b)\sin(\omega t); \end{aligned} \tag{3.1}$$

These equations can be rewritten as:

$$\begin{aligned} y_P &= [h^2 + (\alpha(a-b))^2]^{\frac{1}{2}} \cos(\omega t - \phi_P); \\ y_Q &= [h^2 + (\alpha(c-b))^2]^{\frac{1}{2}} \cos(\omega t - \phi_Q); \end{aligned} \tag{3.2}$$

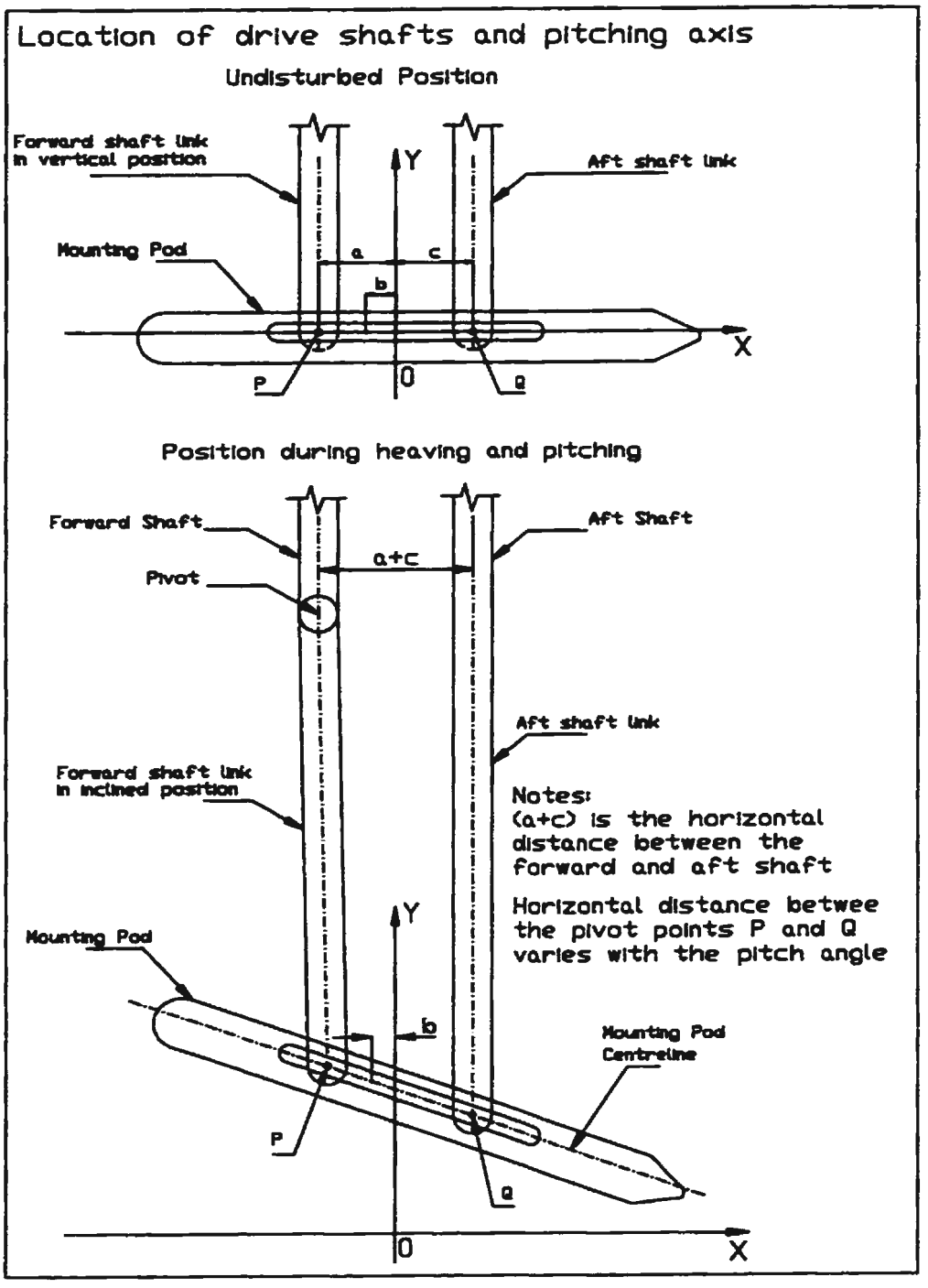

Figure 3.2 Drive Shafts Location and Pitching Axis Position

where:

$$\phi_P = \tan^{-1}\left[\frac{\alpha\,(a-b)}{h}\right];$$
$$\phi_Q = \tan^{-1}\left[\frac{\alpha\,(c-b)}{h}\right]; \qquad (3.3)$$

Using equations (3.1) and (3.2) to define the motions of the drive shafts introduce an error. The equations do not take into account that the forward shaft link does not remain vertically straight, and as a result horizontal distance between the pivot points *P* and *Q* varies with the pitch angle (see figure 3.2). This error increases as the pitching amplitude of the motion increases. For a requested pitch amplitude of 30 deg. a pitch angle amplitude of 30.18 deg. is obtained resulting in 0.62% error (Greening, 1996).

By differentiating equation (3.1) or (3.2) with respect to time, the vertical component of velocity and acceleration of points *P* and *Q* at any instant of time is obtained. The phase difference between the motion of the two drive shafts, in radians is:

$$\phi = \phi_P - \phi_Q \qquad (3.4)$$

Equations (3.1) to (3.4) provided the basis for programming a sinusoidal oscillating motion. Greening (1996), approximated a sinusoidal motion of the shafts by dividing the period of oscillation into *n* time segments. By the use of equation (3.2) the shaft displacement was calculated for each time interval. Then the velocity and acceleration required to reach the desired displacement in the time interval was

calculated based on the velocity and acceleration profiles available in the *Unidex 14* motion controller software. These profiles allowed time for the motors to ramp up to their peak velocities and then ramp back down to a stop at the end of each time segment.

For the purpose of this experiment, a similar approach was used to divide the oscillatory period into a finite number of segments, but the motion was made continuous. That is, at the end of each time segment the motors did not come to a complete stop, but they continued to the new position at the prescribed velocity of the next segment. This was accomplished using the **MV** command. *Unidex® 14* "Operators Manual" has the following description of the command:

> The MV command causes the motor to run to the new ABSOLUTE position (parameter1) at the new velocity (parameter2). When the destination is reached, control will be passed to the next command which should be another MV command.

The absolute position at each time interval was calculated using equation (3.2), and the velocity for each time segment was calculated by differentiating equation (3.2) once with respect to time.

Use of a different motion command than in Greening (1996), was deemed necessary for two reasons. First, work described in this thesis is a second design loop in the development of the computer controlled oscillating motion apparatus. Second, during Greening's (1996) apparatus commissioning, vibrational problems were encountered due to the motors stopping at the end of each time segment. Thus, refinement in the oscillatory motion was necessary.

3.4 Bench Testing

Following the changes made in the motion control, a set of bench tests were performed to examine the behaviour of the apparatus using the new motion command. Overall, It was found that limitations to produce the sinusoidal oscillatory motion were due to the *Unidex 14* motion control software/hardware. The findings from the bench tests are discussed below.

APPROXIMATION OF SINUSOIDAL MOTION

Generally it was found that by increasing the amplitude of oscillation or frequency of oscillation, the motion of the shafts became less sinusoidal and more like a saw tooth. Typically, the motor's peak velocity should not exceed 9,000 steps/sec. if sinusoidal motion is to be obtained. This is illustrated in figure 3.3 which was constructed based on visual observations. On the vertical axis is the heave amplitude h, and on the horizontal axis the frequency of oscillation ω. The curve shown on the plot separates two regions: one in which the obtained shaft motion is sinusoidal, and the other in which the oscillation is non-sinusoidal. Typical shaft displacement time histories from the two different regions are shown in figures 3.4a and 3.4b and are plotted as data points in figure 3.3. For the displacement histories shown, motion particulars were: heave amplitude 20 mm and frequency of oscillation 1.5 rad./sec. (figure 3.4a), and heave amplitude 70 mm and frequency of oscillation 4.4 rad./sec. (figure 3.4b). Reason for selecting the latter motion parameters will become apparent later in the thesis.

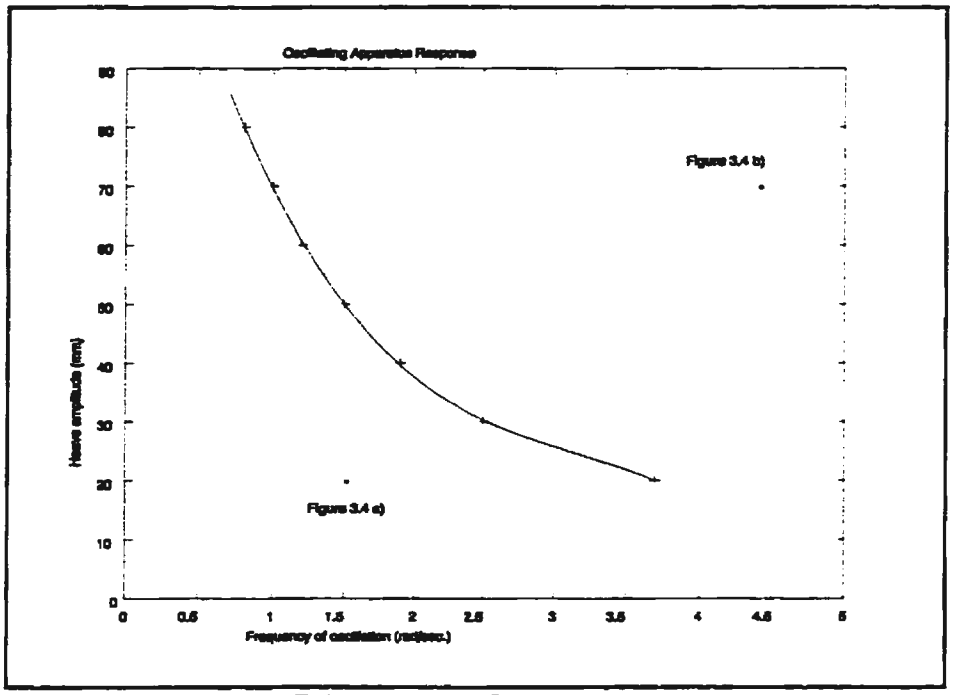

Figure 3.3 Oscillating Foil Apparatus Response

As it can be seen from figure 3.4b the shaft's displacement history was almost linear during the upward and downward stroke, followed by a sudden stop and reversal of direction of travel at the upper and lower limits of the motion. This behaviour is attributed to the substantial weight of the apparatus drive shafts. They are solid and made of stainless steel, therefore at large frequencies of oscillation associated with large accelerations and decelerations, the motors have no capability to decelerate or accelerate during the prescribed time interval.

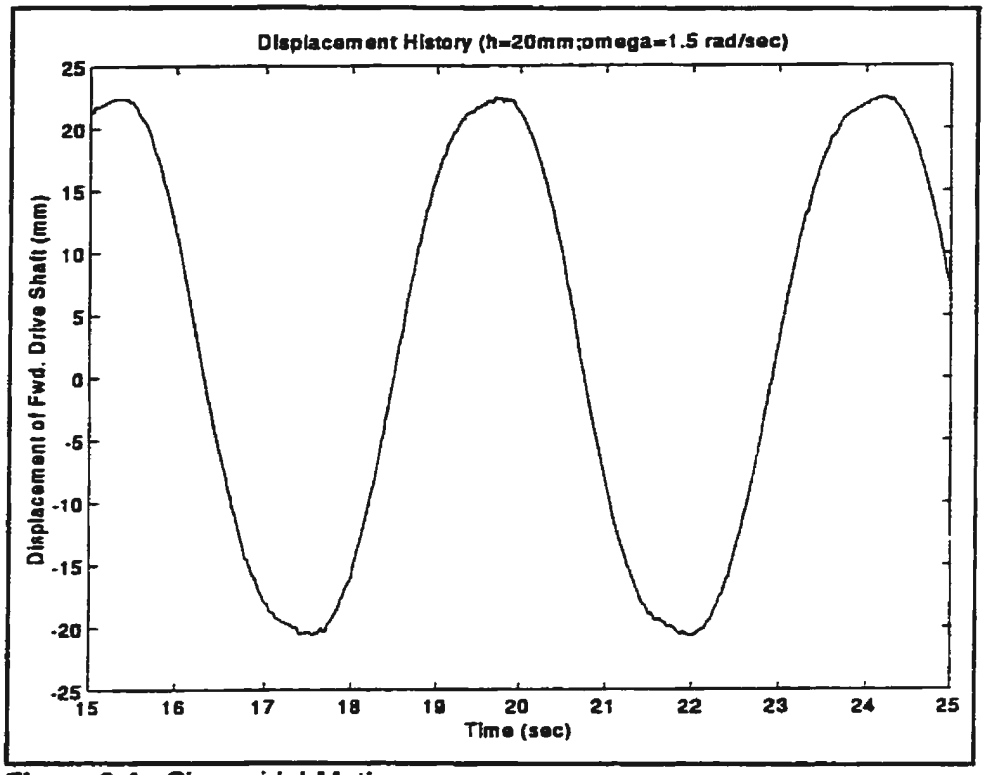

Figure 3.4a Sinusoidal Motion

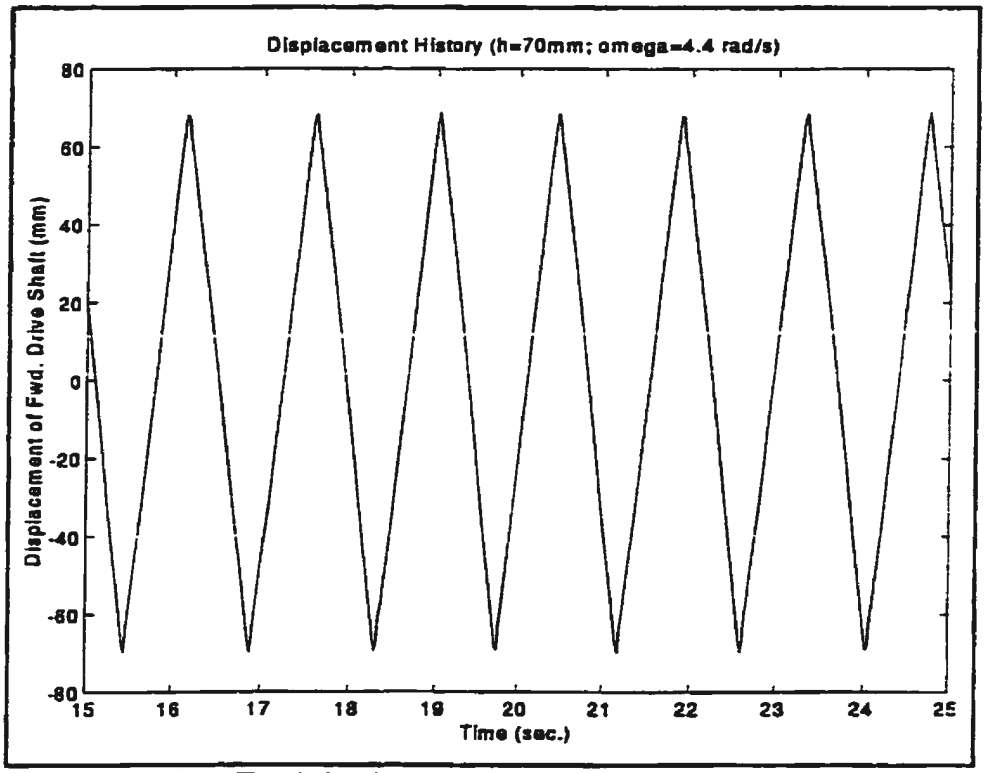

Figure 3.4b Saw-Tooth Motion

A Fast Fourier transform (FFT) analysis of the shaft displacement history shown in figure 3.4b was performed to identify frequency components present in the record. The power spectrum of the displacement history is shown in figure 3.5. From the plot it can be seen that most of the energy in the signal is concentrated around 0.7 Hz, which was the frequency of shaft oscillation of 4.4 rad/sec. This shows that the use of the **MV** motion command eliminated the previous vibrational problems associated with the starting and stopping of motors experienced in Greening (1996).

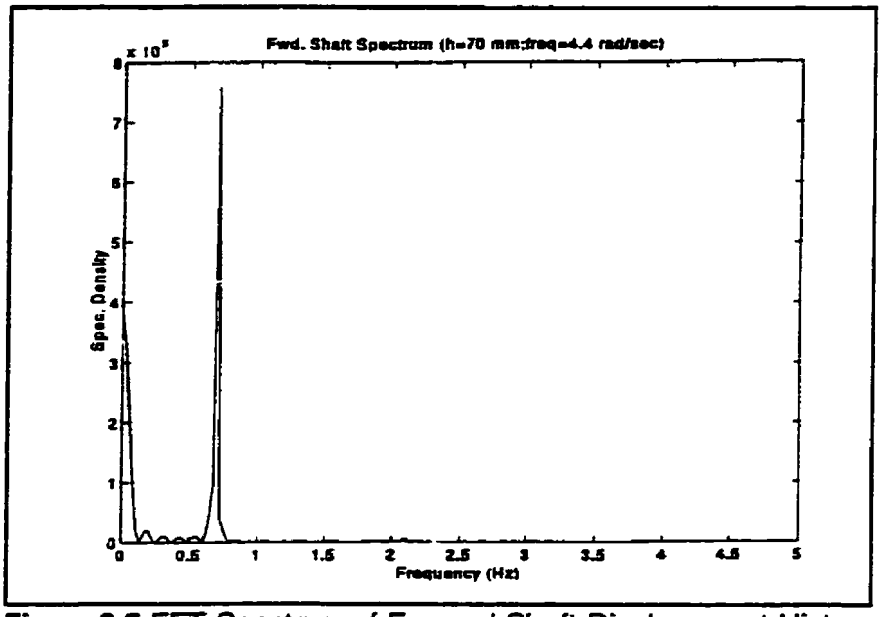

Figure 3.5 FFT Spectrum of Forward Shaft Displacement History

PHASE LAG BETWEEN SHAFTS

The MV command is non-synchronous, i.e. it works with one shaft axis at a time. Here the forward shaft is denoted by the x_1 axis, and aft shaft by the x_2 axis. Thus a new computer program had to be designed in such a way that all motion information was sent, for example to the x_1 axis first, and then to the x_2 axis. This

imposed an approximation to the oscillatory motion. Since there was no coordination between the axes, and it took a finite time to *parse* the information for each axis, an "initial" phase lag[4] was introduced between the shafts. It was possible to obtain an empirical relationship between the initial shaft position and the measured phase lag. However, it was found that this relationship was not unique. Different velocity profiles (different amplitudes or frequencies of oscillation) resulted in different "initial" phase lag between the two shafts.

Bench tests were conducted with the oscillatory motion divided into 6, 12, 20, 24, 30 and 30+ time segments. The number of time segments had an influence on two parameters: the sinusoidal approximation and the "initial" phase lag. More time segments meant a better approximation to sinusoidal motion, but at the same time introduced a larger "initial" phase lag. This was due to the requirement for more information to be sent to the *Unidex 14* indexer, and as a result more time was needed to process and forward this information to each motor. On the other hand, too few time segments resulted in a poor sinusoid. If the mounting pod was connected and there were too many segments then the "initial" phase lag could be so great that it could damage the apparatus. Selection of the number of time steps was a trade off. As a safety precaution it was decided that 24 time steps was an optimal number, with a good sinusoidal approximation and a manageable initial phase lag.

---

[4]Forward and aft drive shafts do not start motion at the same time. What is meant by "initial" phase lag is the time difference between motion initialization of the two shafts.

PITCHING AXIS POSITION

A variation in pitching axis location was obtained by causing the forward and aft shafts to perform oscillations at different amplitudes but same frequency. Due to the approximation of the motion, i.e. having a finite number of time steps, the obtained frequencies of oscillation were slightly different for each shaft. For example, with a heave amplitude of 50 mm, input frequency of 1.5 rad./sec. (T=4.19 sec.), and pitch axis position at +15 mm (this corresponds to a pitch axis at the foil's trailing edge), obtained periods for forward and aft shafts were 4.86 and 5 seconds, respectively. This resulted in a continuous increase in the phase lag between the two shafts. After several cycles, the phase lag was such that if the shafts were connected by the mounting pod, it would have bent the drive shafts. Based on this limitation it was decided to fix the pitching axis position at the origin (b=0, see figure 3.2). By doing this, the forward and aft shaft oscillation history was the same and the phase lag between the shafts remained constant for a given amplitude and frequency of oscillation.

SUMMARY OF RESULTS FROM BENCH TESTS

Based on the limitations of the oscillating apparatus discussed above the following summary of results pertinent to the present experiment can be made:

i) In order to obtain continuous motion of the shafts, the **MV** command has to be used with the present *Unidex 14* hardware.

ii) Velocity profiles for the forward and aft shafts have to be identical in order to obtain constant phase lag between the two shafts. This was obtained by fixing the pitch axis at the origin (b=0).

iii) It is possible to obtain a fairly good sinusoidal motion if the amplitude and frequency of oscillation are below those defined by the empirical curve given in figure 3.3. Other frequencies and amplitudes of oscillation would result in oscillating motion of the "saw tooth" shape.

iv) Pitch amplitude, which is effectively obtained by a phase lag between the shafts cannot be programmed, but it could be estimated prior to the experiment by obtaining a "calibration curve". The aim of the calibration curve was to obtain a relationship between the initial displacement between the forward and aft shaft and the obtained pitch angle. This was accomplished as follows: Initially both shafts were at a displacement corresponding to the heave amplitude. Then forward shaft was displaced 1 to 2 mm further up. Next, motion was started, and from the oscillation time history, the instantaneous difference in displacement between the two shafts could be obtained after a number n of oscillating cycles. The pitch angle was then calculated as:

$$\alpha = \tan^{-1}\left(\frac{D}{40}\right) \tag{3.5}$$

where D in millimetres is the mean of the n number of instantaneous maximum vertical displacements between the shafts, and 40 mm is the horizontal distance between the two shaft's centreline ([a+c] distance in

figure 3.2). This procedure was repeated for several initial displacements between forward and aft shaft. Figure 3.6 shows the dependence of pitch amplitude on the initial shaft position for a heave amplitude of 70 mm and a frequency of oscillation of 2.1 rad/sec. The practical significance of this plot was that during the experiment, for example, if the desired pitch angle is to be approximately 10 deg., then before the motion is initiated the forward shaft would be displaced approximately 1 mm further up from the aft shaft.

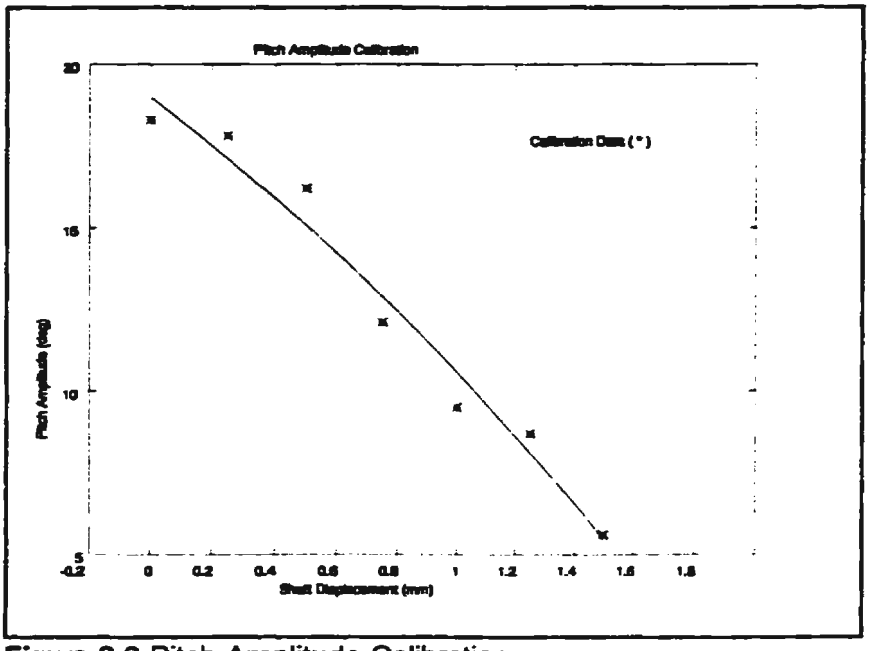

Figure 3.6 Pitch Amplitude Calibration

Chapter 4

Test Rig Design

4.1 General

The aim of the oscillating apparatus as described in Chapter 3 was to produce a coupled heave and pitch motion to drive the foil model. For the purpose of the measurement of hydrodynamic forces developed by an oscillating foil, in the towing tank experiment, a single degree of freedom dynamometer was designed with the aim to separate out the horizontal or thrust (drag) component. In this chapter, design and commissioning of the dynamometer is presented.

4.2 Description of the Dynamometer

The experimental set-up of the dynamometer and oscillating apparatus is given in figure 4.1. The dynamometer was made up of:

i) two thin flexible sheets 0.45 m wide and 0.71 m long made from acrylonitrole-butadiene-styrene (ABS);

ii) 1/2" thick aluminum base plate stiffened with two aluminum 2x2x1/4" angles;

iii) a rigid plate which provided support to the load cell;

iv) one 111.2 N (25 lbs) maximum capacity load cell, and

v) supporting frame.

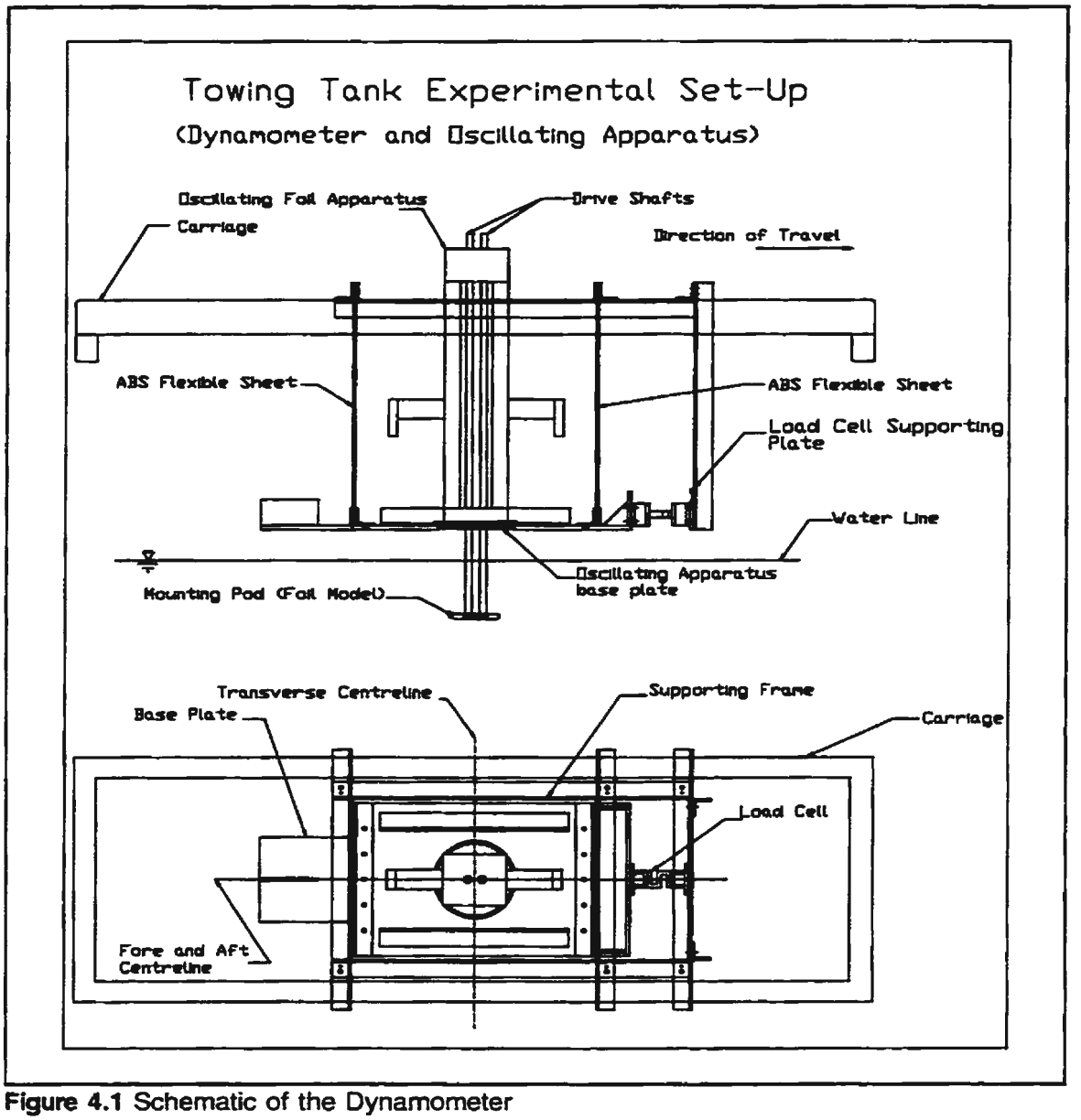

Figure 4.1 Schematic of the Dynamometer

The vertical ABS sheets were bolted to the aluminum base plate forming a U frame which supported the oscillating apparatus. A 210 mm diameter hole was cut in the centre of the aluminum plate to accommodate the base of the oscillating apparatus. Once in place, the oscillating apparatus was rigidly clamped to the aluminum plate. The low stiffness of the thin ABS sheets (k=0.232 N/mm) allowed movement in the fore and aft direction. Because the sheets were wide, transverse

movement of the apparatus was prevented due to the high stiffness in this direction (k=1.16 kN/mm). The plate providing support to the load cell was connected to the supporting frame by two vertical aluminum angles, and two additional angles (not shown in figure 4.1) ran diagonally from the plate to the supporting frame to increase its rigidity. The load cell for thrust measurement was placed on the fore-aft centerline of the dynamometer; one end was connected to the U frame and the other was attached to the supporting plate (see figure 4.1). Due to the substantial mass of the oscillating apparatus (75 kg) the system had to be held rigid during the acceleration and deceleration period of a test run. A vertical plate was placed on the aft end of the dynamometer to accommodate a clamping brake. The function of the supporting frame was to distribute the weight of the dynamometer and oscillating apparatus to the carriage.

When a foil oscillates in a fluid domain with a speed of advance *U*, hydrodynamic forces are generated due to the difference in pressure on the lower and upper surfaces of the foil (Lai, 1990). Figure 4.2 shows the force system acting on an oscillating foil. Forces are derived in the flow coordinate system, i.e the *lift force L* is acting in the perpendicular direction to the incoming resultant flow, and the *drag force D* is acting parallel to the direction of the resultant flow. The vertical and horizontal components of lift and drag that will be transferred through the oscillating apparatus shafts to the dynamometer are also shown in the figure, where angle β is the slope of the resultant velocity vector with respect to the

horizontal.

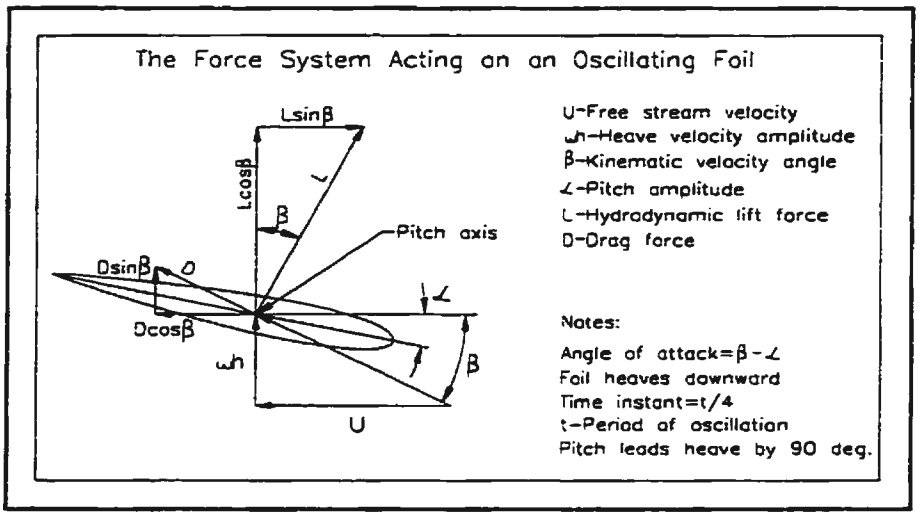

Figure 4.2 Force System Acting on an Oscillating Foil

The forces acting on the oscillating foil are replaced by an equivalent force/couple system acting on the dynamometer as shown in figure 4.3. The position of the oscillating apparatus when it was rigidly clamped to the dynamometer was at the centre of the base plate. For simplicity it was assumed that forces experienced by the dynamometer are acting at this point. Also it is assumed that the position of the centre of gravity of oscillating apparatus lies in the same vertical plane as the dynamometer fore-aft centreline. Four different force systems are acting on the dynamometer during the steady state portion of the run:

i) Static force W due to the weight of the oscillating apparatus;

ii) Hydrodynamic forces experienced by an oscillating foil comprised of a vertical force F_v, and a horizontal force F_h defined as:

$$F_v = L\cos\beta + D\sin\beta$$
$$F_h = L\sin\beta - D\cos\beta \qquad (4.1)$$

where F_h is the developed thrust T and is the main interest in this work. Horizontal hydrodynamic forces were balanced by the reaction at the teflon bearings placed in the base of the oscillating apparatus (see figure 3.1).

iii) Moments M1 and M2 equal to:

$$M1 = L\sin\beta\, d$$
$$M2 = D\cos\beta\, d \qquad (4.2)$$

where d is the instantaneous distance from the foil's pitching axis to the point of action on the bearing where horizontal hydrodynamic forces are acting on the dynamometer (see figure 3.1). If the oscillating foil develops thrust the moment is anticlockwise and equals M1. If the oscillating foil develops drag, the moment is clockwise and its magnitude equals M2.

iv) Dynamic forces F_d due to vertical acceleration and deceleration of the drive shafts and the attached mass (mounting pod/foil assembly).

In designing the dynamometer, care was taken to ensure that the suspension members (vertical sheets) were in tension, otherwise buckling of these members would probably damage the load cell. Estimation of the force systems acting on the dynamometer as well as reaction forces in the dynamometer suspension members are carried out in Appendix I.

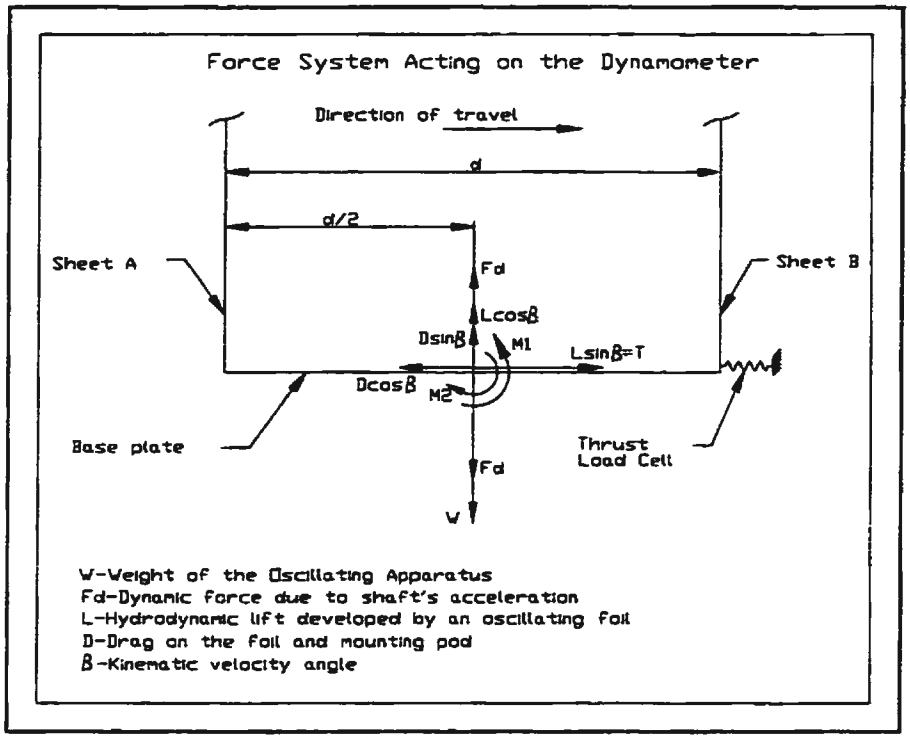

Figure 4.3 Equivalent Force/Couple System Acting on the Dynamometer

4.3 Thrust Load Cell Calibration and Measurement of System Natural Frequency

Static calibration of the thrust load cell was conducted "on the bench" with the oscillating apparatus shaft position at 0 mm displacement. Sixteen data points were collected at 500 points per sample and a sampling rate of 40 Hz resulting in 12.5 sec of data for each applied weight. Calibration was done for tension and compression with compression being positive (forward thrust) and tension being negative (drag). The applied load ranged from -14.72 N (1.5 kg) to +14.72 N.

Prior to the experiment, the dynamometer was fixed to the towing tank carriage

and the oscillating apparatus was clamped to the U frame as shown in figure 4.1. Two measurements of the natural frequency of this set-up were conducted. One with a 0 mm shaft displacement (or heave amplitude) and the other with a -70 mm shaft displacement. In the former the mounting pod together with the attached foil model were entirely above the water line, and in the latter they were completely submerged. Thus, one measured natural frequency will be denoted "in air", and the other "in water". In both cases the mounting pod was in a horizontal position, and the motors were energized. The system was excited by striking the mounting pod with a rubber hammer, and the response of the system or "decay curve" was obtained from the thrust load cell trace.

From the decay curve two important system constants can be estimated, namely the logarithmic decrement and the damped natural frequency. The non-dimensional logarithmic decrement δ can be estimated according to the Steidel (1986) equation:

$$\delta = \frac{1}{n} \ln \left(\frac{X_o}{X_n} \right) \tag{4.3}$$

where X_o and X_n are amplitudes of oscillation at $t=t_o$ and $t=t_n$ measured from the decay curve, and n is the number of oscillating cycles between the two amplitudes.

Once the logarithmic decrement is calculated, the system damping ratio ξ can be estimated according to:

$$\xi = \frac{\delta}{\sqrt{4\pi^2 + \delta^2}} \tag{4.4}$$

The damped natural frequency ω_d can be estimated by measuring time elapsed between two successive peaks from the decay curve.

Table 4.1 Dynamometer Natural Frequency

Test in Air	Test in Water
δ=0.067	δ=0.068
ξ=0.0107	ξ=0.0108
ω_d=9.29 Hz	ω_d=9.26 Hz

Table 4.1 gives estimated values of the logarithmic decrement, damping ratio, and damped natural frequency of the system measured for the two different shaft positions. The natural frequency in water is slightly lower than the one in air. This can be attributed to the added mass of the foil model/mounting pod assembly and the different shaft position for the two tests.

The system will be exposed to harmonic excitation due to the oscillating shafts, as well as the horizontal component of the lift force. It was deemed important to conduct a measurement of the system natural frequency, and show the level of separation between the natural frequency of the system and the frequencies of excitation. Figure 4.4 shows the response of the system (modelled as a damped single degree of freedom system) excited by a harmonic force.The damping ratio used in the calculations was ξ=0.0107. The vertical axis is the dimensionless

amplitude ratio defined as (Steidel, 1989):

$$Amplitude\ Ratio = \frac{1}{\left((1-\frac{\omega^2}{\omega_n^2})^2 + (2\xi\frac{\omega}{\omega_n})^2\right)^{\frac{1}{2}}} \qquad (4.5)$$

and the horizontal axis is the dimensionless frequency ratio ω/ω_n, where ω is the forcing frequency and ω_n is the undamped system natural frequency. The relation between the damped and undamped natural frequency is $\omega_d=\omega_n(1-\xi^2)^{1/2}$, and because damping ratio in our case was very small (see table 4.1), it comes out that $\omega_d=\omega_n$. In the experiment, the forcing frequency (oscillating frequency) was 0.7 Hz (4.4 rad./sec.) and the natural frequency was 9.29 Hz, resulting in a frequency ratio of 0.08. The dimensionless amplitude ratio for this condition was 1.006. This result is significant. It means that in the analysis it will be possible to confidently examine the dynamic behaviour of thrust developed by the oscillating foil using this test set-up.

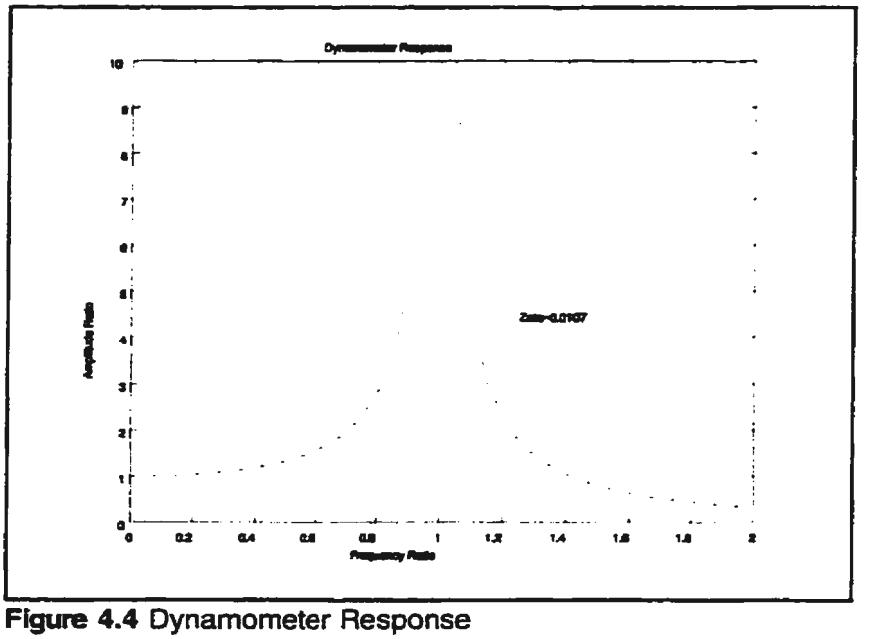

Figure 4.4 Dynamometer Response

Chapter 5

Results: Experimental Performance of the Oscillating Foils

5.1 Description of the Experiment and Theoretical Background

The experimental program was an essential part of this work. Three different foils of the same aspect ratio but different planforms were tested in the Memorial towing tank facility. The aim of this experiment was to investigate the performance of the foil at large angles of attack, and to determine the possible effects that wing planforms may have on the developed thrust.

Following equation (1.1), an oscillating foil moves at constant forward speed U and performs a harmonic vertical motion $h(t)$, of amplitude h and frequency ω, and a harmonic rotational motion $\alpha(t)$, of amplitude α and frequency ω. The instantaneous angle of attack $A(t)_{inst}$ is defined as:

$$A(t)_{inst} = \tan^{-1}\left(\frac{dh}{dt}\frac{1}{U}\right) - \alpha(t) \qquad (5.1)$$

where the first term on the right hand side is the slope of the kinematic velocity vector of the foil's pitch axis with respect to the horizontal and will be denoted by $\beta(t)$ (see figure 4.2). The kinematic velocity angle, and pitch amplitude are time dependent quantities. If the pitch motion has a phase lead of 90 deg. with respect to heave motion, which was the case in this experiment, then the time instant for the occurrence of maximum pitch amplitude will coincide with the time instant of occurrence of maximum kinematic velocity angle $\beta(t)$ which takes the form:

$$\beta_{max} = \tan^{-1}\left(\frac{\omega h}{U}\right) \qquad (5.2)$$

where ωh is the amplitude of the heave motion. Thus the angle of attack that will be referred to in this section is the maximum instantaneous angle of attack. According to equation (5.1) to have a positive angle of attack the kinematic velocity angle has to be greater than the maximum pitch amplitude. In the experiment care was taken to ensure that this was the case.

Prior to each run, the shafts and hence the foil were homed to an initial position which was the top of the upper stroke. Then the forward shaft was displaced further up (according to the calibration curve similar to the one shown in figure 3.6) as to obtain desired pitch angle. Then data collection was started and several seconds of zero readings were taken. Shafts motion was then initiated, the acceleration brake was applied to hold the dynamometer in place, and the carriage accelerated to the desired speed. Once steady velocity was obtained the brake was released and approximately 15 to 20 seconds of steady state data were collected. Then the brake was applied again, and the carriage decelerated to a full stop.

Due to limitations of the apparatus described in Chapter 3, the pivot point was set to the origin which corresponded to the foil's mid chord position ($c/2$). All tests were conducted at a heave amplitude of 70 mm and frequency of oscillation of 4.4

rad./sec. For each foil planform several pitch amplitudes were tested, α: 6, 13, 17.5, and 21 deg. These pitch amplitudes were obtained from the displacement time history and by the use of equation (3.5). For each foil planform and pitch amplitude, the speed of advance was varied at small increments in the range of 0.1 to 0.55 m/s.

5.2 The Foils

The foils tested consisted of a rectangular planform, a straight tapered and swept back planform with swept back angle of 30 deg., as well as a planform with a curved leading edge, similar to the flukes of a fin whale. The particulars for each foil planform together with the illustration of the mounting pod/foil assembly are shown in figure 5.1a, b and c. The cross section of all foils was the symmetrical NACA 0019 shape defined by the formula (Moran, 1994):

$$T(x) = 10\tau c\left[0.2969\sqrt{\frac{x}{c}} - 0.126\frac{x}{c} - 0.3537\left(\frac{x}{c}\right)^2 + 0.2843\left(\frac{x}{c}\right)^3 - 0.1015\left(\frac{x}{c}\right)^4\right]$$

Here T is the thickness distribution, c is the foil chord length, and x is the distance along the chord line from the leading edge. The parameter τ is the thickness ratio of the foil (maximum thickness/chord) and for NACA 0019 τ=0.19. The foils had the same aspect ratio of 6, and standardized roots such that they would fit into the mounting pod. The two foils were fabricated out of brass, and another was made out of wood. The brass foils had a span of 200 mm, while the wooden foil had a span of 400 mm.

In the experiment the heave amplitude to chord ratio was an important parameter, and throughout this thesis the reference chord length is the root chord *c*. All three foils have different root chord length. They are 56.7 mm for a sweptback foil, 58 mm for a whale fluke and 66.6 mm for a rectangular foil. Therefore for a heave amplitude of 70 mm, the heave to chord ratio *h/c* was 1.23, 1.21, and 1.05 respectively. In the following sections the foils will be referred to by the letter shown in the figure caption of each foil.

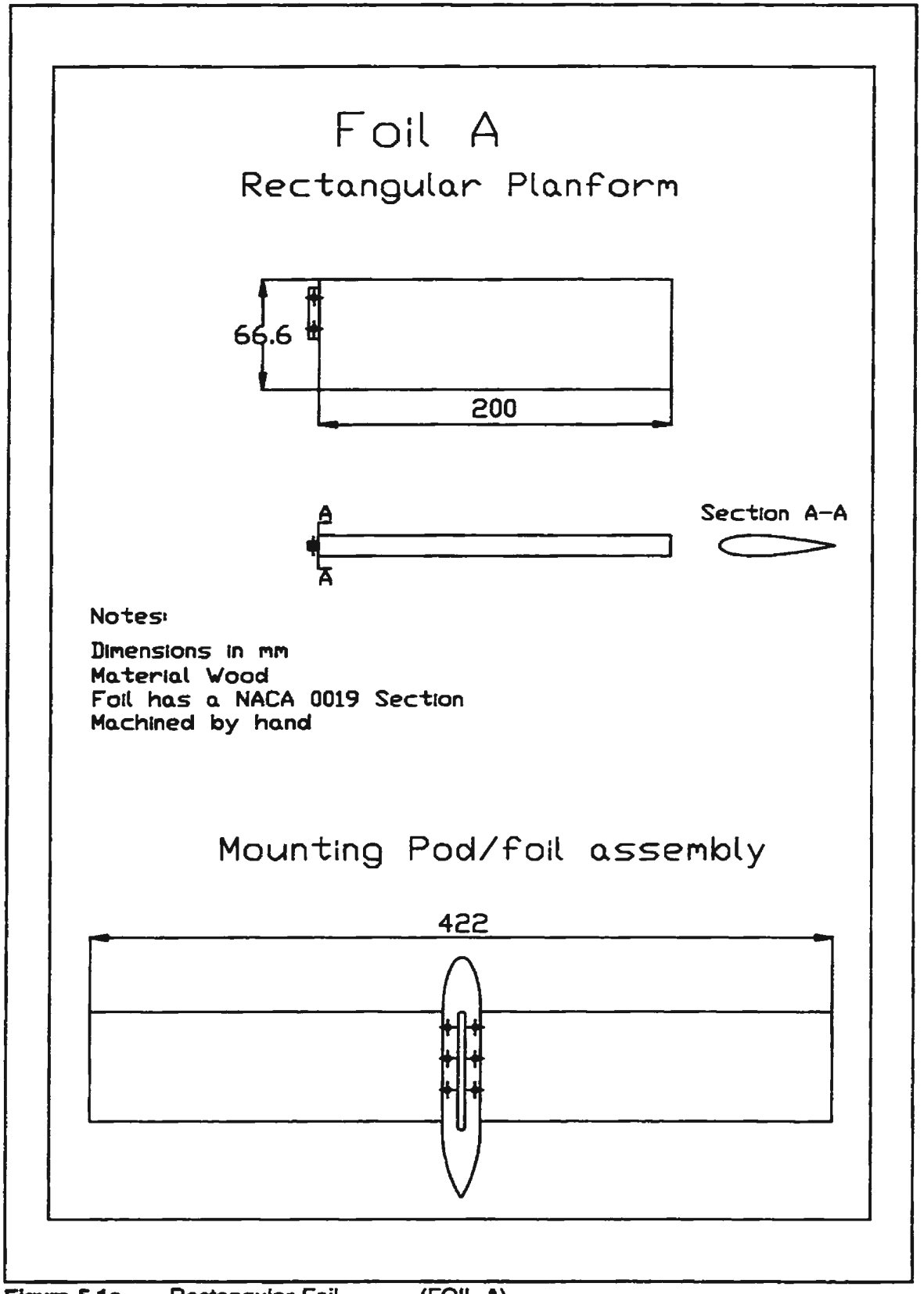

Figure 5.1a Rectangular Foil (FOIL **A**)

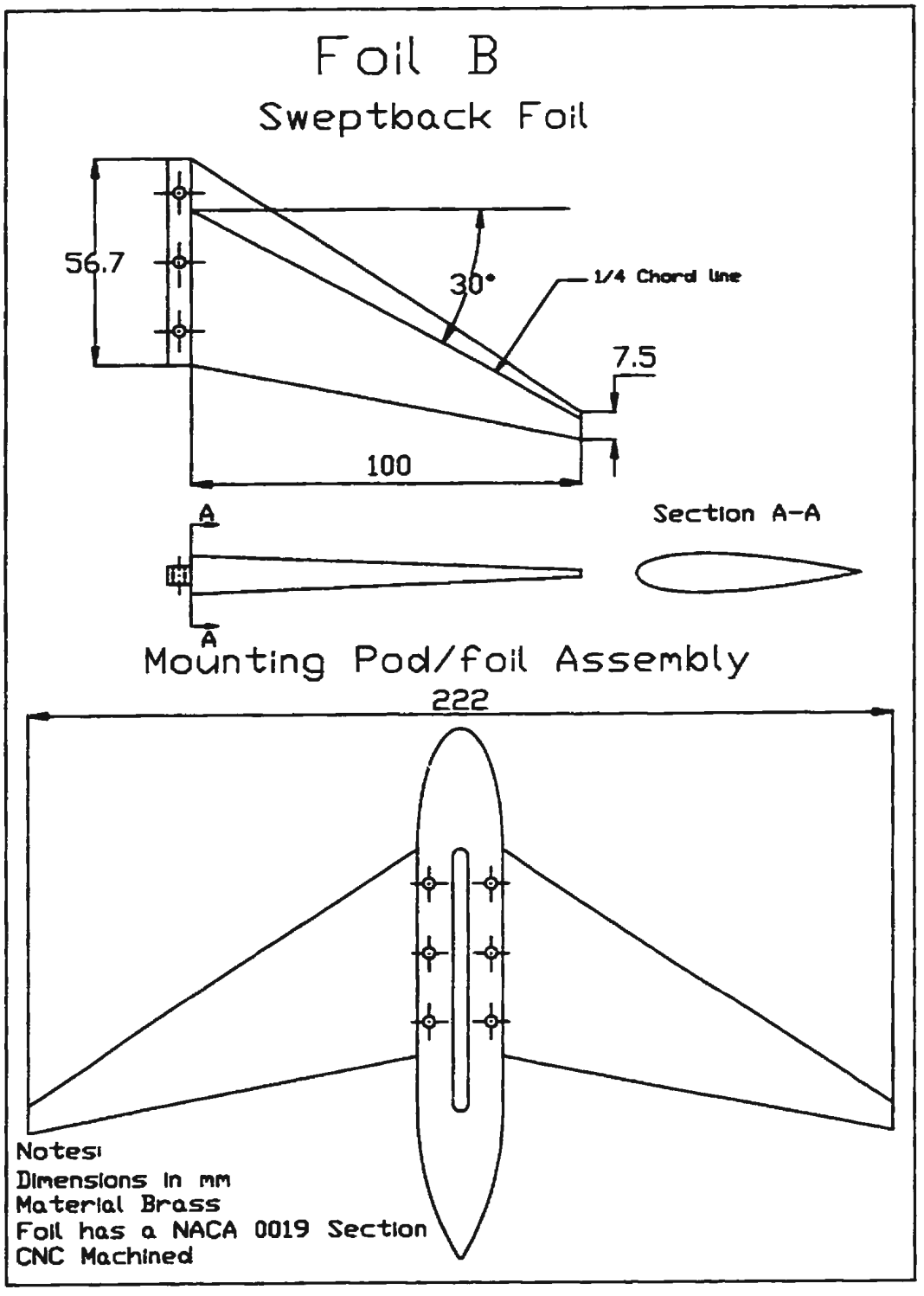

Figure 5.1b Sweptback Foil (FOIL B)

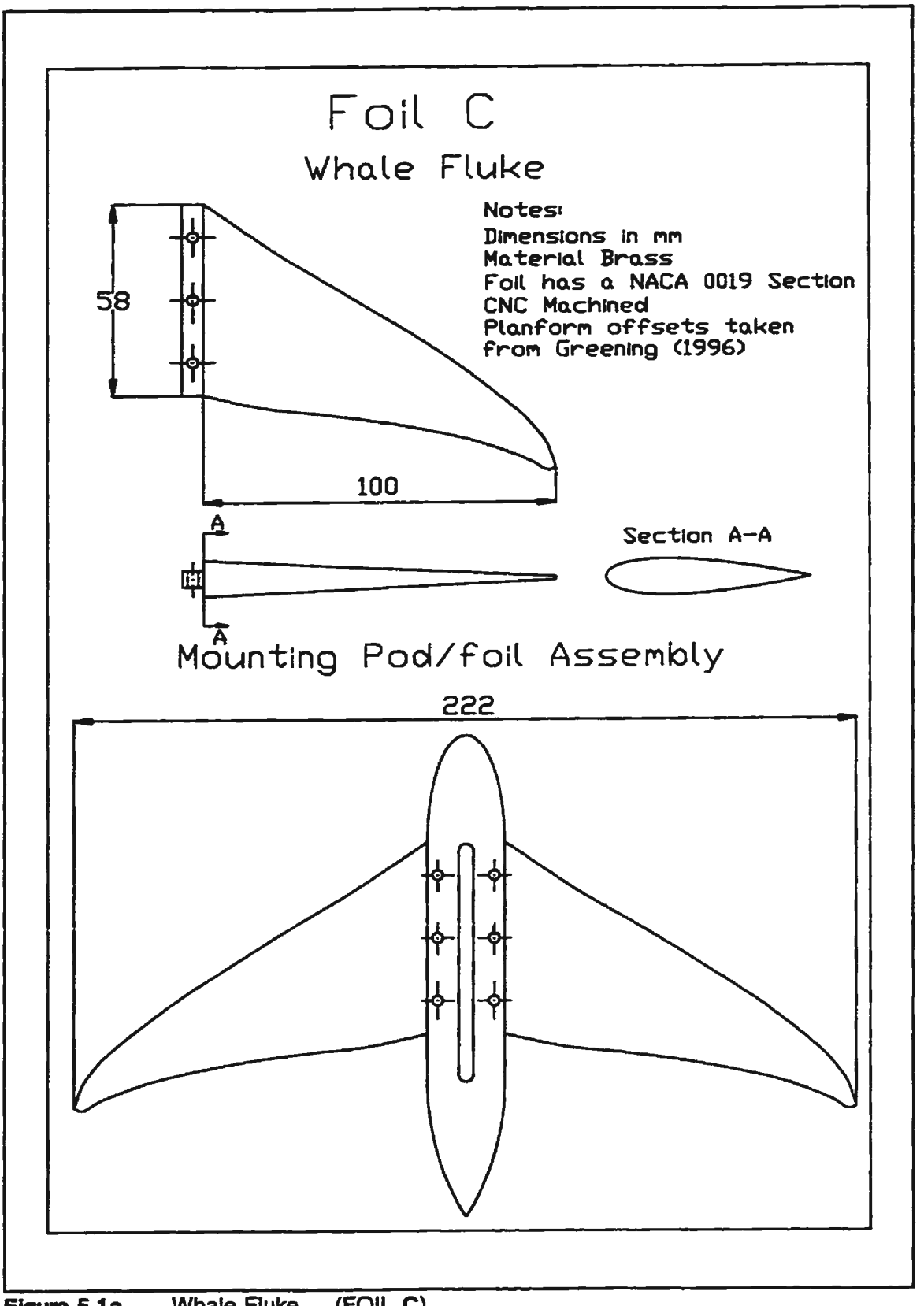

Figure 5.1c Whale Fluke (FOIL C)

5.3 Data Acquisition System and Transducer Calibration

Four parameters were recorded during the tests: developed thrust or drag by an oscillating foil, displacement history of the forward and aft shaft motion, and the speed of advance (carriage speed). The output thrust or drag was measured by a dynamometer load cell, while each shaft displacement was recorded by a LVDT. The carriage speed was measured by an optical transducer.

Prior to the experiment, calibration of all transducers was conducted. Thrust load cell static calibration was described in section 4.3. LVDT calibration consisted of thirteen data points collected at 100 points per sample at the sampling rate of 40 Hz resulting in 2.5 sec of data for each displacement. This was straight forward because shaft displacement was computer controlled. The range of shaft displacement for calibration varied from -90 to 90 mm for both shafts. Calibration of carriage speed was conducted at 50 points per sample at the sampling rate of 40 Hz. Speed ranged from 0.1 to 0.7 m/s.

Four channels of data were recorded for each run in the experiment:

i) Channel 1 for measuring forward shaft displacement

ii) Channel 2 for collecting aft shaft displacement

iii) Channel 3 recorded data from the thrust load cell

iv) Channel 4 measured carriage speed

The displacement and force traces were analog low-pass filtered at 20 Hz and

then recorded on a 80486 PC-class computer equipped with a 16 bit KEITHLEY A/D input converter. The sampling frequency for all four channels was 40 Hz throughout the experiment, and the maximum frequency of oscillation of the foils was 0.7 Hz (4.4 rad/sec). Therefore the number of samples to describe an oscillating cycle at this frequency was 57.

5.4 Experimental Corrections

The measured propulsive thrust or drag was masked by two parameters: aerodynamic drag on the dynamometer lateral plates, and the effects of the mounting pod oscillation and drive shaft movement through the fluid. To account for this, prior to the experiment a set of preliminary tests were conducted at the conditions as close to the conditions in the actual experiment. These conditions were as follows:

i) Same motion files were used. Thus the motion history of the mounting pod including pitch amplitude and frequency of oscillation were the same in the preliminary tests as the motion history of the foil in the actual experiment.

ii) Forward speed was not exactly the one used in the experiment. There was a slight mismatch in the velocities obtained in preliminary tests compared with the ones obtained in the experiment. This is attributed to the fact that the towing tank at Memorial is manually controlled. Therefore the ideal situation, to repeat a run at exactly the same speed in the tests and actual

experiment, was impossible to accomplish.

iii) The flow conditions around the oscillating mounting pod during the preliminary tests were not the same as the flow conditions during the experiment, where the foil model was attached to the mounting pod. There was no way to account for this in the experiment. This will contribute to the uncertainty in the experiment.

iv) For aerodynamic drag measurements on the dynamometer lateral plates, the mounting pod was disconnected and the drive shafts were above the waterline. As a result, in these measurements only the drag experienced by the lateral plates was recorded by the thrust load cell.

It was found that the magnitude of aerodynamic drag measured was within the non-linear range of the load cell (+/- 0.033 N), for the range of speeds tested. It was decided to disregard this correction.

The mean propulsive thrust or drag for the mounting pod at four tested pitch amplitude settings and different speeds of advance is plotted in figure 5.2 In the subsequent data analysis the experimental value of mean thrust for the different foils was corrected by the appropriate value of thrust or drag obtained from the regression curves shown in this figure.The correction equation was:

$$T_{corr} = T_{exp} - T_{mpod} \tag{5.3}$$

where T_{exp} was the mean thrust or drag obtained from experiment and T_{mpod} was

the thrust or drag obtained from the regression equation. For example, if the T_{mpod} was negative, i.e. mounting pod developed drag, and T_{exp} was positive, i.e. mounting pod and foil together developed thrust, then the overall thrust T_{corr} developed by the foil was greater than T_{exp} by the amount equal to the T_{mpod}. This physically means that to see positive thrust, the foil had to overcome the drag developed by the mounting pod and the portion of the oscillating shafts immersed in the fluid.

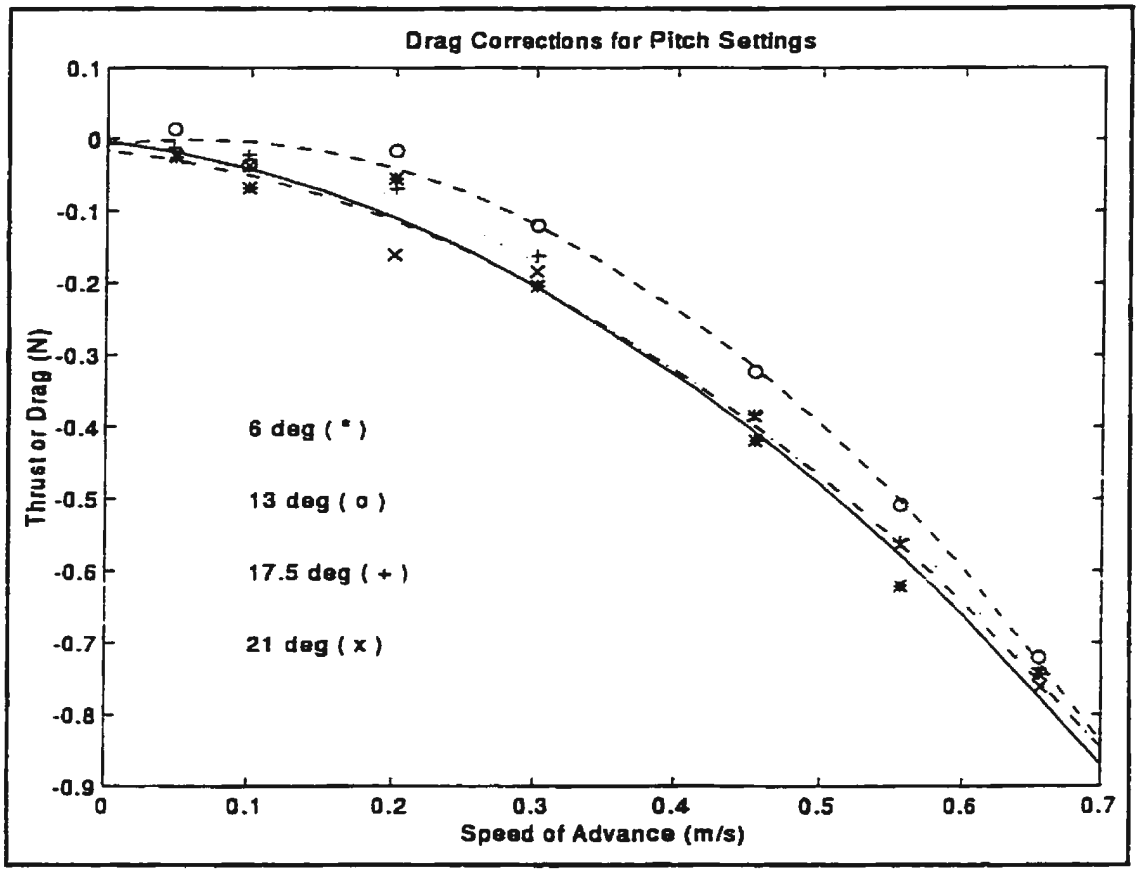

Figure 5.2 Drag Correction Data

5.5 Results: Developed Thrust

In this section experimental results are presented and discussed. Non-dimensional parameters which are used to present the results were derived in section 1.4. In the plots the horizontal axis is the reduced frequency k defined as:

$$k = \frac{\omega c}{U} \tag{5.4}$$

and the vertical axis is the mean thrust coefficient C_t of the form:

$$C_t = \frac{T}{\frac{1}{2}\rho S U^2} \tag{5.5}$$

where S is the foil surface area, U is the speed of advance, and T is the mean developed thrust and is equal to T_{corr} in equation (5.3). A negative value of C_t corresponds to drag and a positive value indicates thrust. According to equation (5.1), the maximum angle of attack is a function of two parameters: maximum pitch amplitude α, and the maximum kinematic velocity angle β. In this experiment for a given pitch amplitude, the maximum kinematic velocity angle was varied by varying the speed of advance U. Therefore in the plots for the given pitch amplitude, small values of reduced frequency correspond to small values of β and small angles of attack. Conversely, large values of reduced frequency indicate larger angles of attack. Also for a fixed reduced frequency (fixed maximum kinematic velocity angle) the larger the pitch amplitude, the smaller the angle of attack. Information on the data points will be reported as is necessary in this analysis.

FOIL A

Figure 5.3 shows experimental data in the form of C_t as a function of reduced frequency *k* for foil **A**. The plot contains results obtained at pitch oscillation amplitudes of 6, 13, 17.5 and 21 deg. From the plot it can be seen that at the lower range of reduced frequencies tested there is no marked difference in the thrust coefficient magnitudes between 6 and 13 deg. pitch amplitudes, and between 17.5 and 21 deg. pitch amplitudes. As the reduced frequency increases, particularly for k>1.5, the difference in the thrust coefficient data for different pitch amplitudes becomes more pronounced.

The foil produced thrust for 6 and 13 deg. pitch amplitudes for the range of reduced frequencies tested. For k<0.64 the foil developed drag for the 17.5 deg. pitch amplitude, and for the 21 deg. pitch amplitude the foil developed drag for the reduced frequency range k<0.83.

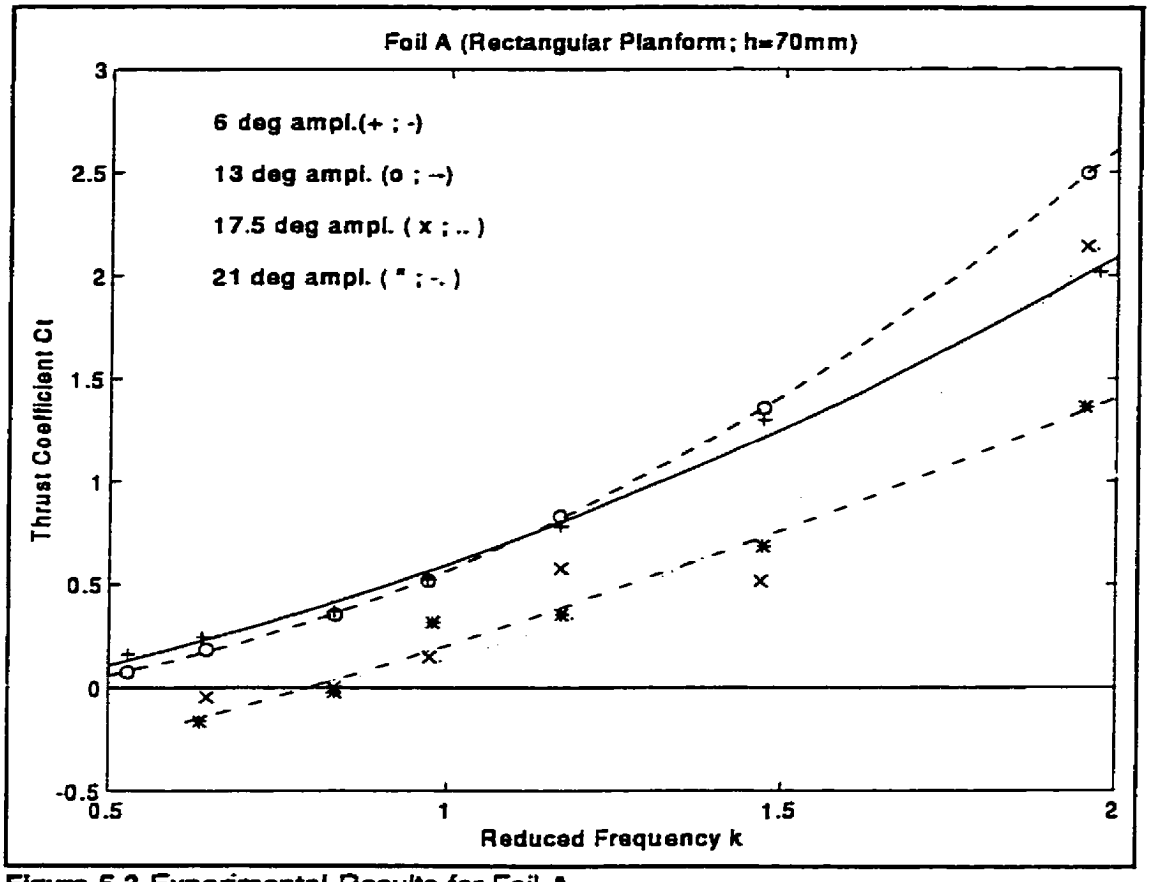

Figure 5.3 Experimental Results for Foil **A**

The thrust coefficient at reduced frequencies of 0.64, 1.17, 1.47, and 1.96 as a function of the pitch amplitude are shown in figure 5.4. The aim was to demonstrate the effect of the foil's pitch amplitude and angle of attack on the developed thrust at different reduced frequencies. At each corresponding data point the maximum angle of attack is given in brackets.

For the small reduced frequency of k=0.64 the thrust coefficient increases as the pitch amplitude decreases. The rate of increase with pitch amplitude assumes an almost linear trend, although measured thrust levels off slightly at 6 deg. pitch

amplitude. This trend is attributed to the case where the maximum angle of attack is within the linear part of the relation between the lift and the angle of attack (Katz and Plotkin, 1991).

A similar trend as for k=0.64 between pitch amplitude and thrust coefficient can be observed at k=1.17. At this value of reduced frequency a decrease in pitch amplitude in the range from 21 deg. down to 13 deg. is accompanied by a linear increase in thrust coefficient. 13 deg. pitch amplitude corresponded to 38 deg. angle of attack. For a 6 deg. pitch amplitude and 45 deg. angle of attack the thrust coefficient drops off. This was probably due to separation and dynamic stall of the flow around the foil which is usually accompanied by a deterioration in developed thrust. To avoid a stall the angle of attack for the NACA 0019 airfoil in steady flow should be below 16 deg (Moran, 1984). However, based on the linear trend of the C_t data at k=1.17 up to 38 deg. angle of attack (13 deg. pitch amplitude) dynamic stall did not appear to occur.

For k=1.47 the relationship between pitch amplitude and developed thrust is less well defined. All values of thrust coefficient except at 17.5 pitch amplitude are larger in magnitude than the corresponding values of thrust coefficient at k=1.17. This is depicted in the plot by a second degree polynomial fitted through the data. On the contrary to the curve fits shown at other reduced frequencies, this curve has no qualitative meaning of explaining the trend in the data with changes in pitch

amplitude. The thrust coefficient data seem to cluster between 1.30 and 1.36 for 6 and 13 deg. pitch amplitudes, while C_t values lie between 0.52 and 0.68 for 17.5 and 21 deg. pitch amplitudes, respectively.

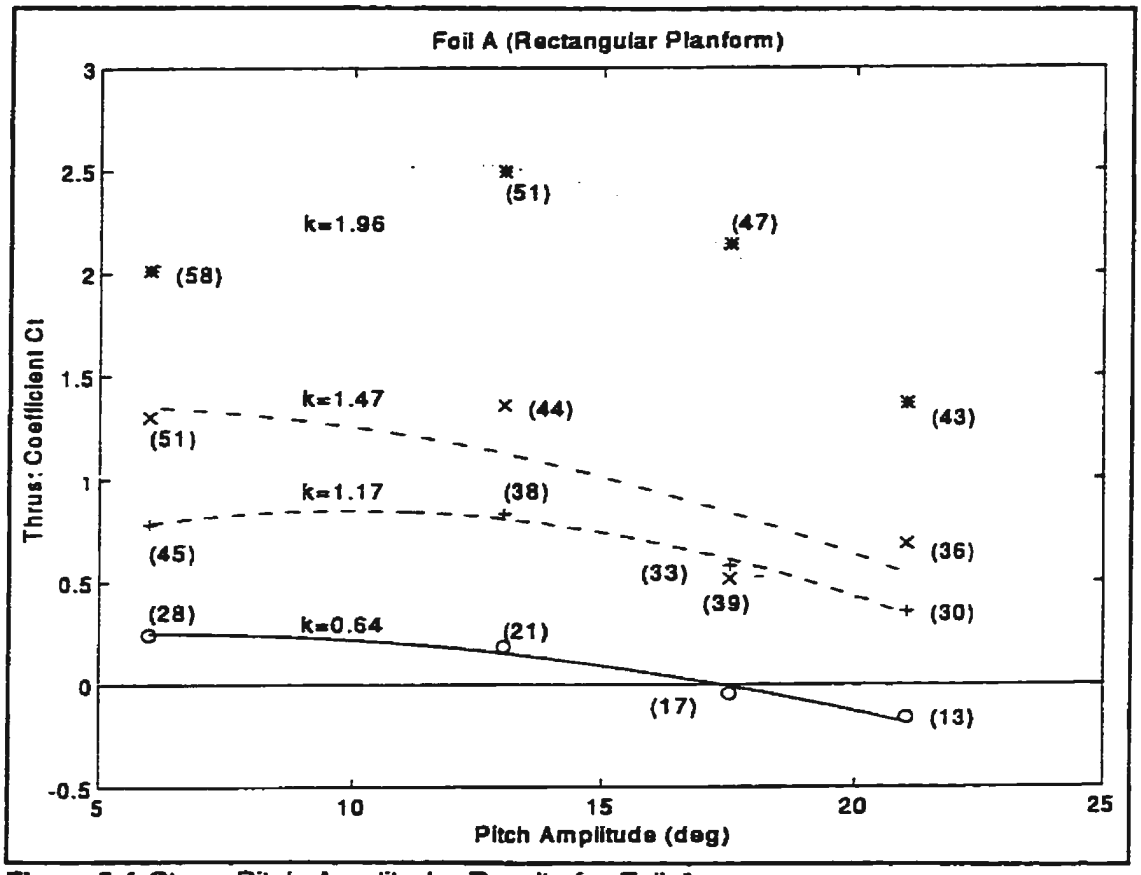

Figure 5.4 Ct vs. Pitch Amplitude. Results for Foil **A**

The most striking results in this experiment for foil **A** were obtained at the reduced frequency of k=1.96. The effect of high reduced frequency combined with the large angles of attack resulted not only in a substantial increase in C_t magnitude, but also altered the linear relationship between thrust coefficient and pitch amplitude present at small reduced frequencies. At this reduced frequency maximum thrust coefficient of C_t=2.50 was obtained at a pitch amplitude of 13 deg., and 51 deg.

angle of attack.

The flow field around an oscillating foil at large angles of attack is usually accompanied by a flow separation and dynamic stall (McCroskey, 1982). Also, large reduced frequency combined with large amplitude motion of a foil results in the shed vortex breaking up into an array of individual vortices immediately behind or within one chord length of a foil (Triantafyllou et. al, 1993). Freymuth's (1988) flow visualization photographs gave evidence of the above behaviours. As was discussed in Chapter 2, Freymuth observed leading edge separation for a heaving foil (h/c=0.2) of 10 cm chord and AR=∞ at a reduced frequency of k=2.7 and angle of attack at 52.2 deg. His visualization photographs show that at these flow conditions the leading edge vortex merged with the vortex of the same sign created by the trailing edge at the end of the downward stroke; thus reinforcing the propulsive vortical pattern in the wake behind the heaving foil.

In the present experiment the maximum thrust coefficient was obtained at the reduced frequency of k=1.96 and a 51deg. angle of attack. This is the same angle of attack at which, in Freymuth's study (1988), enhancement of the propulsive vortical signature in the foil's wake occurred. This comparison, however is inconclusive because other things complicate the issue. First, the flow conditions were not the same between the two experiments because of the difference in reduced frequency and amplitude of oscillation. Reduced frequency is a very

important parameter as it signifies the frequency of vortex shedding. Therefore, the proper timing for the leading edge vortex merger with vortices of the same sign in the wake is strongly dependent on the reduced frequency. Secondly, in the present experiment the foil had a finite aspect ratio, while in the Freymuth's flow visualization experiment the foil had AR=∞, thus the effects that tip vortices would have on the propulsive vortical signature are not known.

FOILS **B** AND **C**

Figures 5.5 and 5.6 show thrust coefficient C_t as a function of reduced frequency for the foils **B** and **C** respectively. Similarly to foil **A**, at 6 and 13 deg. pitch amplitude foils **B** and **C** produced thrust for the range of reduced frequencies tested. For foil **B**, at 17.5 deg. pitch amplitude drag was measured up to k=0.45, while for a pitch amplitude of 21 deg. the foil produced drag up to k=0.55. For foil **C** drag was measured up to k=0.46.

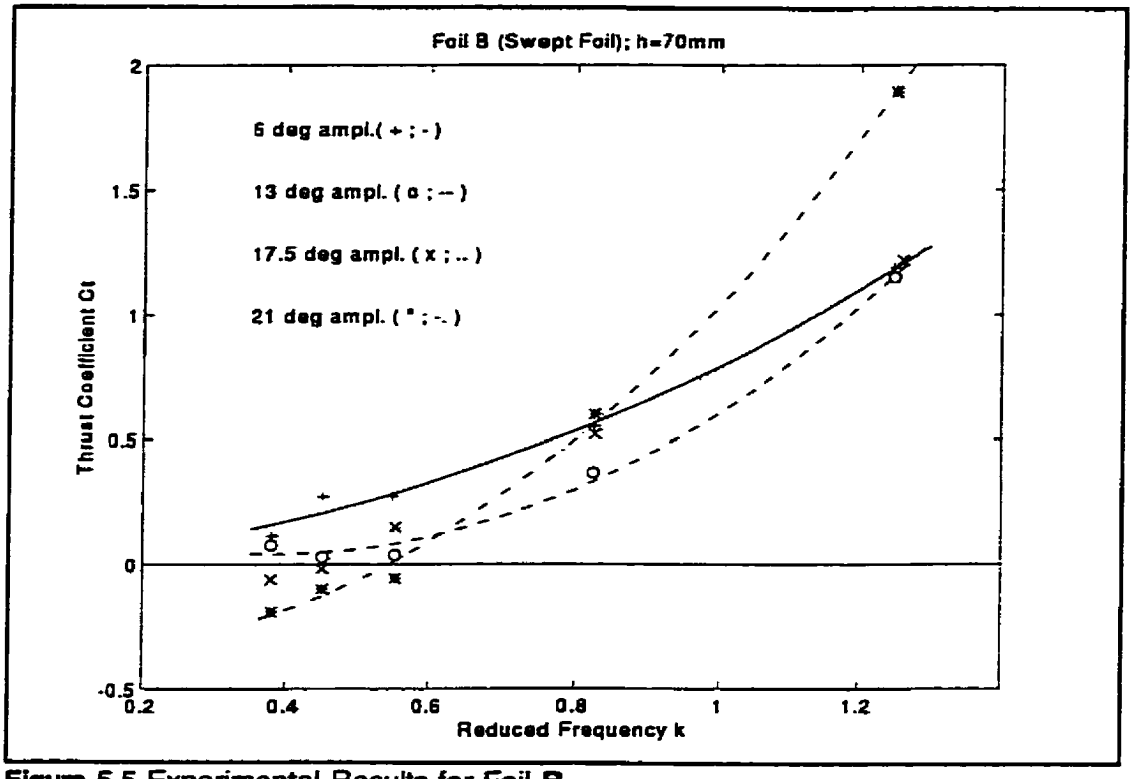

Figure 5.5 Experimental Results for Foil **B**

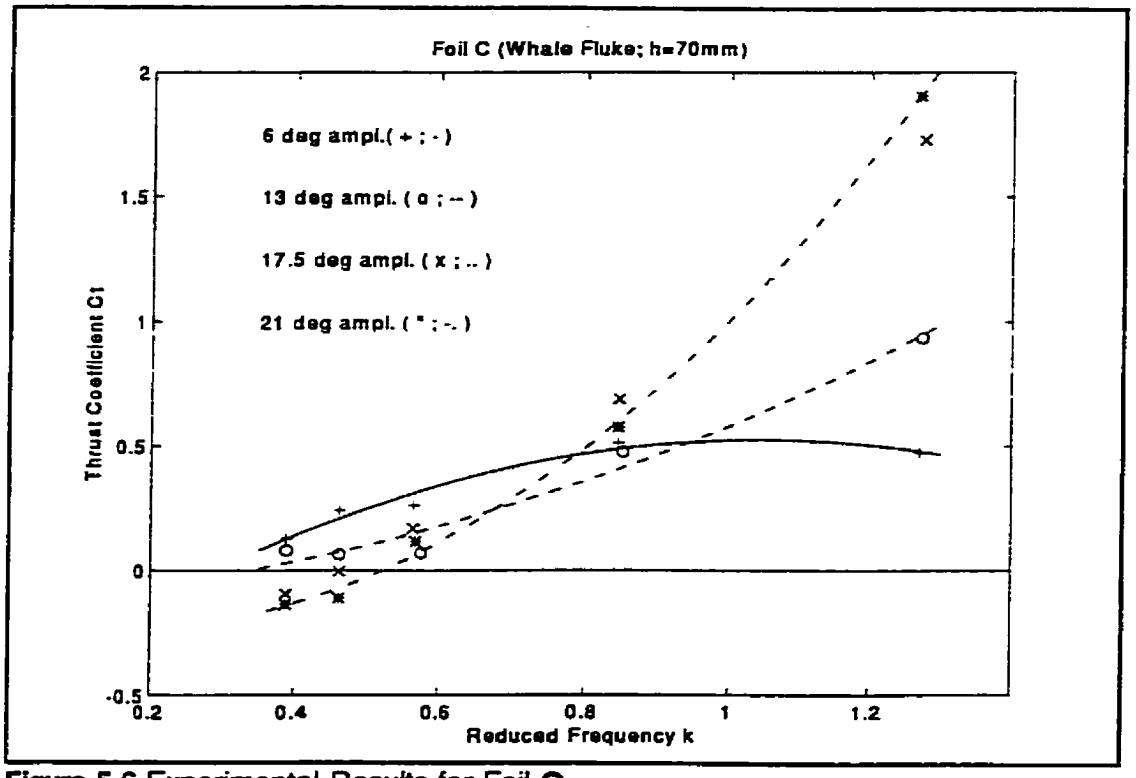

Figure 5.6 Experimental Results for Foil **C**

The reduced frequencies at which the drag force was replaced by propulsive thrust for 17.5 and 21 deg. pitch amplitudes for foil **A** were k=0.64 and k=0.83, respectively. By comparing the reduced frequencies at which the onset of the propulsive thrust occurs between foil **A** and **B**, two points can be noted. First, the reduced frequencies at which drag changed to thrust for 21 deg. pitch amplitude was consistently higher than for 17.5 deg pitch amplitude. This suggests that developed thrust for both foils **A** and **B** depends on oscillation amplitude. Similar conclusions for a pitching foil can be found in Koochesfahani (1989).

Second, reduced frequencies for the onset of forward thrust differ between foils **A** and **B**. Drag was measured for foil **A** up to k=0.64 which corresponded to 17 deg. angle of attack and 17.5 deg. pitch angle. For foil **B** drag was measured up to k=0.55 and 12 deg. angle of attack at 17.5 deg. pitch angle. A larger angle of attack for foil **A** implies that it experienced more drag than foil **B**. This is attributed to the fact that foil **A** is twice the size of foil **B**, and it has a different planform than foil **B**. Also foil **A** was fabricated by hand, meaning that the shape and the thickness of foil **A** was not exactly that of the NACA 0019 section, while foil **B** was CNC machined and therefore the sectional shape was more accurate.

Figures 5.7 and 5.8 show thrust coefficient as a function of the pitch amplitude for foils **B** and **C** respectively. Reduced frequencies shown are 0.42, 0.85 and 1.25 for foils **B**, and **C**. At each corresponding data point the maximum angle of attack

is given in brackets.

For the reduced frequency of k=0.42 it can be seen that the thrust coefficient increases as the pitch amplitude decreases for both foils **B** and **C**. A second degree polynomial fitted to the data, indicates that the rate of C_t increase with pitch amplitude is closely linear for both foils. The quadratic term for foil **B** was 0.0009 and thus negligible, and the quadratic term in the curve fit equation for foil **C** was 0. The slope of the curve fits for foil **B** and **C** were -0.0492 and -0.0229 respectively. As was the case for foil **A**, at small reduced frequencies, a linear relation between the thrust coefficient and pitch amplitude exists for foils **B** and **C**. This is attributed to the situation where the maximum angle of attack is below the stall angle, and the lift force assumes a linear relation with increasing angle of attack.

For the intermediate value of reduced frequency at k=0.85 for foil **C**, the rate of change of thrust coefficient with pitch amplitude is found to be linear (quadratic term in the curve fit was 0.0001), with a positive slope of +0.006. A positive slope means that the thrust coefficient decreases with decreasing pitch amplitude, or in other words, thrust decreases with increasing angles of attack (see figure 5.8). At the reduced frequency of k=0.85 for foil **B**, the similar behaviour of decrease in thrust as pitch amplitude decreases (or as angle of attack increases) is observed up to 13 deg. pitch amplitude corresponding to 33 deg. angle of attack.

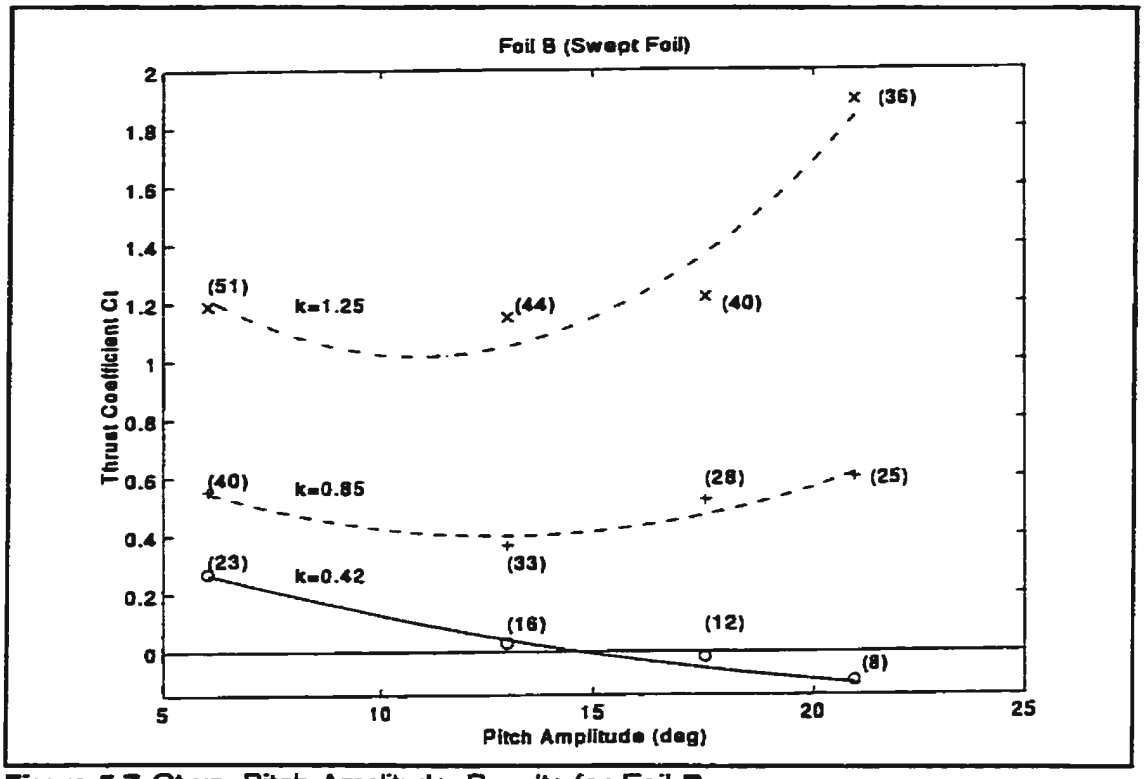

Figure 5.7 Ct vs. Pitch Amplitude. Results for Foil B

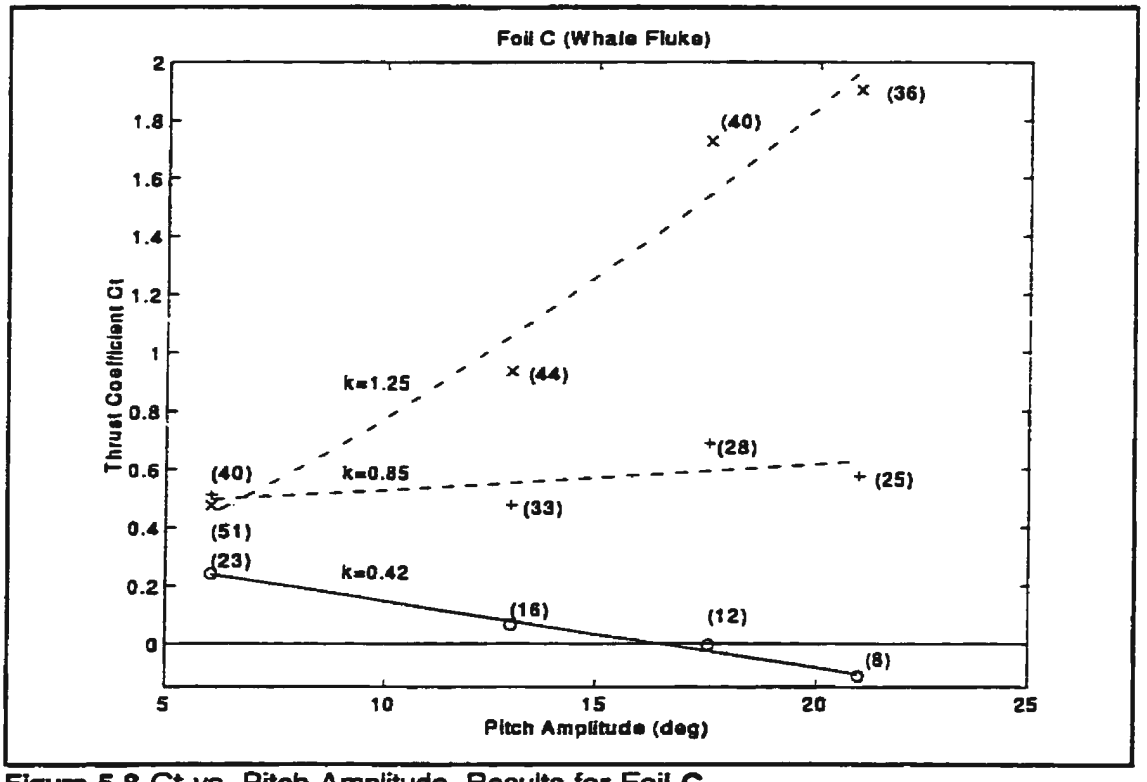

Figure 5.8 Ct vs. Pitch Amplitude. Results for Foil C

At the reduced frequency of k=1.25, experimental data for foil **B** shows a substantial increase in the thrust coefficient compared to the values at k=0.85. A high magnitude is maintained for the angles of attack from 51 to 40 deg. corresponding to pitch amplitudes from 6 to 17.5 deg. For 21 deg. pitch amplitude and the smallest angle of attack of 36 deg., at k=1.25 developed thrust showed a further increase in the magnitude. This represents the largest thrust coefficient obtained in this experiment for foil **B**, C_t=1.89.

For foil **C** maximum thrust, C_t=1.91 was measured at the same conditions as for foil **B** (21 deg. pitch amplitude and 36 deg. angle of attack at a reduced frequency of k=1.25). However, the trend in developed thrust with decreasing pitch amplitude was somewhat different from that of foil **B** (compare figures 5.7 and 5.8). The tendency observed in the experimental data for foil **C** at the reduced frequency of k=1.25 was that larger angles of attack, or smaller pitch amplitudes, resulted in lower developed thrust. The curve fit slope was positive (+0.0532) with a quadratic term of 0.0018, indicating that the relationship was not linear. For 6 deg. pitch amplitude and 51 deg. angle of attack, the thrust coefficient deteriorated so much that the magnitude was smaller than for k=0.85 at the same pitch amplitude and 40 deg. angle of attack.

The drop in developed thrust with increasing angle of attack observed for foils **B** and **C** at high reduced frequencies, is attributed to the dynamic stall condition.

Both foils **B** and **C** have the same NACA 0019 cross section, as well as the same sweep back angle of 30 deg. The stalled flow field over wings with leading edge sweep is characterized by the inception of leading edge vortices whose effect is to create large suction peaks on the upper surface of the wing. Consequently this increases the lift force. These leading edge vortices are unstable and eventually break downstream from the foil. The position of breakdown depends on the angle of attack. As the angle of attack increases the onset of vortex breakdown moves gradually forward, closer to the foil. A further increase in the angle of attack causes the vortex to breakdown over the surface of the foil and consequently a deterioration of the lift force (Katz and Plotkin, 1991).

EFFECT OF DIFFERENT PLANFORMS ON DEVELOPED THRUST

Up to this point the developed thrust has been presented from a qualitative perspective. The results for foils **B** and **C** suggest a noticeable difference in the behaviour of developed thrust over those for foil **A** at large reduced frequencies and angles of attack. This may be because dynamic stall for swept foils **B** and **C** is completely different from the dynamic stall of a straight leading edge foil (Katz and Plotkin, 1991). In order to obtain an idea of the quantitative effects that different planforms may have on the developed thrust, the data in figures 5.3, 5.5 and 5.6 were curve fitted with second degree polynomials and these are replotted in the figures 5.9a to d. Each plot represents one pitch amplitude and contains curves for the three different planforms. As before the vertical axis is the thrust

coefficient C_t, and the horizontal axis is the reduced frequency *k*.

From the plots it can be seen that there is no marked difference in developed thrust between foils **B** and **C** for the reduced frequencies approximately k<0.8 for the pitch amplitudes tested. At reduced frequencies k>0.8 foil **B** produced larger thrust for 6 deg. pitch amplitude (figure 5.9a), and conversely foil **C** developed more thrust than foil **B** for 17.5 deg. pitch amplitude (figure 5.9c). This result suggests that for the largest angles of attack in the experiment corresponding to 6 deg. pitch amplitude, and reduced frequencies k>0.8, the sweptback planform (foil **B**) performed better, while at relatively smaller angles of attack corresponding to 17.5 deg. pitch amplitude the whale fluke (foil **C**) produced more thrust. This is attributed to the difference in the planform shape between foils **B** and **C**. The leading edge of foil **B** has a straight (linear) curvature, while the leading edge of foil **C** has a non-linear "crescent moon" shape (see figure 5.1b and c).

At 13 and 21 deg. pitch amplitude C_t curves for foil **B** and **C** are very similar. At small reduced frequencies foil **C** showed somewhat increased thrust, and at larger reduced frequencies foil **B** developed larger thrust. Overall, results indicate that for these pitch amplitudes, developed thrust was relatively insensitive to the difference in planform shape between foils **B** and **C**.

By comparing the performance of foils **A** and **B** or **A** and **C**, it is possible to obtain

the combined effect of leading edge sweep and taper on developed thrust. For pitch amplitudes of 17.5 and 21 deg. the slope of the C_t curve is larger for foils **B** and **C** compared to foil **A**. A similar situation, that foil **B** and **C** produced larger thrust than foil **A**, can be observed for 6 deg. pitch amplitude except that the curve for foil **C** levels off at approximately k=0.8. This suggests that sweepback and taper of the foil planform has the effect to increase the level of thrust at the same reduced frequency. This observation is in accordance with the analytical lifting surface calculations of a finite flat-plate wing by Chopra and Kambe (1977) of planforms similar to the ones used in this work.

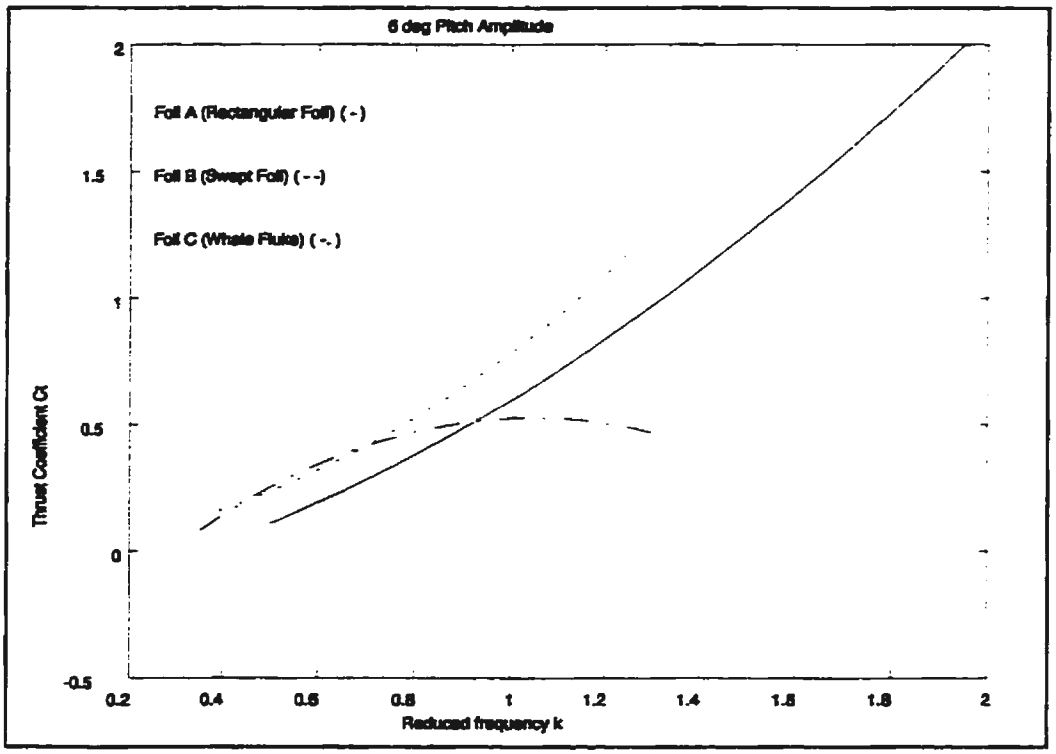

Figure 5.9a 6 deg Pitch Amplitude

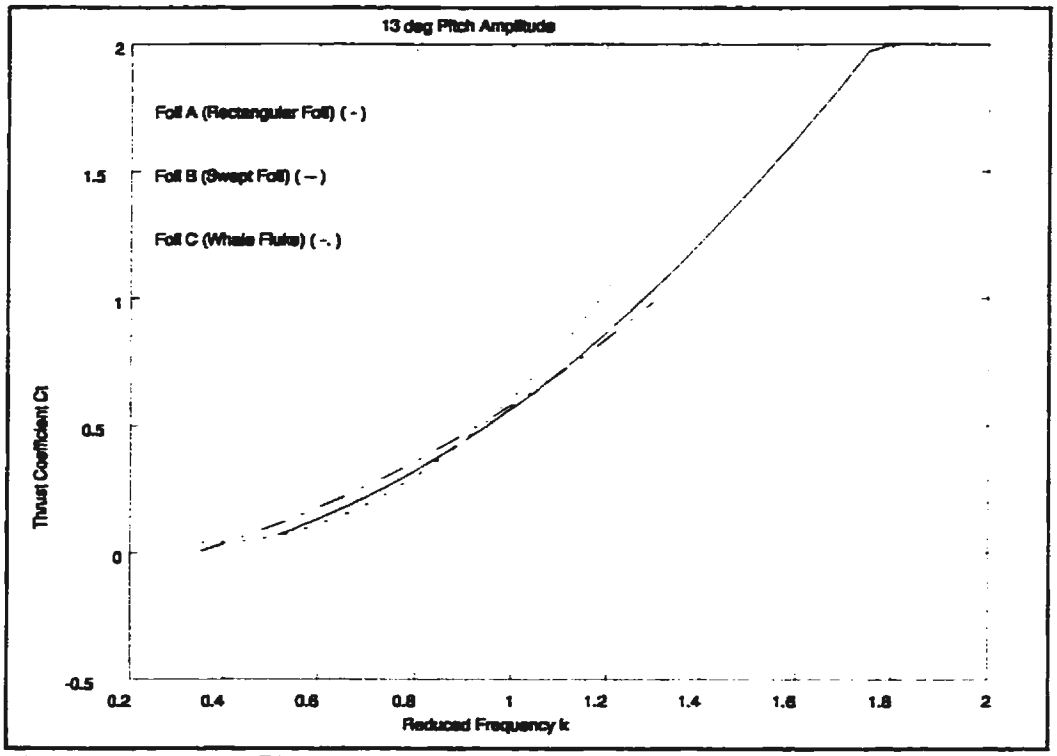

Figure 5.9b 13 deg Pitch Amplitude

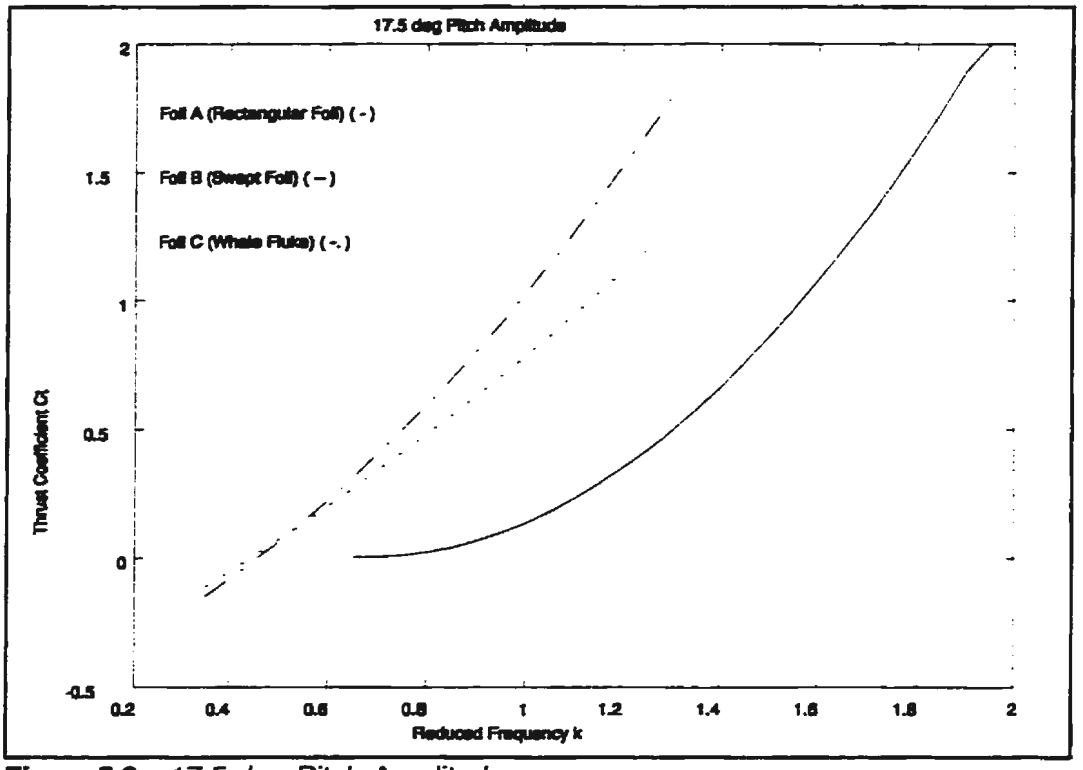

Figure 5.9c 17.5 deg Pitch Amplitude

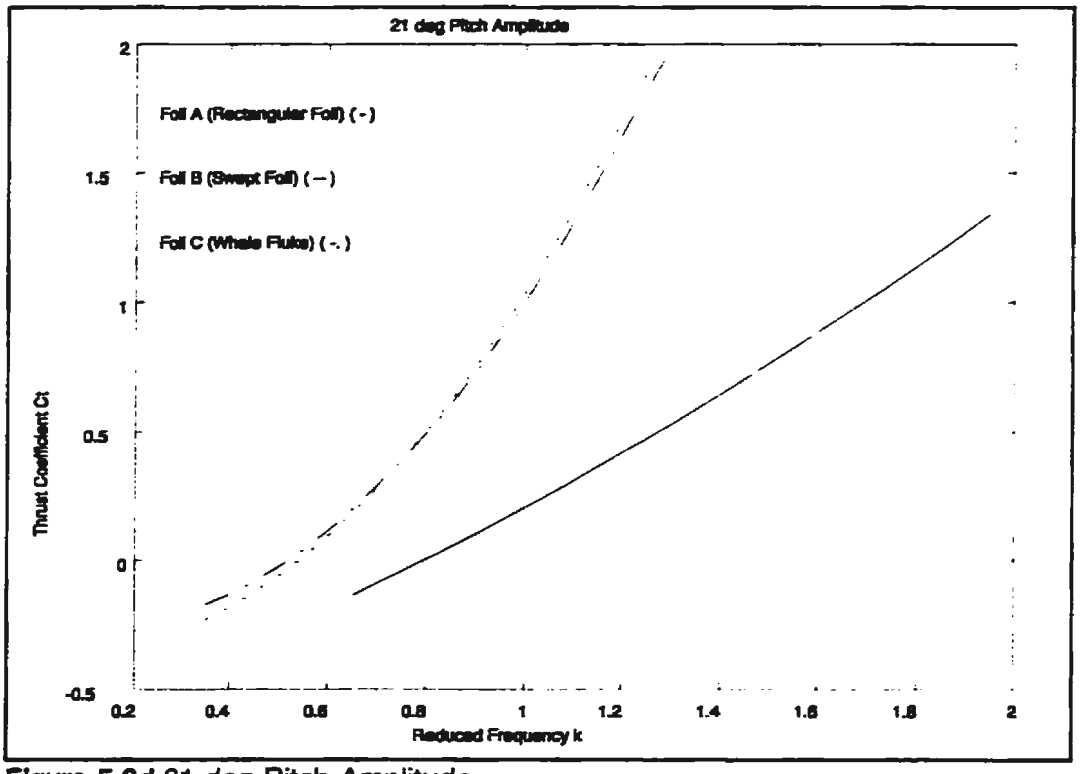

Figure 5.9d 21 deg Pitch Amplitude

5.6 Uncertainty Analysis

In this section an estimate of errors associated with the experimental data is evaluated. The approach used is described by Coleman and Steele (1989) in their book *Experimentation and Uncertainty Analysis for Engineers.*

Every measurement system is influenced by a number of elemental error sources manifested as a *bias error limit* B_i (constant component of the total error), and a *precision error limit* P_i (random component of the total error). These errors in the measured variables propagate through the data reduction equation and yield the bias and precision limit in the experimental result. These two errors are then combined to obtain the overall uncertainty in a experimental result by:

$$u = (B_i^2 + P_i^2)^{1/2} \tag{5.6}$$

The aim during the present experiment was to obtain values of thrust coefficient C_t defined as:

$$C_t = \frac{T - T_o}{\frac{1}{2}\rho S U^2} \tag{5.7}$$

where T_o refers to the correction due to thrust/drag on the mounting pod and is equal to T_{mpod} in equation (5.3). The bias and precision limit for C_t is found from the uncertainty analysis expression (Coleman and Steele, 1989):

$$\left(\frac{u_{Ct}}{C_t}\right)^2 = \left(\frac{1}{C_t}\frac{\partial C_t}{\partial T}u_T\right)^2 + \left(\frac{1}{C_t}\frac{\partial C_t}{\partial T_o}u_{T_o}\right)^2 + \left(\frac{1}{C_t}\frac{\partial C_t}{\partial V}u_V\right)^2 \tag{5.8}$$

where u_{Ct} is the bias and precision limit of the experimental result, and u_T, u_{To}, and

u_V represent precision and bias limits of the measured variables: thrust T, drag/thrust on the mounting pod T_o, and speed of advance V[5] respectively. After partial differentiation the data reduction equation takes the form:

$$\left(\frac{u_{C_t}}{C_t}\right)^2 = \left(\frac{u_T}{T-T_o}\right)^2 + \left(\frac{u_{T_o}}{T-T_o}\right)^2 + 4\left(\frac{u_V}{V}\right)^2 \qquad (5.9)$$

A summary of estimates of the bias and precision limits for each measured variable is presented in table 5.1, and numerical details are given in Appendix II.

Table 5.1 Bias and Precision Limits of Measured Variables

Variable	Bias Errors and Bias Limit	Precision Errors and Precision Limit
Velocity *V*	curve fit:+/-0.0001 m/s tide:+/-0.001 m/s calibration:+/-0.005 m/s **Bias Limit=+/- 0.0051 m/s**	**Precision Limit= +/- 0.0004 m/s**
Thrust *T*	nonlinearity:+/-0.0134 N applied load:+/-0.01 N curve fit:+/-0.0337 N **Bias Limit=+/- 0.0376 N**	**Precision Limit= +/- 0.0399 N**
Thrust/Drag on the pod T_o	nonlinearity:+/-0.0134 N applied load:+/-0.01 N curve fit:+/-0.0337 N **Bias Limit=+/- 0.0376 N**	**Precision Limit= +/- 0.0413 N**

After the bias and precision limits were found for each of the variables, they were propagated through the data reduction equation (5.9) to obtain overall bias and

[5]Since uncertainty has the symbol u, in this section the speed of advance will be denoted by V. In other sections U refers to the speed of advance.

precision limits in the experimental result of thrust coefficient. This was done separately for the bias and precision limits. Since typical values of each variable are required in the calculations, three overall bias and precision uncertainties in thrust coefficient were calculated corresponding to reduced frequencies k=0.64, 1.47, 1.95 for the 13 deg pitch amplitude case, covering the range of frequencies in the experiment.

Table 5.2 Overall Uncertainty in Experimental Result

Reduced Frequency	Thrust Coefficient Bias Error	Thrust Coefficient Precision Error	Overall Uncertainty in Thrust Coefficient	Percentage Error in C_t
0.64	+/- 0.0199	+/- 0.0210	+/- 0.0289	+/- 15.6
1.47	+/- 0.1220	+/- 0.1088	+/- 0.1630	+/-12.0
1.95	+/- 0.2460	+/- 0.1926	+/- 0.3124	+/- 12.5

The overall bias and precision uncertainties representing a 95% confidence interval are given in table 5.2. When combined using equation (5.6) these led to an overall uncertainty in the thrust coefficient given in the third column of table 5.2.

As stated above, the typical values used in the calculation of overall bias and precision uncertainties were for 13 deg. pitch amplitude. Uncertainties at other pitch amplitudes were approximately the same because the relative magnitudes of terms on the right hand side of the data reduction equation were approximately the same for all pitch amplitudes.

Overall the relative percent error of data in the experiment is approximately between 12 and 15% for the range of reduced frequencies tested.

5.7 Comparison with Theory

In this section experimental data are compared with theoretical results. For foil **A** together with the experimental data, analytical and numerical inviscid solutions for a foil of the same aspect ratio, planform shape, and pitching axis position are presented. The small amplitude theory of a thin plate of finite aspect ratio, as given by Chopra (1974) was used for the analytical predictions, while the 3-D panel method by Liu (1996) was used to simulate the large amplitude response of the foil. For foils **B** and **C**, experimental results are contrasted against Liu's (1996) numerical solution only, for the same planform shape, aspect ratio and pitching axis position. The present author carried out all the runs using Liu's panel method code. Also results from the uncertainty analysis are plotted with the experimental data. This is shown by error bars in the plots, where the width of the bars represent a 95% confidence interval.

FOIL **A**

Figure 5.10a to d show plots of C_t as a function of reduced frequency for foil **A**. Each plot contains experimental data for one pitch amplitude, together with analytical and numerical inviscid solutions.

It can be seen that results from the analytical method (Chopra, 1974) overestimate developed thrust for the range of reduced frequencies and pitch amplitudes tested. Although they agree in trend with experimental data, the disagreement in magnitude increases with increasing reduced frequency. This can be attributed to several factors. In the experiment, the foil had to overcome viscous drag that does not exist in the inviscid analytic theory. Second, in lifting surface theory, a foil has an infinitely small thickness while foil **A** had finite thickness. A thin (zero-thickness) wing section has a large leading edge suction force which contributes to the developed thrust (Liu, 1996). Thirdly, in Chopra's work small amplitude motion is assumed. This implies that the slope of the instantaneous kinematic velocity of the foil's pitch axis with respect to the horizontal is calculated as:

$$\beta = \frac{\omega h}{U} \tag{5.10}$$

This is an approximation which holds for small angles. Equation (5.2) should be used for large angles where:

$$\beta = \tan^{-1}\left(\frac{\omega h}{U}\right) \tag{5.11}$$

For example, at k=1.47, equation (5.10) estimates the kinematic velocity angle β=88.59 deg., and β according to equation (5.11) is 57.11 deg. Thus, small amplitude theory overestimates the kinematic velocity angle by more than 55%. A consequence of this is that overestimation of the kinematic velocity angle β resulted in overestimation of the maximum angle of attack. This is so, because the maximum kinematic velocity angle is directly related to the maximum angle of

attack through the relation given by equation (5.1). In potential theory, which is the theory Chopra used, the larger the angle of attack of the foil, the larger the developed thrust. This error in calculating the kinematic velocity angle resulted in overestimation of the thrust coefficient. This error, however decreases with decreasing reduced frequency. At k=0.53, the error in kinematic velocity angle is reduced to 9.6%, resulting in less disagreement between the analytical solution and experimental results.

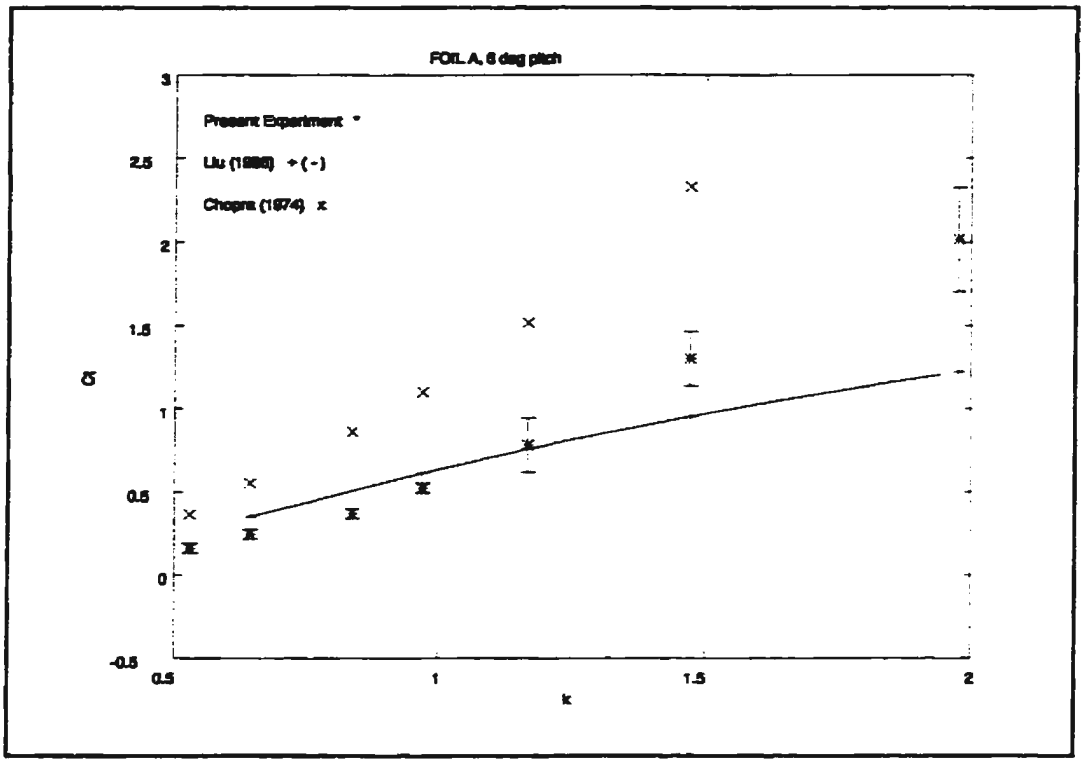

Figure 5.10a 6 deg Pitch Amplitude Foil **A**

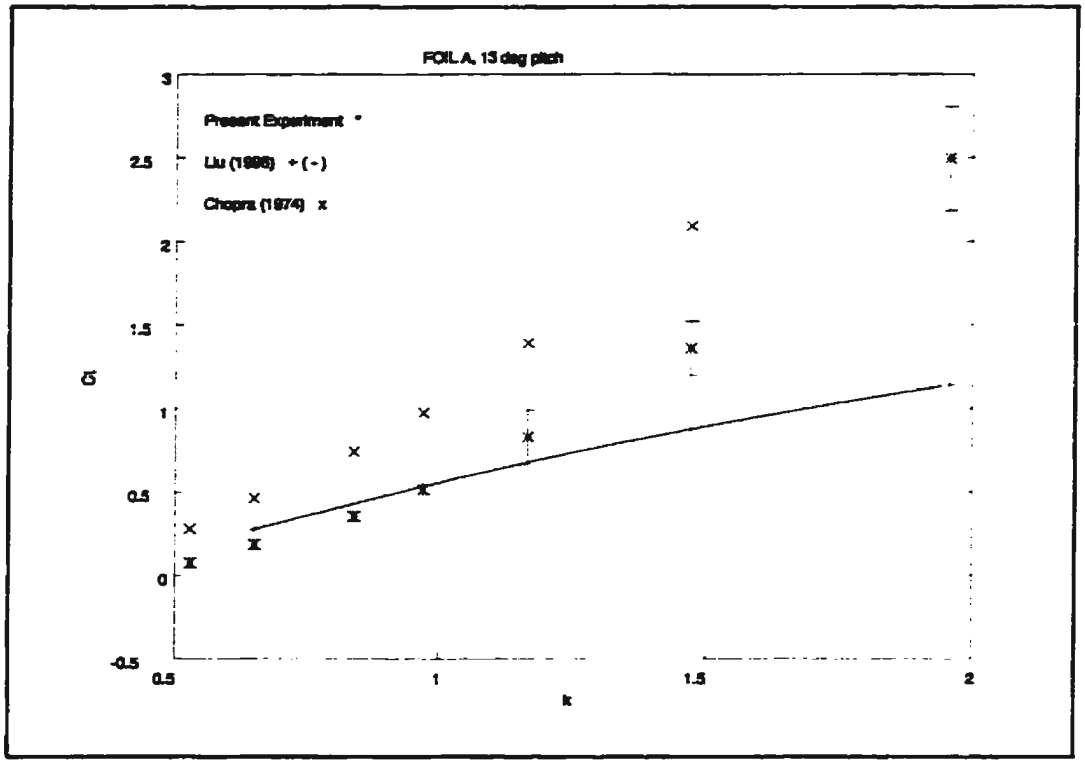

Figure 5.10b 13 deg Pitch Amplitude Foil **A**

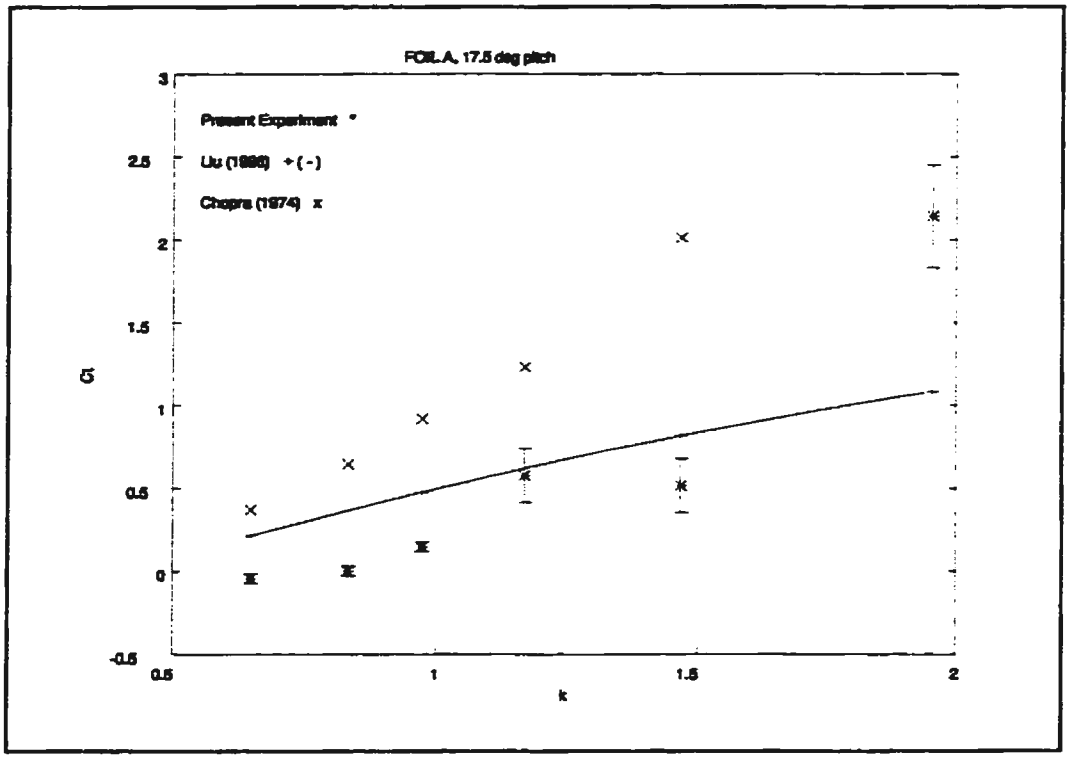

Figure 5.10c 17.5 deg Pitch Amplitude Foil **A**

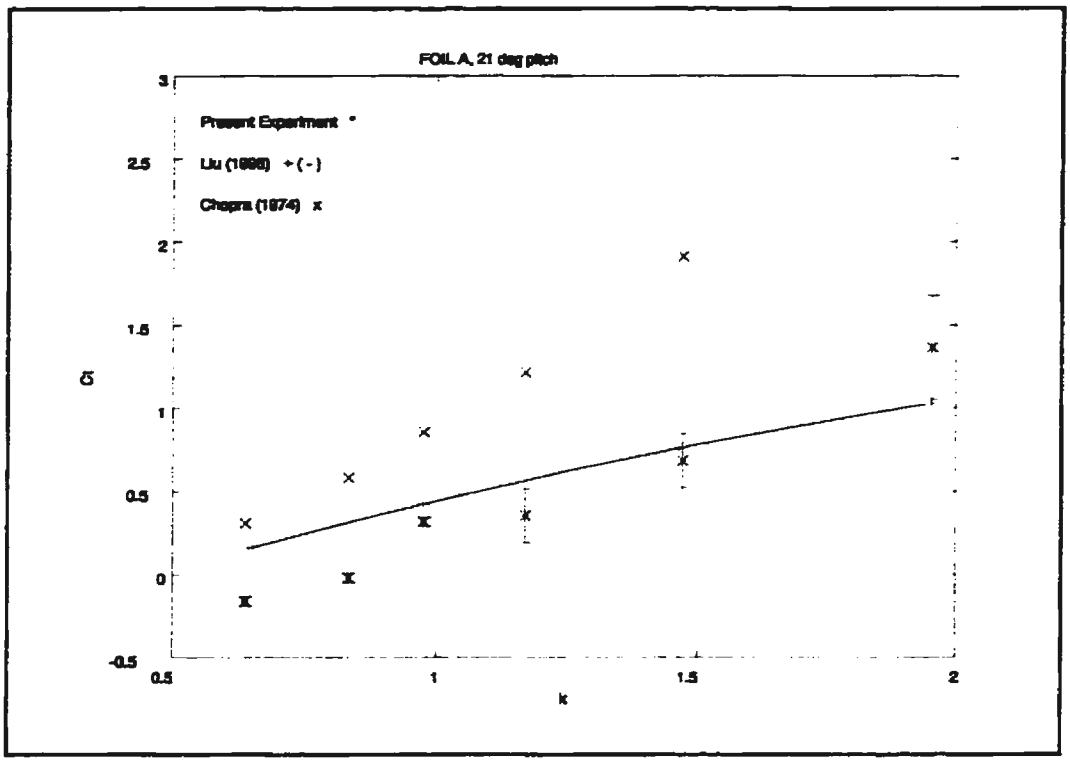

Figure 5.10d 21 deg Pitch Amplitude Foil **A**

The discrepancy between experimental data and the results from the Liu (1996) large amplitude numerical solution is less pronounced. The comparison can be classified into two regions. In the first region, corresponding to small reduced frequencies agreement between the results is relatively good. The numerical solution overestimated the developed thrust in this region due to viscous drag present in the experiment which does not exist in the inviscid potential theory on which the numerical solution was based. In the second region the disagreement between the results increases with increasing reduced frequency. This disagreement was characterized by larger experimentally obtained developed thrust than predicted by the numerical solution. The reduced frequency at which the numerical results start to underestimate the developed thrust varies with the pitch amplitude. However, the maximum instantaneous angle of attack at these reduced frequencies was approximately the same for all four pitch amplitudes. This "cut-off" maximum angle of attack ranged from 33 to 40 deg.

FOILS **B** AND **C**

Figures 5.11a to d, and 5.12a to d show the thrust coefficient as a function of reduced frequency for foils **B** and **C** respectively. Each plot contains two sets of data for one pitch amplitude. The first set are the experimental results and the second set are the numerical results obtained using the Liu (1996) panel code. The best agreement between experimental results and numerical prediction for foils **B** and **C** was obtained at small reduced frequencies and angles of attack for

all four pitch amplitudes tested. With increasing reduced frequency and angles of attack discrepancy in results increases in both trend and magnitude.

Overall, at small reduced frequencies and angles of attack numerical results correlated relatively well with the experimental results for all three foils tested. Therefore, the assumed flow conditions modeled in the Liu (1996) panel method were probably similar to those of the flow conditions in the real fluid during the present experiment. Based on the same argument, the substantial disagreement between Liu's numerical prediction and experimental results at large reduced frequencies and angles of attack indicates a violation of the panel code assumptions.

In the Liu (1996) panel method the foil performs large amplitude sinusoidal motion and the thin wake vortex sheet left behind the foil has a sinusoidal shape. The wake is assumed to be rigid, or in other words, the influence of the vortex sheet roll-up on the creation of lift force was neglected in the numerical method. In reality however this is not the case, particularly at large reduced frequencies, because vortex sheets are inherently unstable and result in vortex sheet distortion and break-up into discrete vortices (Prandtl and Tietjens, 1934). Further, the flow field around an oscillating foil at large angles of attack is usually accompanied by a dynamic stall and the development of leading edge vortices (Freymuth, 1988; Triantafyllou et al., 1996). Thus, the additional assumption of attached flow around the foil, inherent to the numerical method is violated.

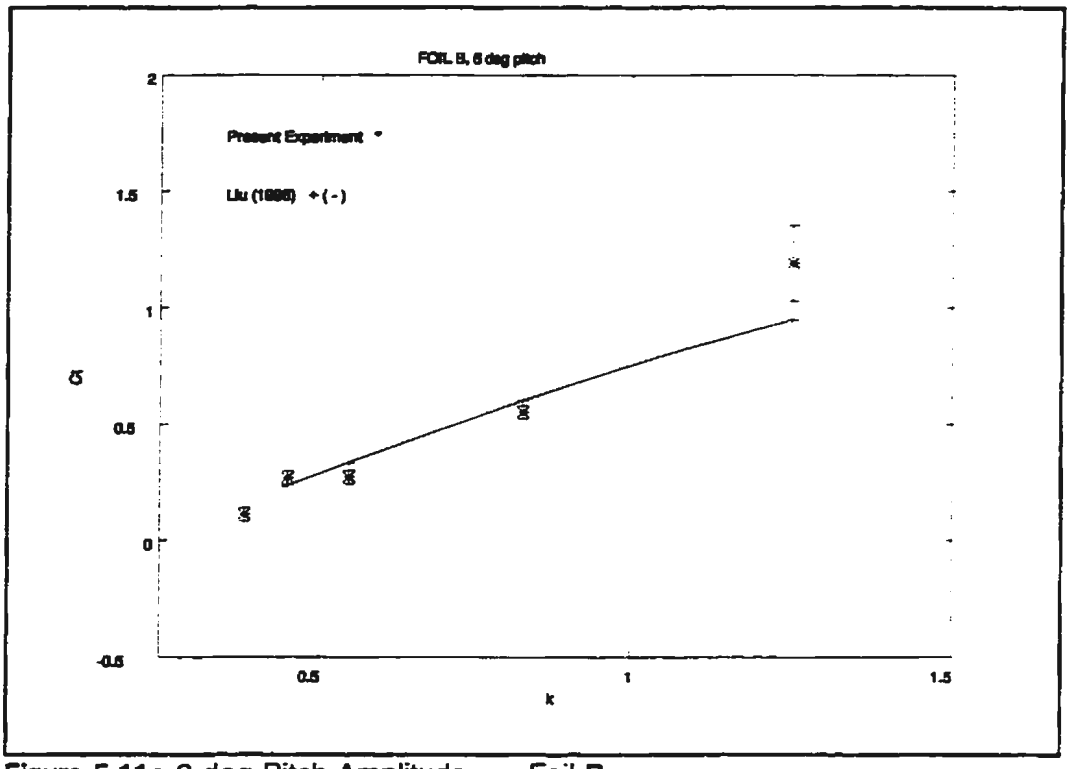

Figure 5.11a 6 deg Pitch Amplitude Foil B

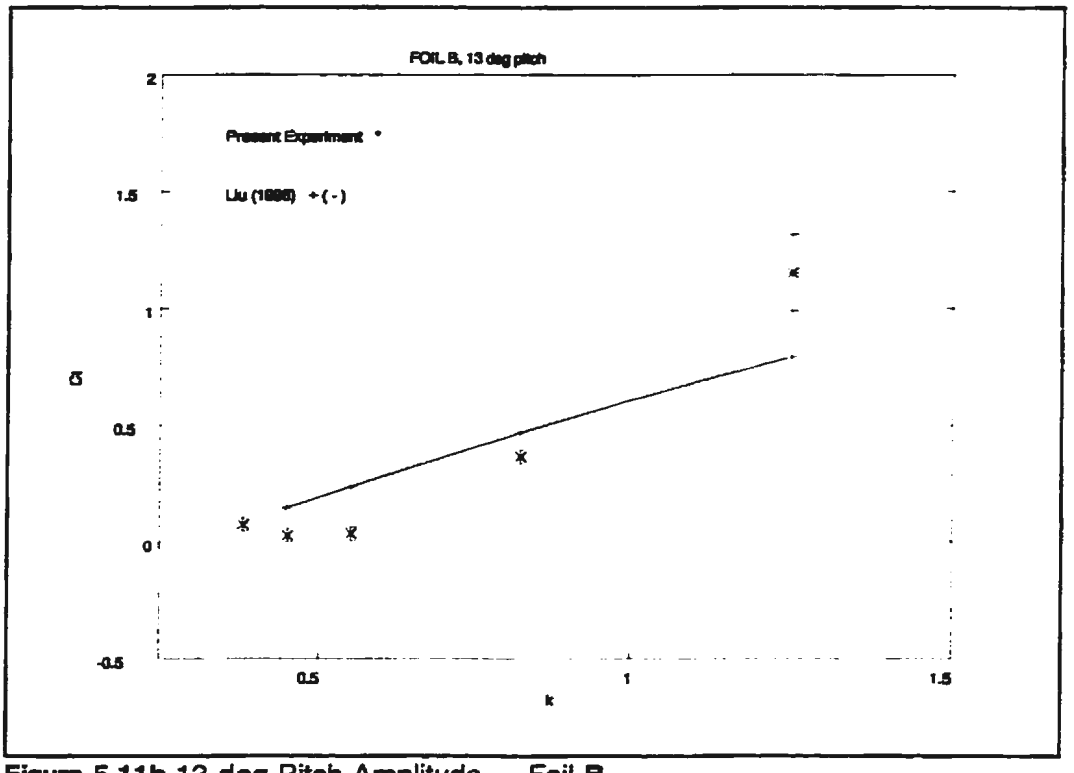

Figure 5.11b 13 deg Pitch Amplitude Foil B

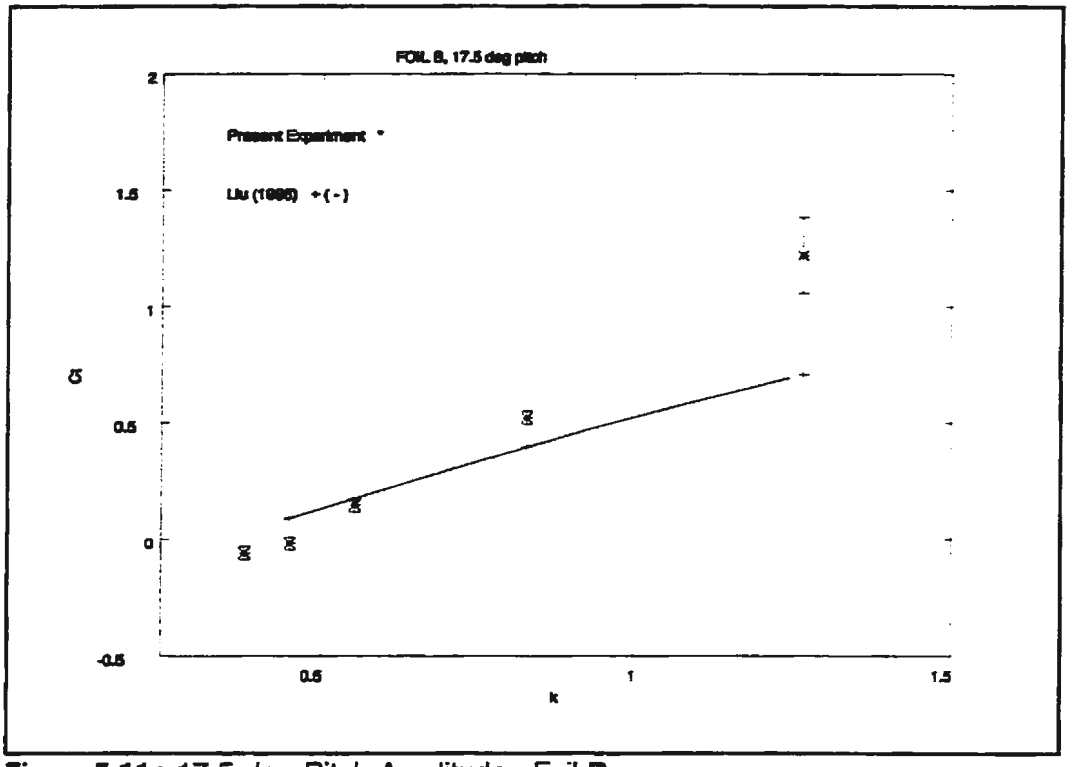

Figure 5.11c 17.5 deg Pitch Amplitude Foil B

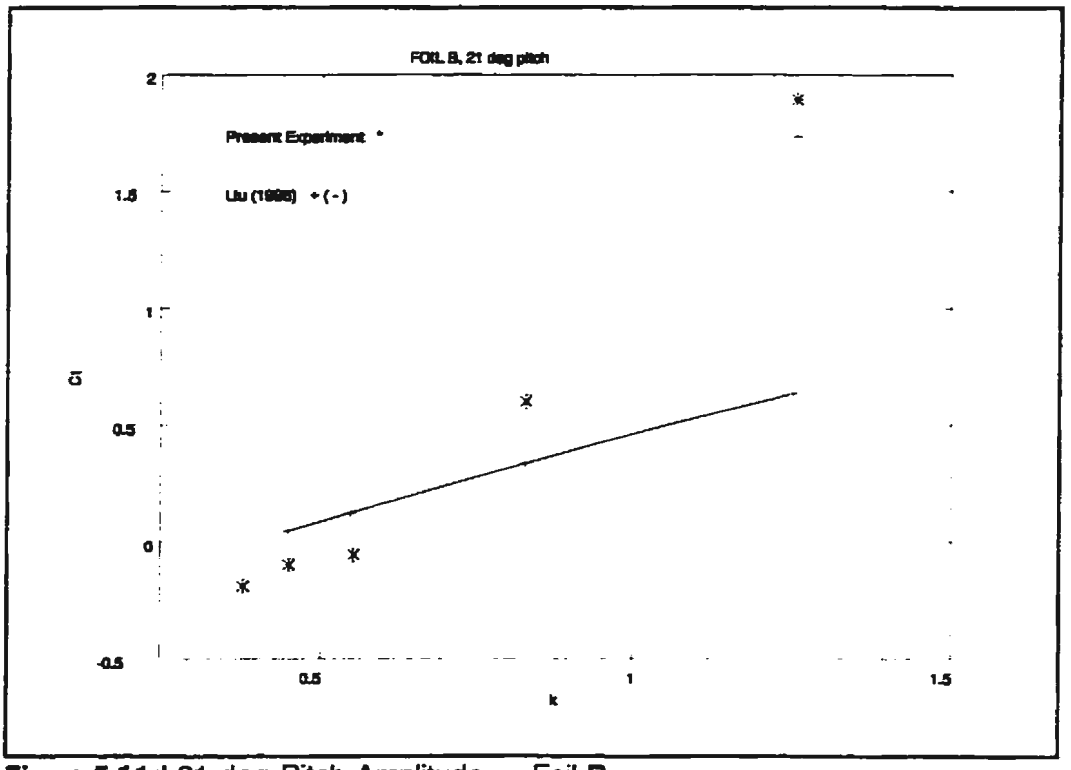

Figure 5.11d 21 deg Pitch Amplitude Foil B

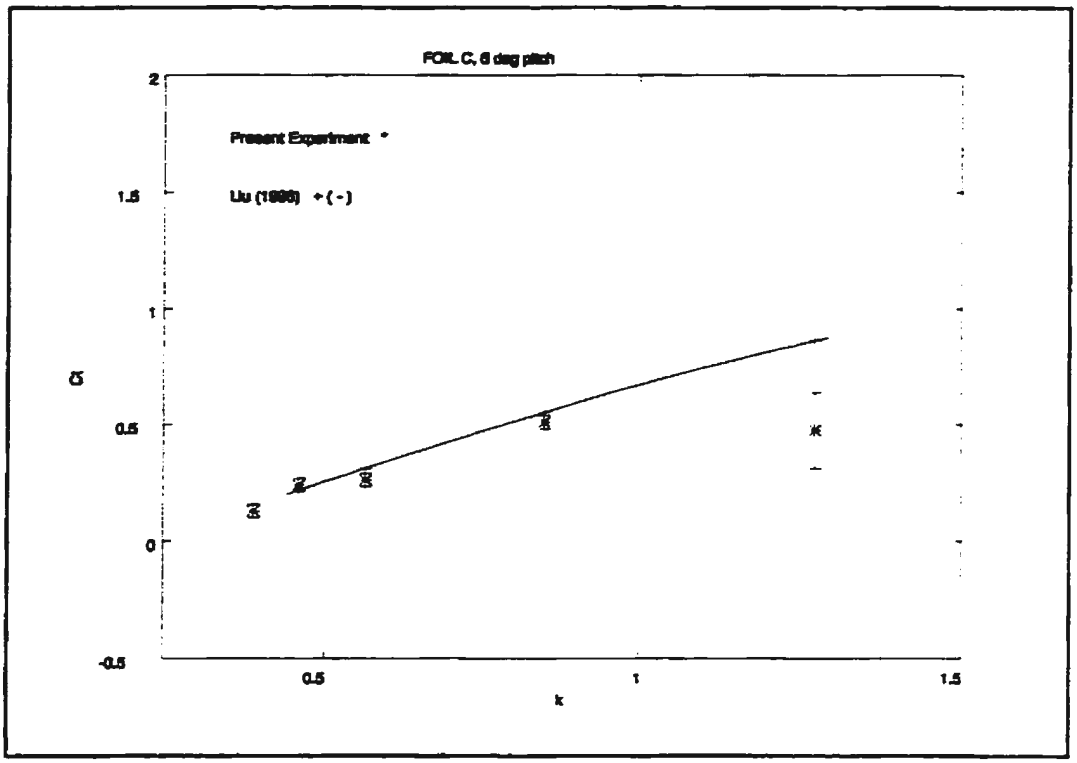

Figure 5.12a 6 deg Pitch Amplitude Foil **C**

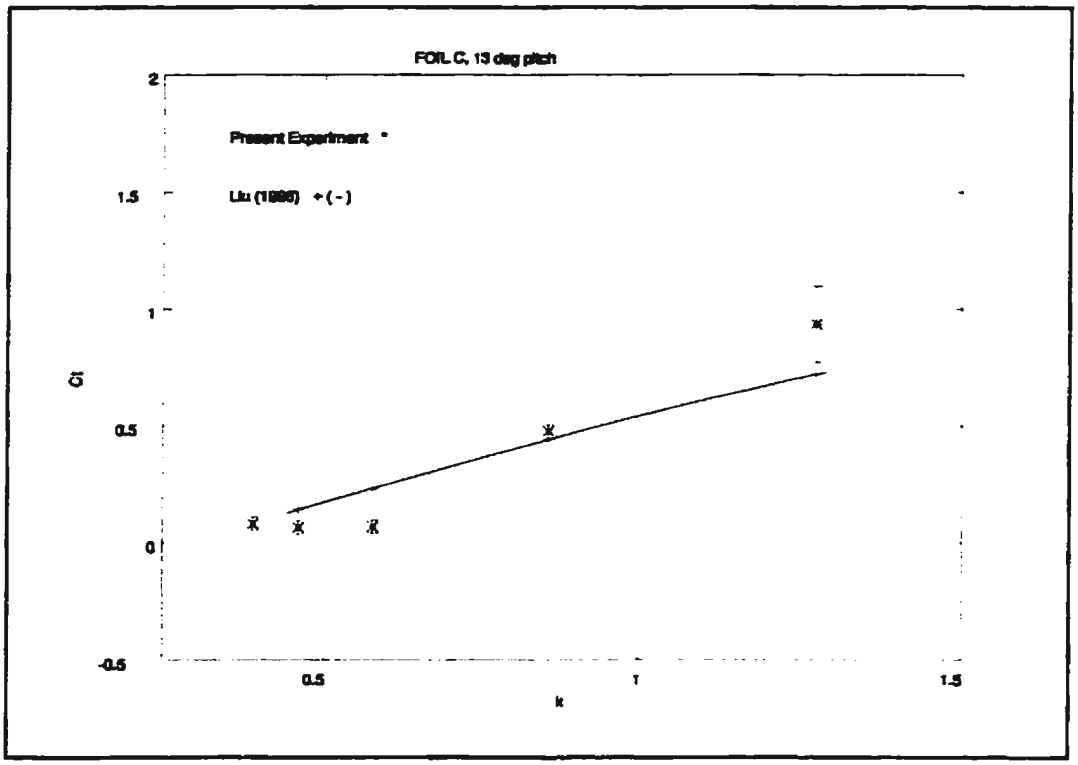

Figure 5.12b 13 deg Pitch Amplitude Foil **C**

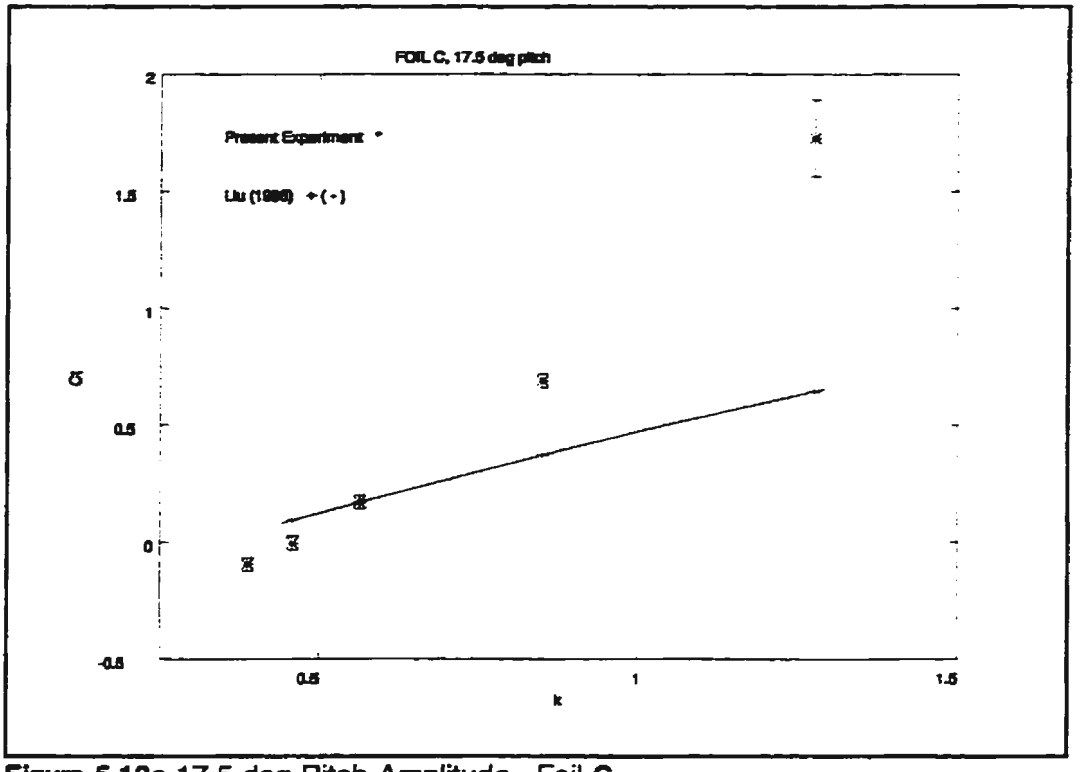

Figure 5.12c 17.5 deg Pitch Amplitude Foil C

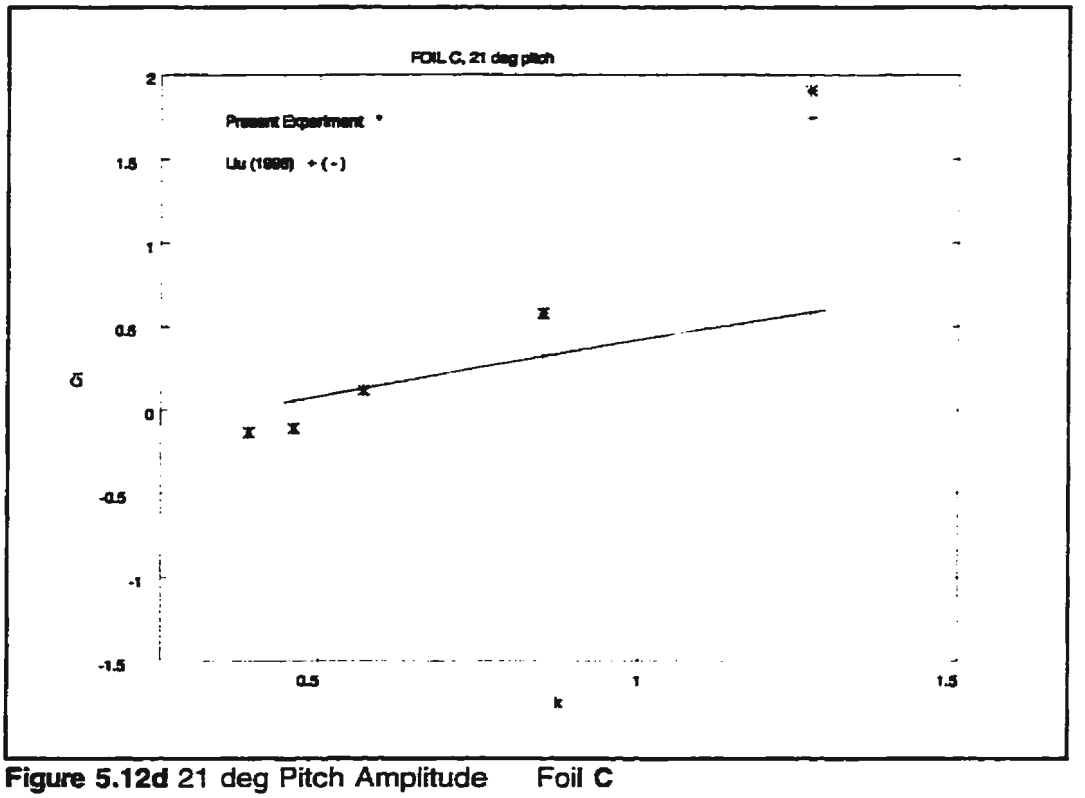

Figure 5.12d 21 deg Pitch Amplitude Foil C

Chapter 6

Conclusions and Recommendations

6.1 Oscillating Apparatus and Motion Control

A second design loop in the development of the computer controlled oscillating motion apparatus was completed as part of this research. Specifically, work was concentrated in two areas: first, modifications to the existing motion control software with the aim to eliminate vibrational problems experienced during commissioning of the original apparatus (Greening, 1996), and second, design of a dynamometer to more accurately measure the thrust developed by the oscillating foil.

The refinement of the motion control consisted of a computer program which incorporated a new motion command. This was followed by a set of bench tests to examine the behaviour of the oscillating apparatus using the new motion command. The following conclusions from the bench tests were drawn about the limitations of the oscillating apparatus:

i) The use of the new motion command eliminated vibrational problems experienced in previous tests with the oscillating apparatus. Thus in order to obtain continuous motion the **MV** command has to be used.

ii) The obtained approximation of the sinusoidal motion strongly depends on the requested input parameters, namely frequency and amplitude of

oscillation. Typically, motion parameters should be selected such that the motor's peak velocity does not exceed 9,000 steps/sec if sinusoidal motion is desired. For a shaft velocity greater than this, motion of the two shafts becomes less sinusoidal and more like a saw tooth.

iii) With the new motion command, pitch amplitude cannot be programmed, but it can be estimated by obtaining a calibration curve between the two shafts initial position and the obtained phase lag between them.

iv) Due to the nature of the approximation, that is having a finite number of time segments at which displacement and velocity are evaluated, the actual velocity profiles differ for forward and aft shafts. This caused a constant increase in the phase lag between the two shafts, and if the mounting pod was connecting the shafts, this increase would have caused damage. This problem was alleviated by fixing the pitching axis position at the origin, making the velocity profiles for both shafts identical.

6.2 Forward Thrust Developed by an Oscillating Foil

Overall in oscillating foil theory there have been two approaches to the analysis of thrust from an oscillating propulsor. One follows classical principles by stating that the developed thrust of an oscillating foil can be calculated from the difference in the pressure between the upper and lower surface of the foil. In these calculations it is assumed that the flow remains attached. Large amplitude motion is taken into account by properly calculating the kinematic velocity angle, but the

shed vortex is not allowed to relax, and so the full effect of the induced velocities from a rolled up wake are disregarded. This approach is represented by the numerical panel method of Liu (1996). The second approach is represented by the work of Triantafyllou et al. (1993) where it is proposed that thrust development is related entirely to the propulsive vortical pattern developed in the wake of an oscillating foil.

Experimental results in this thesis show evidence of the correctness of both approaches. This is illustrated in figure 6.1a to c where experimental results and Liu (1996) panel method predictions for the rectangular foil (foil **A**), swept back foil (Foil **B**), and whale fluke (Foil **C**) are plotted against maximum instantaneous angles of attack for three reduced frequencies obtained in the experiment. Also shown in the plot are errors associated with the experimental measurement and are represented by the vertical bars indicating 95% confidence intervals.

Agreement in the magnitude of the thrust coefficient is relatively good between the numerical and experimental results at reduced frequencies of k=0.64 and k=1.17 for the rectangular foil. At k=1.17 and 33 deg. angle of attack the panel method starts to underpredict the developed thrust. At an even larger reduced frequency and angles of attack the numerical solution fails to predict the trend and magnitude of measured thrust. The level of thrust developed at k=1.96 is much larger than predicted by the numerical solution. Even by taking into account the uncertainty

levels at this reduced frequency, the magnitudes of measured developed thrust are larger than those predicted by the theory.

Similar to the rectangular foil, at small reduced frequencies of k=0.42 and k=0.85 for the swept back foil and the whale fluke, the disagreement in C_t data obtained from the panel method compared to the measured thrust coefficient is relatively small. For a large reduced frequency of k=1.25, the panel method yielded consistently lower values in the thrust coefficient as well as a dissimilar trend for both the swept back foil and whale fluke (figure 6.1 b and c).

Comparison of the numerical method with experimental results suggest the following:

- At small reduced frequencies and angles of attack the panel method is in good agreement with experimental results, thus flow characteristics existing at these conditions are modelled correctly in the panel method.

- Inherent assumptions such as rigid vortex wake and attached flow in the panel code are violated at large reduces frequencies and angles of attack, resulting in a large discrepancy between experimental and numerical results.

- Results form the present experiment can be used as verification data for the numerical model. Based on figure 6.1 a,b and c it can be said that the Liu (1996) panel method is valid to predict unsteady loading of oscillating foils up to approximately k=1, and angles of attack between 30 to 44 deg.

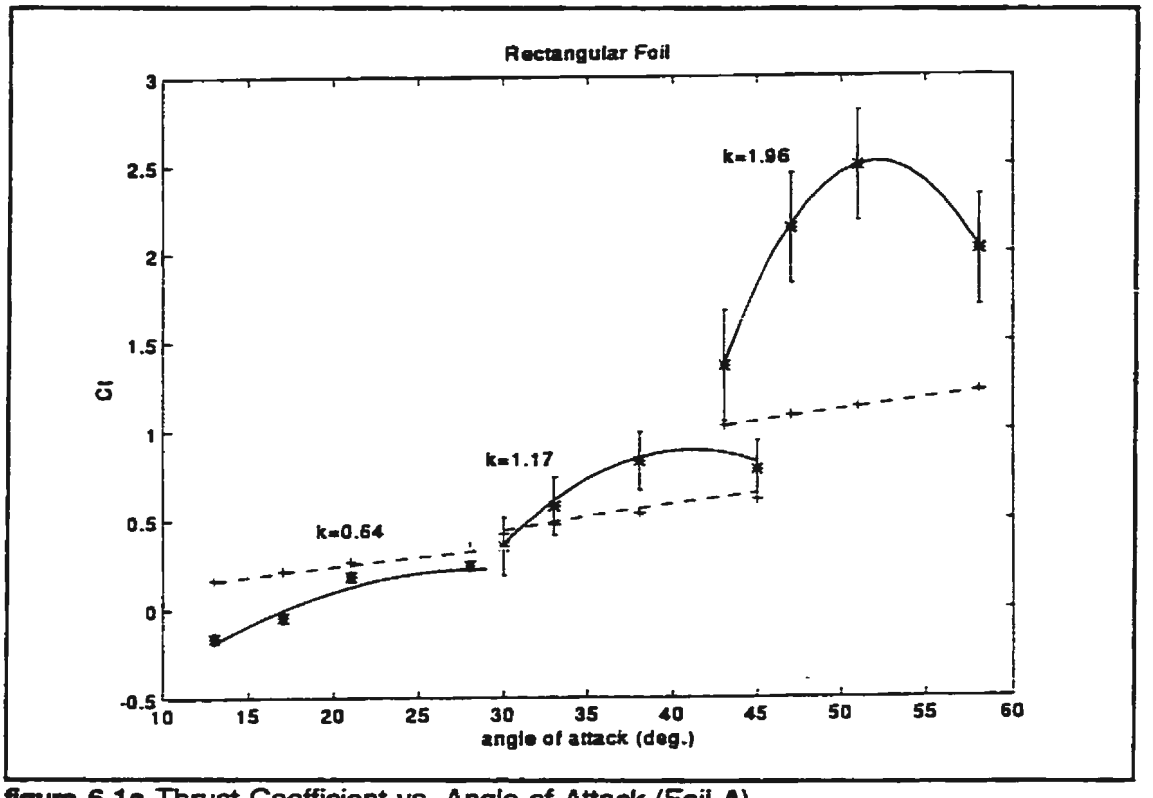

figure 6.1a Thrust Coefficient vs. Angle of Attack (Foil A)

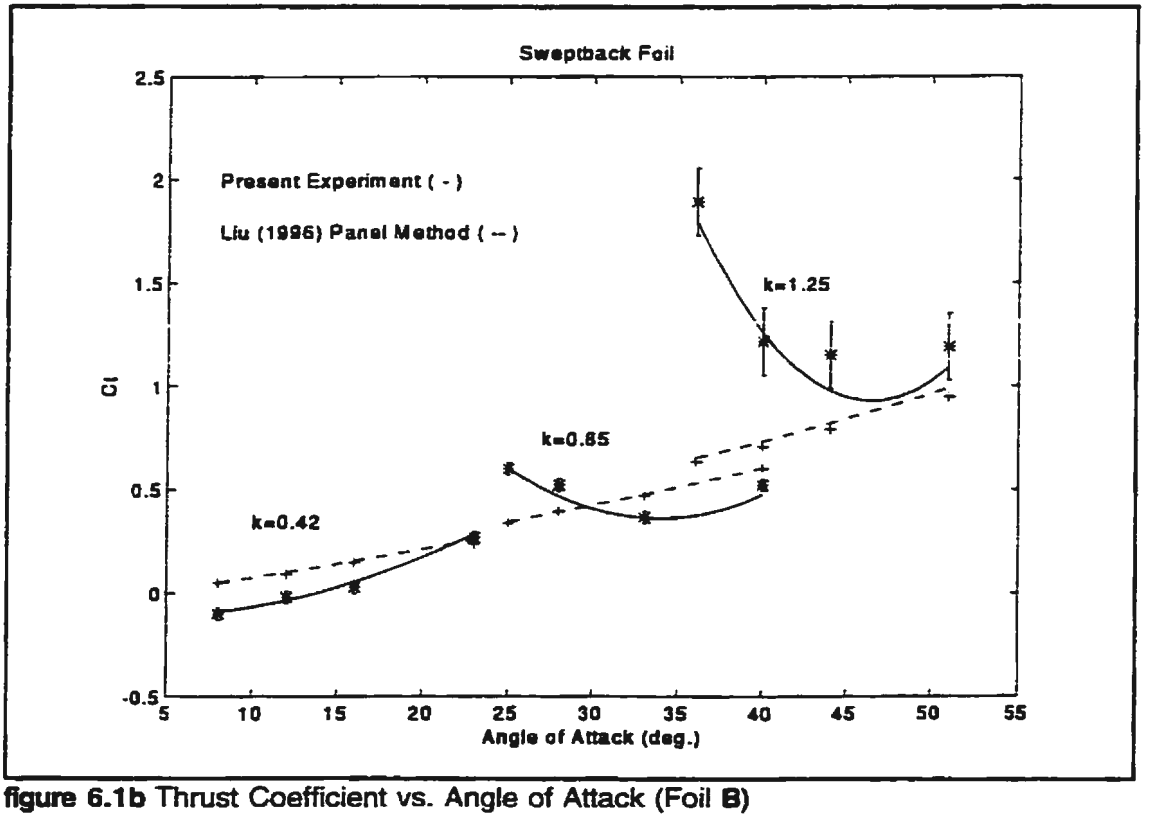

figure 6.1b Thrust Coefficient vs. Angle of Attack (Foil B)

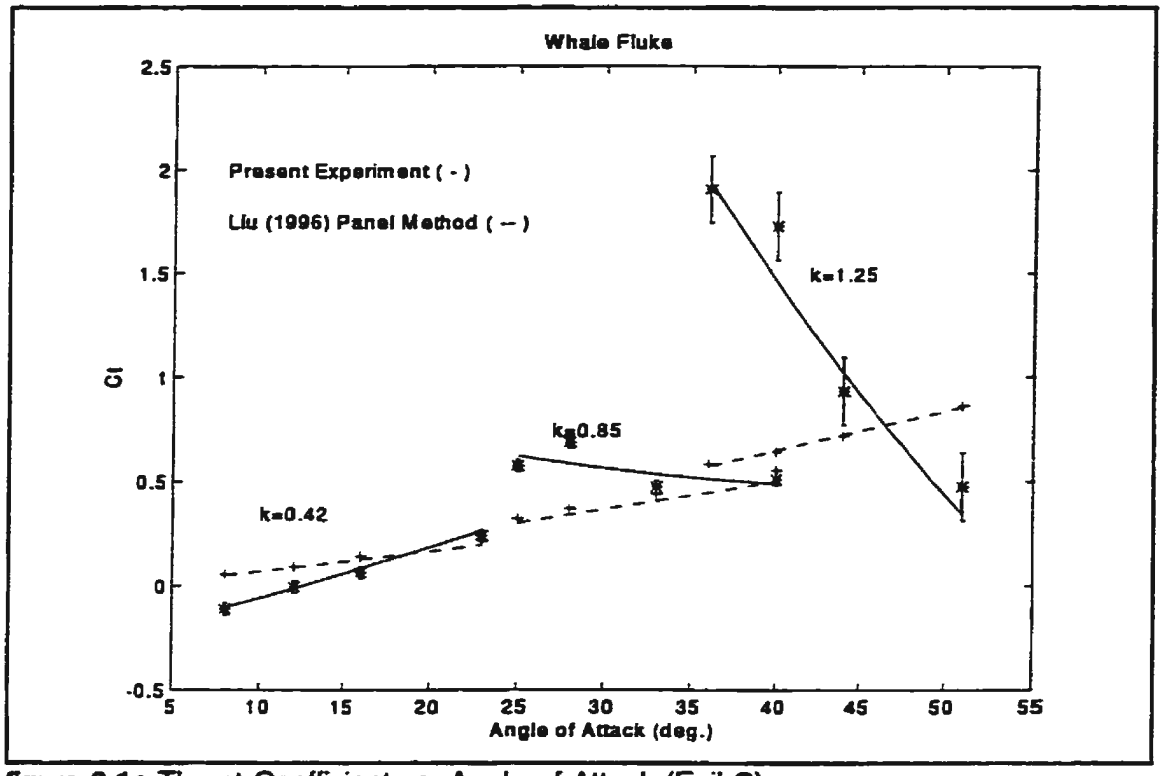

figure 6.1c Thrust Coefficient vs. Angle of Attack (Foil C)

From figure 6.1a it can be seen that up to 38 deg. angle of attack and at k=1.17, the experimentally obtained thrust coefficient shows a gradual increase with increasing angle of attack, and then starts to drop off at a 45 deg. angle. This may be an indication of separation and dynamic stall of the flow around the foil which is usually accompanied by a deterioration in developed thrust. That separation and dynamic stall was delayed up to a 38 deg. angle, may be substantiated by the visual observations of Triantafyllou et. al (1996) who reported that in their experiment noticeable stall for a heaving and pitching foil occurred for angles of attack greater than 30 deg. For the present experiment, the level of uncertainty associated with measurements at a reduced frequency of k=1.17, should be noted.

Figure 6.1 a to c also demonstrates qualitative differences between the performance of the foils of different planforms. For all three foils at small reduced frequencies and angles of attack the thrust coefficient increases with increasing angle of attack, suggesting that at these conditions developed thrust was insensitive to the planform shape. The experimental results at large reduced frequencies combined with the large angles of attack suggest a noticeable difference in performance between the foils. It can be observed that the combination of a leading edge sweep and taper of the foil's planform (the swept back foil and the whale fluke) has a marked qualitative difference in developed thrust compared to the foil with a straight leading edge (rectangular foil). The rectangular foil at k=1.96 showed an increase in thrust coefficient with angle of attack, with a maximum measured thrust, C_t =2.5 occurring at 51 deg. angle of attack. On the contrary the swept foil and whale fluke at k=1.25 showed a decrease in thrust coefficient with increasing angle of attack. The maximum measured thrust, C_t =1.89 and 1.91 for the swept back foil and whale fluke occurred at 36 deg. angle of attack. This was attributed to the fact that the stall behaviour over foils with leading edge sweep is completely different than the stall of foils with a rectangular planform.

6.3 Recommendations

It is recommended that flow visualization studies of the unsteady fluid flow phenomena around the oscillating foil at large reduced frequencies and angles of

attack be conducted. This would result in an improved understanding of the physics of the flow such as the characteristics of the vortical signature in the wake, as well as the development of a leading edge vortex and its subsequent manipulation in the foil's wake. These qualitative results could then be used in conjunction with numerical results from the Navier-Stokes solvers, which in the present author's opinion have great potential in the study of oscillating foils, for verification of the numerical methods.

In the experimental measurement of forward thrust developed by an oscillating foil, more sophisticated ways of obtaining thrust or drag should be used. This would improve the quality and reliability of the obtained results. The recent purchase of the Laser Doppler Velocimeter (LDV) by the Institute for Marine Dynamics (IMD) provides such a capability. LDV can measure in a non-intrusive and simultaneous manner, the vertical and horizontal components of the velocity vector. For example, LDV measurements can be performed at several vertical locations across the full width of the foil's wake (assuming that foil oscillates in vertical plane), providing information on the mean velocity profile behind the oscillating foil. In addition, this procedure can be repeated for a number of downstream locations, in the wake, so that a 3D picture of the unsteady wake behind the oscillating foil can be obtained. Having the wake surveyed in this way, the following can be deduced:

- From the shape of the velocity profile it can be deduced whether the foil develops drag or thrust. If the velocity profile has a velocity deficit, then the foil develops drag. If the measured velocity profile has a velocity suficit, then the oscillating foil experiences forward thrust.

- As the foil attains forward momentum by the oscillating motion, the propulsive force pushes the fluid backward with a net total momentum equal and opposite to that corresponding to the propulsive force (Chopra, 1974). Thus, the mean velocity profile can be used to quantitatively estimate the mean thrust or drag force developed by the foil. This velocity profile has to be taken in the near wake or as close to the foil's trailing edge as possible so that losses in the jet due to viscosity are minimized.

Since the LDV has a capability to measure the horizontal component of the velocity, distribution of velocity in the horizontal plane or across the foil span can be obtained. This would provide invaluable information of the loadings on the foil across the span, as well as insight into the conditions that exist at the foil's tip. To the author's knowledge this has not been done before, experimentally.

References

Bose, N., Lien, J. (1989). "Propulsion of a Fin Whale (Balaenoptera physalus): Why the Fin Whale is a Fast Swimmer," *Proceedings of the Royal Society of London,* B237, pp. 175-200.

Chopra, M. G., (1974). "Hydromechanics of lunate-tail swimming propulsion," *J. Fluid Mech.*, Vol. 64, part 2, pp. 375-391.

Chopra, M. G., Kambe, T. (1977). "Hydromechanics of lunate-tail swimming propulsion. Part 2," *J. Fluid Mech.*, Vol. 79, part 1, pp. 49-69.

Coleman, H. W., Steele, Jr., W. G. (1989). *Experimentation and uncertainty analysis for engineers,* John Wiley & Sons, Inc., 205 p.

Freymuth, P. (1988). "Propulsive Vortical Signature of Plunging and Pitching Airfoils," *AIAA Journal*, Vol. 26, No. 7, pp. 881-883.

Gopalkrishnan, R., Triantafyllou, M., S., Triantafyllou, G., S., Barrett, D. (1994). "Active vorticity control in a shear flow using a flapping foil," *J. Fluid Mech.*, Vol. 274, pp. 1-21.

Gray, J. (1936). "Studies in animal locomotion - VI. The propulsive powers of the dolphin," *Journal of Experimental Biology*, Vol.13, pp. 192-199.

Greening, D. L. (1996). "Design and Commissioning of a Computer Controlled Oscillating Hydrofoil Dynamometer," *M.Eng. thesis*, Memorial University of Newfoundland, St. John's, Newfoundland, Canada, 198 p.

Kadlec, R. A., Davis, S. S. (1979). "Visualization of Quasiperiodic Flows," *AIAA Journal*, Vol. 17, No. 11, pp. 1164-1169.

Karman von, Th., Burgers, J. M. (1935). "General Aerodynamic Theory," *Aerodynamic Theory*, Vol. II, ed. W. F. Durand, Julius Verlag, Berlin, pp. 308.

Katz, J., Plotkin, A. (1991). *Low Speed Aerodynamics (From Wing Theory to Panel Methods),* McGraw-Hill, Inc., 632 p.

Katz, J., Weihs, D. (1978). "Behaviour of Vortex Wakes from Oscillating Airfoils," *Journal of Aircraft*, Vol. 15, No. 12, pp. 861-863.

Koochesfahani, M. (1989). "Vortical Patterns in the Wake of an Oscillating Airfoil," *AIAA Journal*, Vol. 27, No. 9, pp. 1200-1205.

Juvinall, R. C., Marshek, K. M. (1991). *Fundamentals of Machine Component Design*, second edition, John Wiley & Sons, 804 p.

Lai, P. S. K. (1990). "Oscillating Foil Propulsion," *Ph.D. thesis*, Dept. of Naval Architecture and Ocean Engineering, University of Glasgow, Scotland, 384 p.

Lamb, H. (1945). *Hydrodynamics*, sixth edition, Dover Publications, New York.

Lighthill, M. J. (1969). "Hydromechanics of Aquatic Animal Propulsion," *Annu. Rev. Fluid Mech.*, Vol. 1, pp. 413-446.

Lighthill, M. J. (1970). "Aquatic animal propulsion of high hydrodynamical efficiency," *J. Fluid Mech.*, Vol. 44, part 2, pp. 265-301.

Moran, J. (1984). An Introduction to Theoretical and Computational Aerodynamics, Wiley, New York.

McCroskey, W. J. (1982). "Unsteady Airfoils," *Annu. Rev. Fluid Mech.*, Vol. 14, pp. 285-311.

McCroskey, W. J. (1977). "Some Current Research in Unsteady Fluid Dynamics," *Journal of Fluids Engineering*, Vol. 99, Series I, No. 1, pp. 8-38.

Oertel, Jr., H. (1990). "Wakes Behind Blunt Bodies," *Annu. Rev. Fluid Mech.*, Vol. 22, pp. 539-564.

Prandtl, L., Tietjens, O. G. (1934). *Fundamentals of Hydro-and Aeromechanics*, Dover Publications Inc., New York, 270 p.

Sharp, J. J. (1981). *Hydraulic Modelling*, Butterworth & Co. Ltd., 242 p.

Sharp, J. J., Moore, E. (1983). "Partial Analysis and Matrix Methods," *Int. J. Math. Educ. Sci. Technol.*, Vol. 14., No.4, pp. 393-402.

Steidel, Jr., R. F. (1989). *An Introduction to Mechanical Vibrations*, third edition, John Wiley & Sons, 439 p.

Triantafyllou, M. S., Barrett, D. S., Yue, D. K. P., Anderson, J. M., Grosenbaugh, M. A., Streitlien, K., Triantafyllou, G. S. (1996). "A New Paradigm of Propulsion and Maneuvering for Marine Vehicles," SNAME *Transactions*.

Triantafyllou, M. S., Triantafyllou, G. S. (1995). "An Efficient Swimming Machine," Scientific American, pp. 64-70.

Triantafyllou, G. S., Triantafyllou, M. S., Grosenbaugh, M. A. (1993). "Oscillating Foils with Application to Fish Propulsion," *J. of Fluids and Structures*, Vol. 7, pp. 205-224.

Triantafyllou, G. S., Triantafyllou, M. S., Chryssostomidis, C. (1986). "On the formation of vortex streets behind stationary cylinders," *J. Fluid Mech.*, Vol. 170, pp. 461-477.

Van Dam, C. P. (1987). "Efficiency characteristics of crescent-shaped wings and caudal fins," *Nature*, Vol. 325, pp. 435-437.

Yamaguchi, H., Bose, N. (1994). "Oscillating Foils for Marine Propulsion," *Proceedings of the Fourth International Offshore and Polar Engineering Conference*, Osaka, Japan.

Wang, C., Salmon, C.G. (1984). *Introductory Structural Analysis*, Prentice-Hall, Inc., 591 p.

Wu, T. Y. (1961). "Swimming of waving plate," *J. Fluid Mech.*, Vol. 10, pp. 321-344.

Wu, T. Y. (1971). "Hydromechanics of swimming propulsion. Part 1. Swimming of a two dimensional flexible plate at variable forward speed in an inviscid fluid," *J. Fluid Mech.*, Vol. 46, pp. 561-568.

Appendix I

Calculation of Forces Acting on the Dynamometer

Estimation of Expected Forces Acting on the Dynamometer

i) Static force due to the weight of the oscillating apparatus. The mass of the apparatus is approximately 77 kg. Thus, W=756 N.

ii) Hydrodynamic forces developed by the foil. These forces were estimated using the Chopra (1974) (his figure 4a) inviscid analytical calculations for developed thrust of an oscillating flat plate of aspect ratio 6 pitching at mid chord. For k=0.50, kinematic velocity angle β=46 deg, and small amplitude feathering parameter equal to zero (condition of maximum thrust), the thrust coefficient is Ct≈1. The thrust coefficient in Chopra (1974) work is defined as:

$$Ct = \frac{T}{2\rho c s \omega^2 h^2} \qquad \text{(AI.1)}$$

where c and s are the foil's semichord and semispan, respectively, and the other terms are as defined in the main body of this document. Using the values of the present experiment where frequency of oscillation was ω=4.4 rad/sec, heave amplitude h=0.07 m, c=33.3x10^{-3} m, s=0.4 m, the mean developed thrust T was calculated to be 1.3 N. Therefore, assuming D=0 (inviscid case), from equation 4.1 it follows

$$F_h = L\sin\beta = T = 1.3\,N$$
$$F_v = L\cos\beta = \frac{T}{\tan\beta} = 1.26\,N \qquad \text{(AI.2)}$$

iii) Dynamic forces due to acceleration and deceleration of the drive shafts.

These forces were estimated experimentally. It was found that the maximum axial force in one shaft was approximately F_d=32.5 N. Thus, the total dynamic force transferred to the dynamometer base plate is 2x32.5 N.

iv) The moment acting on the dynamometer is:

$$M = Td \tag{AI.3}$$

where d is the distance from the foil's pitching axis to the point of action on the bearing, where horizontal hydrodynamic forces are acting on the dynamometer. Assuming that maximum immersion of the foil models in the water for the present experiment is approximately 25 cm from the water line, and adding an additional 5 cm from the water line to the dynamometer base plate, x is taken to be 30 cm. Thus, the maximum moment was M=0.3x1.3=0.4 Nm.

Dynamometer Frame Loads

Figure AI.1 shows the free body diagram of the vertical forces acting on the dynamometer. First, vertical loads in sheets A and B will be estimated.

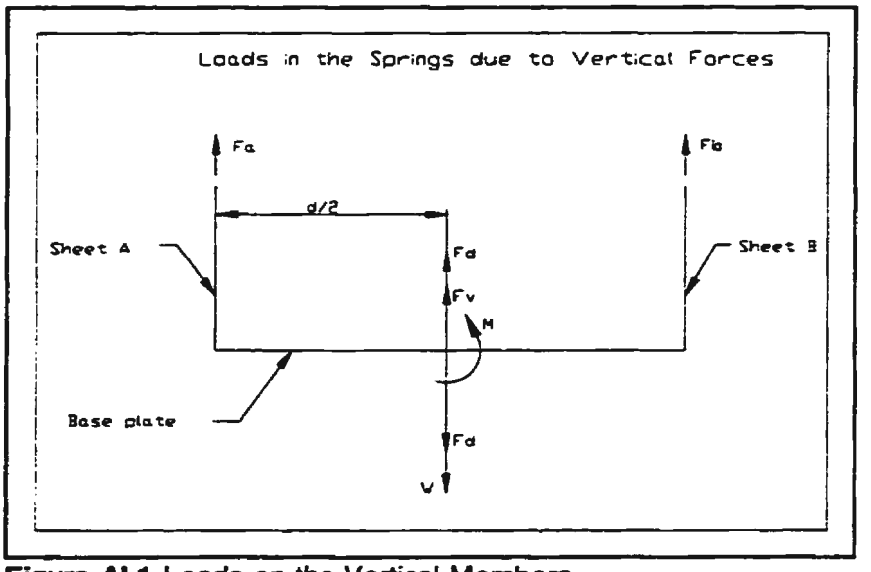

Figure AI.1 Loads on the Vertical Members

Table AI.1 summarizes the loads in the vertical members (springs) A and B. The moment acting on the dynamometer is taken to be anticlockwise due to the positive thrust force. This causes tension in sheet A and compression in sheet B. If the foil develops drag, the moment on the dynamometer would be clockwise and this would cause compression in sheet A and tension in sheet B. A positive force is taken to act downward.

Table AI.1 Summary of Loads in the Vertical Members

Force	W	F_v	F_d	M
Sheet A	W/2 (tension)	$-F_v/2$ (compression)	$-F_d/2$ (compression)	+2M/d (tension)
Sheet B	W/2 (tension)	$-F_v/2$ (compression)	$-F_d/2$ (compression)	-2M/d (compression)

The resultant forces F_a and F_b in sheets A and B due to vertical forces are, respectively:

$$F_a = \frac{W}{2} + \frac{2M}{d} - \frac{1}{2}(F_v + F_d)$$
$$F_b = \frac{W}{2} - \frac{2M}{d} - \frac{1}{2}(F_v + F_d) \qquad \text{(AI.4)}$$

where d is the distance between the vertical sheets (d=0.66 m).

Figure AI.2 shows the free body diagram of the loads in members A and B due to the horizontal force T. Here it is assumed that sheets A and B have the same stiffness, and that the dynamometer base plate is rigid. If this is the case then at distance l/2 (where l is the length of the vertical members), the moment in the members is zero (Wang and Salmon, 1984). Here a positive force is taken to act downward.

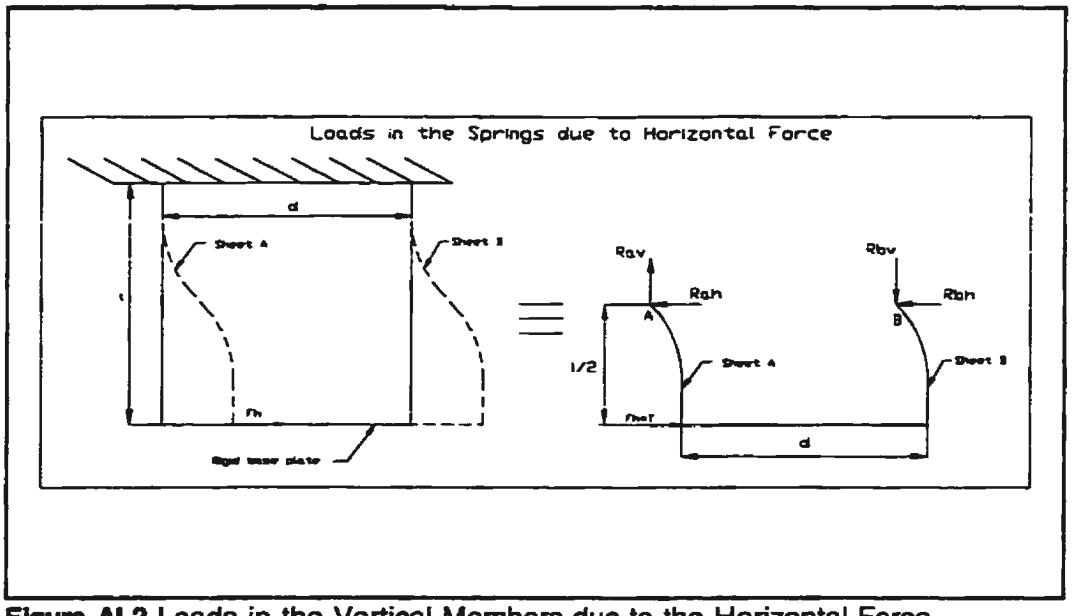

Figure AI.2 Loads in the Vertical Members due to the Horizontal Force

Taking moments about point A:

$$\Sigma Ma = 0$$
$$F_h \frac{l}{2} - R_{bv} d = 0 \rightarrow R_{bv} = \frac{F_h l}{2d} \quad \text{(AI.5)}$$

The sum of the vertical forces yields the relation:

$$\Sigma R_v = 0$$
$$R_{bv} - R_{av} = 0 \rightarrow R_{bv} = R_{av} \quad \text{(AI.6)}$$

This result indicates that for the orientation of the horizontal thrust force as shown in figure AI.2, sheet A will be in tension, and sheet B compression.

The total vertical force in the sheets is equal to:

$$F_{a\,toc} = F_a + R_{av} = 346.7\,N$$
$$F_{b\,toc} = F_b + R_{bv} = 323.0\,N \quad \text{(AI.7)}$$

It can be seen from these calculations that both sheets A and B will be in tension, suggesting that buckling of the vertical members is not possible.

Horizontal forces in the sheets can be found from the free body diagram shown in figure AI.2. If the stiffness of the members is the same, then

$$R_{ah} = R_{bh} = \frac{F_h}{2} \quad \text{(AI.8)}$$

Design of the ABS Flexible Sheets

The vertical sheets were fabricated from the Acrylonitrile-Butadiene-Styrene (ABS) family of resins. The tensile yield strength σ_y of ABS is 31 MPa (4,500 psi), and the modulus of elasticity E=1379 MPa (2×10^5 psi) (Juvinall and Marshek, 1991). The

thickness of the sheets was 6.35 mm (1/4").

The nominal stress in the vertical member is

$$\sigma = \frac{P}{A} = \frac{347}{2.56 x 10^{-3}} = 0.14 MPa \qquad \text{(AI.9)}$$

where A is the area of the sheet cross section based on the dimensions given in figure AI.3. The stress concentration due to bolt holes was estimated using the graph 4.39b in Marshek (1991) as σ_{max}=2.73xσ=0.4 MPa. Since $\sigma_y >> \sigma_{max}$ the member can safely carry the expected load.

Stiffness was estimated by considering the sheets as cantilever beams. The maximum deflection for a cantilever beam with a concentrated load P at the end is (Marshek, 1991):

$$\delta = \frac{P l^3}{3 E I} \qquad \text{(AI.10)}$$

where l is the length of the sheet (see figure AI.2). Stiffness is defined as load over deflection, thus:

$$k = \frac{3 E I}{l^3} \qquad \text{(AI.11)}$$

Using this equation, stiffness of one vertical member was found to be k=115.8 N/m in the fore and aft direction (direction of thrust or drag force); k=581.6 kN/m in the transverse direction.

Since vertical sheets A and B are identical, the total stiffness in the fore and aft

direction is 2x115.8=231.6 N/m (0.232 N/mm). Similarly, the total stiffness in the transverse direction is 2x581.6=1163.2 kN/m (1.163 kN/mm). From this it can be seen that the sheets are flexible in the fore and aft direction and very stiff in the transverse direction.

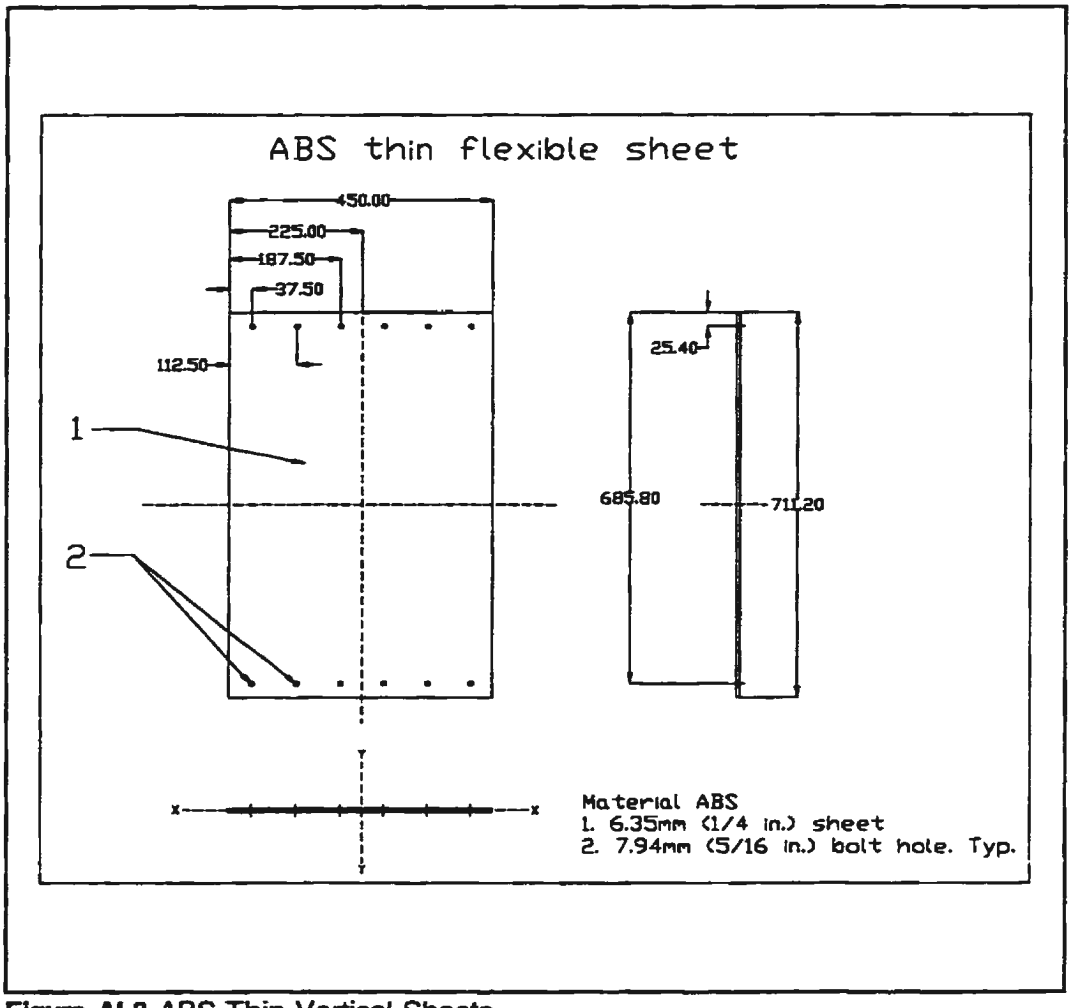

Figure AI.3 ABS Thin Vertical Sheets

Appendix II

Bias and Precision Limits of Measured Variables

Bias and Precision Limit Calculations of Measured Variables

•Velocity - V (Elemental biases)

i) curve fit: +/-2 SEE[6]=+/- 0.0001 m/s (assumption)

ii) tide: +/- 0.001 m/s (estimate)

iii) calibration: +/- 0.005 m/s (readability of the digital scale; taken as 1/2 of the least scale)

Velocity bias limit: $B_V=[0.0001^2+0.001^2+0.005^2]^{1/2}=0.0051$ m/s

•Velocity - V (Precision limit)

Only one carriage speed time history was analyzed to find the precision limit associated with the average value of the speed. Values are shown in the Precision Limit Table.

Velocity precision limit: $P_V=+/-0.0004$ m/s

•Thrust - T (Elemental biases)

i) nonlinearity of the thrust load cell (0.03% of the rated output): +/- 0.0134 N

ii) applied load: +/- 0.01 N

iii) curve fit: +/- 2SEE=+/- 0.0337 N

Thrust bias limit: $B_T=[0.0134^2+0.01^2+0.0337^2]^{1/2}=0.0376$ N

•Thrust - T (Precision limit)

Only one thrust time history was analyzed to find the precision limit. Values are

[6]SEE is Standard Error of Estimate. +/-2 SEE band around the curvefit will contain approximately 95% of the data points (Coleman and Steele, 1989), page 173.

shown in the Precision Limit Table.

Thrust precision limit: P_T=+/- 0.0399 N

•Thrust/Drag on the pod - T_o (Elemental biases)

Thrust/Drag on the pod bias limit: B_{To}=0.0376 N (same as for thrust T)

•Thrust/Drag on the pod - T_o (Precision limit)

Only one thrust time history was analyzed to find the precision limit. Values are shown in the Precision Limit Table.

Thrust/Drag on the pod precision limit: P_{To}=+/- 0.0413 N

Precision Limit Calculation

Precision limits were estimated by analyzing the time history of the measured variables. This time history was divided into 10 sections and the mean was taken of each of the 10 sections and are given in table AII.1. These values were used in calculating the precision index of the sample population given by:

$$S_r = \left(\frac{1}{M-1}\sum_{k=1}^{M}(r_k - r)^2\right)^{1/2} \qquad \text{(AII.1)}$$

where M=10, r_k is each of the 10 means, and r is the mean of the 10 means. The precision index of these 10 readings was taken as:

$$S_P = \frac{S_r}{M^{1/2}} \qquad \text{(AII.2)}$$

Finally, the precision limit was calculated as:

$$P_x = tS_x \qquad \text{(AII.3)}$$

where t=2.262 was the value from the t-distribution for a 95% confidence level and M-1 degrees of freedom (Coleman and Steele, 1989).

Table AII.1 Readings for Precision Limit Calculations

Reading #	T_o[N]	T[N]	V[m/s]
1	-0.15953	0.784503	0.20158
2	-0.15656	0.754575	0.19961
3	-0.168842	0.833196	0.20086
4	-0.119467	0.743072	0.20109
5	-0.024517	0.752236	0.20054
6	-0.103772	0.816380	0.20005
7	-0.210517	0.85810	0.20075
8	-0.06249	0.70803	0.20009
9	-0.13789	0.72737	0.20011
10	-0.193945	0.86444	0.20007